UNIVERSITY OF OKLAHOMA

GRADUATE COLLEGE

BOND PERFORMANCE OF ADVANCED ENVIRONMENTALLY FRIENDLY CONCRETE MATERIALS FOR RAPID INFRASTRUCTURE REPAIR AND REHABILITATION

A THESIS

SUBMITTED TO THE GRADUATE FACULTY

in partial fulfillment of the requirements for the

Degree of

MASTER OF SCIENCE

By COURTNEY ELICE DAWSON

Norman, Oklahoma

2025

Downloaded from SHAREOK. Persistent Handle URL: https://hdl.handle.net/11244/341623

BOND PERFORMANCE OF ADVANCED ENVIRONMENTALLY FRIENDLY CONCRETE MATERIALS FOR RAPID INFRASTRUCTURE REPAIR AND REHABILITATION

A THESIS APPROVED FOR THE

SCHOOL OF CIVIL ENGINEERING AND ENVIRONMENTAL SCIENCE

BY THE COMMITTEE CONSISTING OF

Dr. Royce Floyd, Chair

Dr. Shreya Vemuganti

Dr. Jeffery Volz

© Copyright by COURTNEY ELICE DAWSON 2025
All Rights Reserved.

Acknowledgments

I have many people to thank for their unique contributions to my academic and personal life. I truly would not have been able to do this without such a strong group of people behind me. I'm not sure if I can properly articulate how much these people mean to me, but this is my attempt.

First, I would like to thank my advisor, Dr. Royce Floyd, for his unwavering patience and faith in me—even after I called him to come tow the forklift out of a mud pit. Dr. Floyd hired me for undergrad research before I knew a single thing about concrete, and from there, taught me pretty much everything that I know. I greatly appreciate the opportunity and your support throughout the past few years.

I would also like to thank my committee members, Dr. Shreya Vemuganti and Dr. Jeffery Volz. Dr. Vemuganti, thank you for your encouragement and contagious enthusiasm. I'm sorry about the day that I missed your class to power wash wet concrete because I used the wrong type of cement. Dr. Volz, thank you for your sense of humor and for helping me to keep John in check. I am grateful that you both took the time to be on my committee and to share your knowledge with me.

The next person that I would like to thank is the Fears Structural Engineering Laboratory Manager, John Bullock. John, thank you for your technical and emotional support during these past couple of years. You have fostered such amazing camaraderie in the lab and have made it a fun place to be. I can always count on you to hype me up and to be there if I am having a bad day. Thank you for always being eager to share your expertise for and teaching me how to do countless things in the lab. Lastly, thank you for being someone that I know I can call for help. Thank you for coming to change my tire when it was a million degrees out and for driving me to the ER to get stitches after a non-work related incident. All of this being said, I forgive you for the many times that you embarrassed me at Home Depot and other public establishments.

I have worked with numerous amazing people throughout my time at Fears lab, all of whom deserve gratitude and recognition. In no particular order, thank you to Omar Yadak, Mujtaba Ahmadi, Sijan Adhikari, Isaiah Shoulders, Isabella Mendoza, Cade Harris, Jackson Milner, Jacob Starks, Zach Tiry, and Steve Roswurm. There are numerous other people who were also instrumental in my research experience. These people have not only been my peers and colleagues, but have also come to be my friends. We have all shared laughs and dreadfully hot days at the lab. The work that we have done is impossible to do alone, and I owe all of you a huge thank you for your role in the completion of my research. My research would not have been possible, let alone enjoyable, without the people that I have been lucky enough to work with.

Next, I would like to acknowledge my friends, boyfriend, and family who have been the best support system. Thank you to all of you for being there when I was stressed out or needed to vent. Thank you for being so uplifting and supportive. Thank you for making my life easier and more meaningful. My family deserves special acknowledgement. Mom, Dad, and Tyler, thank you for making me the person that I am today. Thank you for your vital role in allowing me to grow up believing that I can do anything I want to if I try hard enough.

Lastly, I would like to acknowledge and thank the generous individuals and companies whose donations and technical knowledge made this study possible. Specimen fabrication would not have been possible without material donations from Dolese, CTS Cement Manufacturing Corporation, and BASF MasterFiber. I would also like to acknowledge and thank University of Arkansas researchers Dr. Cameron Murray and Bette Poblete for their technical contribution to one of the concrete mix designs used in this study.

Table of Contents

Abstract xvi

Chapter 1. Introduction 1

1.1. Background 1

1.2. Research Question 3

Chapter 2. Literature Review 5

2.1. Quantification of CO_2 Emissions from OP, CSA, and HB-CSA Cement 5

2.2. Performance of Concrete Using CSA Cements 8

2.2.1. CSA Cement 8

2.2.2. Challenges of Implementing CSA Cement Concrete 9

2.2.3. Mechanical Performance of CSA Cement Concrete 10

2.2.3.1. Mechanical Benefits of CSA Cement 10

2.2.3.1.1. Time-Dependent Deformation 11

2.2.3.1.2. Bond and Development Length of Prestressing Strand 12

2.2.3.1.3. CSA Cement Concrete as a Repair Material 12

2.2.3.2. Mechanical Challenges of CSA Cement 13

2.2.3.2.1. Strength Loss of CSA Cement Concrete 14

2.2.3.2.2. Modulus of Elasticity of CSA Cement Concrete 14

2.2.4. Durability of CSA Cement Concrete 15

2.2.4.1. Freeze-Thaw Resistance of CSA Cement Concrete 17

2.2.4.2. Resistance of CSA Cement Concrete to De-Icing Salts 20

2.3. Analysis of Supplementary Cementitious Materials 22

2.4. Aspects for Future Research 25

Chapter 3. Materials and Methodologies 26

3.1. Specimen Preparation 26

3.1.1. Mix Designs 26

3.1.2. Mixing, Casting, and Curing of Class AA Concrete 31

3.1.3. Surface Preparation 32

3.1.4. Preparation of Small-Scale In-Service Concrete Bases 33

3.1.5. Mixing, Casting, and Curing of Overlay Materials 35

3.1.5.1. RS-SCC and RS-SCCHA Mixing Procedure 36

3.1.5.2. FR-SCC Mixing Procedure 37

3.1.5.3. RS-SCCUA Mixing Procedure 38

3.2. Small-Scale Testing 39

3.2.1. Pull-Off Testing 39

3.2.2. Freeze-Thaw Testing 43

3.3. Large-Scale Repair Specimens 46

Chapter 4. Results and Discussion 50

4.1. Pull-Off Testing 50

4.1.1. Monolithic Specimen Pull-Off Testing 50

4.1.2. Composite Specimen Pull-Off Testing 54

4.1.2.1. Effects of Surface Preparation on Tensile Bond Strength 55

4.1.2.1.1. Composite Specimens with RS-SCC Overlays 55

4.1.2.1.2. Composite Specimens with RS-SCCHA Overlays 56

4.1.2.1.3. Composite Specimens with RS-SCCUA Overlays 58

4.1.2.1.4. Composite Specimens with FR-SCC Overlays 61
4.1.2.2. Effects of Repair Material on Tensile Bond Strength 62
4.1.2.3. Summary of Composite Pull-Off Test Results 63
4.2. Freeze-Thaw Testing 66
Chapter 5. Conclusions and Recommendations 95
5.1. Conclusions on General Material Performance 95
5.2. Conclusions on Bond Strength 96
5.3. Conclusions on Freeze-Thaw Durability 96
5.4. Recommendations for Future Research 97
References 98
Appendix A : Fresh Properties and Compressive Strength Data 104
Appendix B : Pull-Off Test Data 108
Appendix C : Freeze-Thaw Test Data 112

List of Tables

Table 1: Comparison of Theoretical CO_2 Emissions from Cement Production 7

Table 2: Quantification of CO_2 Emissions for Supplementary Cementitious Materials [31] 23

Table 3: Summary of Mixes and Corresponding Specimens 27

Table 4: Material Sources 29

Table 5: Summary of Mix Designs 30

Table 6: Average Tensile Strength and Standard Deviation for Monolithic Specimens 50

Table 7: Summary of Average Tensile Strength Values (psi) 55

Table 8: Percentage of ASTM C1583 Failure Modes by Surface Preparation 64

Table 9: 28-Day Compressive Strength of RS-SCC Specimens for Environmental and Controlled Curing Conditions 91

Table 10: Admixture Dosages, Slump, and Air Content of Class AA Concrete 104

Table 11: Admixture Dosages, Slump Flow, and Air Content of FR-SCC 104

Table 12: Admixture Dosage and Slump Flow of RS-SCC 104

Table 13: Admixture Dosage and Slump Flow of RS-SCCHA 104

Table 14: Admixture Dosage and Slump Flow of RS-SCCUA 105

Table 15: Compressive Strength Data for Class AA Concrete 105

Table 16: Compressive Strength Data for RS-SCC 105

Table 17: Compressive Strength Data for RS-SCCHA 106

Table 18: Compressive Strength Data for RS-SCCUA 106

Table 19: Compressive Strength Data for FR-SCC 107

Table 20: Pull-Off Results for Class AA Monolithic Specimen 108

Table 21: Pull-Off Test Results for 7-Day RS-SCC Monolithic Specimen 108

Table 22: Pull-Off Test Results for 28-Day RS-SCC Monolithic Specimen 108

Table 23: Pull-Off Test Results for RS-SCCHA Monolithic Specimen 108

Table 24: Pull-Off Test Results for RS-SCCUA Monolithic Specimen 109

Table 25: Pull-Off Test Results for FR-SCC Monolithic Specimen 109

Table 26: Pull-Off Results for RS-SCC Composite Specimens 109

Table 27: Pull-Off Results for RS-SCCHA Composite Specimens 110

Table 28: Pull-Off Results for RS-SCCUA Composite Specimens 110

Table 29: Pull-Off Results for FR-SCC Composite Specimens 111

Table 30: Monolithic RS-SCC (7-Day) Freeze-Thaw Data 112

Table 31: Monolithic RS-SCC (28-Day) Freeze-Thaw Data 112

Table 32: Monolithic RS-SCCUA Freeze-Thaw Data 112

Table 33: Monolithic RS-SCCHA Freeze-Thaw Data 113

Table 34: Composite RS-SCCHA Resonant Frequency Data (Hz) 113

Table 35: Composite RS-SCCHA Relative Dynamic Modulus of Elasticity Data (%) .. 113

Table 36: Composite FR-SCC Resonant Frequency Data (Hz) 113

Table 37: Composite FR-SCC Relative Dynamic Modulus of Elasticity Data (%) 114

Table 38: RS-SCCHA/CH Bridge Repair Freeze-Thaw Data 114

Table 39: RS-SCCHA/SB-D Bridge Repair Freeze-Thaw Data..... 114

Table 40: FR-SCC/CH Bridge Repair Freeze-Thaw Data 115

Table 41: FR-SCC/SB-D Bridge Repair Freeze-Thaw Data..... 115

List of Figures

Figure 1: Diagram of Cement Production Process [6] 6

Figure 2: CO_2 Emissions for Concrete with Supplementary Cementitious Materials [31] 24

Figure 3: Compressive Strength Data for Fly Ash and GGBFS Replacement Ratios [31] 25

Figure 4: Visible Layer of Unset Paste (a) and Exposed Aggregate Finish (b)..... 34

Figure 5: Chipping Hammer (a) and Sandblasted Surface Preparations (b) 35

Figure 6: Pull-Off Specimen Before Testing 40

Figure 7: ASTM C1583 [40] Pull-Off Testing Schematic (a) and Testing Device (b) 41

Figure 8: Specimen Orientation for Resonant Frequency Testing..... 44

Figure 9: Target Temperature Fluctuation of Freeze-Thaw Specimens 45

Figure 10: Large-Scale Slab for Repair 46

Figure 11: Large Scale Repair Slab During Cutting (a), Chipping (b), and Sandblasting Processes (c) 47

Figure 12: Large Scale Repair Slab Formwork (a) and Finished Specimen (b) 49

Figure 13: Tensile Strength of Monolithic Materials Measured Using Pull-off Test 52

Figure 14: Polypropylene Fiber Bridging Failure Plane of Monolithic FR-SCC Pull-Off Specimen 53

Figure 15: ASTM C1583 Results for Composite Specimens with RS-SCC Overlay 56

Figure 16: ASTM C1583 Results for Composite Specimens with RS-SCCHA Overlay 58

Figure 17: ASTM C1583 Results for Composite Specimens with RS-SCCUA Overlay 60

Figure 18: ASTM C1583 Results for Composite Specimens with FR-SCC Overlay..... 61

Figure 19: Composite Pull-Off Test Results by Material 63

Figure 20: FR-SCC-EA Pull-Off Specimen Failure Surface 65

Figure 21: Relative Dynamic Modulus of Elasticity Results for Monolithic RS-SCC 67

Figure 22: 7-Day (a) and 28-Day (b) Monolithic RS-SCC Specimens After Freeze-Thaw Exposure 69

Figure 23: Relative Dynamic Modulus of Elasticity Results for Monolithic RS-SCCHA . 71

Figure 24: RS-SCCHA Monolithic Specimens Before (a) and After (b, c) 93 Freeze-Thaw Cycles 71

Figure 25: Relative Dynamic Modulus of Elasticity for Monolithic RS-SCCUA Specimens 72

Figure 26: Deterioration of RS-SCCUA After Freeze-Thaw Exposure 73

Figure 27: Relative Dynamic Modulus of Elasticity Results for RS-SCCHA Repair 75

Figure 28: Crumbling of Edge and Surface of RS-SCCHA Specimen After Freeze-Thaw Exposure 76

Figure 29: RS-SCCHA-SB-D1 Specimen Before (a) and After (b) Freeze-Thaw Exposure 77

Figure 30: Poorly Consolidated FR-SCC Specimen Before (a) and After (b) Freeze-Thaw Exposure 79

Figure 31: Failure Surface of FR-SCC-SB-1 Specimen Showing Fractured Aggregate Particles at the Interface 80

Figure 32: Relative Dynamic Modulus of Elasticity Results for FR-SCC Repair 81

Figure 33: FR-SCC Composite Specimen after 307 Exposure Cycles 82

Figure 34: Delamination of RS-SCCHA-CH Repairs on Bridge Deck Specimens, (a) RS-SCCHA-CH Specimen 2 and (b) RS-SCCHA-CH Specimen 1 84

Figure 35: Relative Dynamic MOE Data for RS-SCCHA Bridge Deck Repair Specimens 84

Figure 36: Relative Dynamic MOE Data for FR-SCC Bridge Deck Repair Specimens . 85

Figure 37: Bridge Deck Repair Specimens After Initial Exposure Period: RS-SCCHA-SB Specimen After 97 Cycles (a), FR-SCC-CH Specimen After 95 Cycles (b), and FR-SCC-SB Specimen after 95 Cycles (c) 86

Figure 38: RS-SCC Interfaces on Large-Scale Repair Slab 88

Figure 39: Shrinkage Crack on Large-Scale RS-SCC Repair Slab 89

Figure 40: RS-SCC Large-Scale Repair Slab (a) and Compressive Strength Cylinders (b) with Ice Accumulation 90

Figure 41: RS-SCC Large-Scale Repair Slab with the CH plus SB Surface Condition (a) and Close-up of the RS-SCC Material (b) After Environmental Exposure 90

Figure 42: Large-Scale FR-SCC Repair Slab Before Exposure 93

Figure 43: Comparison of FR-SCC Repair Material Before (a) and After (b) Exposure 94

Figure 44: Interface Zone of FR-SCC Repair Slab 94

List of Equations

Equation 1: Bond or Tensile Strength of Pull-Off Specimens [40] 42

Equation 2: Relative Dynamic Modulus of Elasticity [41] 66

Abstract

Portland cement production results in approximately 2.5 gigatons of direct CO_2 emissions per year, or between 5% and 10% of human produced CO_2 emissions. Calcium sulfoaluminate (CSA) cements are promising alternative hydraulic cements with nearly half the CO_2 emissions during production and with high early strength (rapid setting) or controlled expansion (shrinkage compensating). These properties make CSA cement attractive and effective for transportation structure and pavement repair applications by increasing the speed of the repair and/or mitigating shrinkage cracking. Half of the bridges in the United States already have or will reach their anticipated design life in the next 10 years. Many can have their service life safely extended – with reduced environmental impact – by targeted repair and rehabilitation using CSA cements. Using concrete mix designs developed at the University of Oklahoma (OU) and the University of Arkansas (UARK), the ability of CSA cement to bond to traditional concrete substrates and the durability of those bonds over time were studied. The objectives of this study were to evaluate CSA cement concrete bond performance for varying substrate conditions, evaluate freeze-thaw durability of CSA cement concrete repairs, and to develop and communicate recommendations for CSA cement concrete repairs. The results of the study suggest that the tensile bond strength between CSA cement concrete and ordinary portland cement (OPC) concrete is generally sufficient and, in some cases, may surpass the tensile strength of the OPC concrete. The freeze-thaw durability of these repairs is generally sufficient as well. Therefore, relative to tensile bond strength and resistance to freeze-thaw deterioration, CSA cement concretes have proven to be a feasible option for rapid infrastructure repair.

Chapter 1. Introduction

1.1. Background

Portland cement production results in approximately 2.5 gigatons of direct CO_2 emissions per year, or between 5% and 10% of human produced CO_2 emissions. Growing concerns about aging infrastructure and greenhouse gas emissions necessitate advanced concrete repair materials that are both functional and environmentally friendly. Concrete is one of the most widely used materials in the world, second only to water [1]. Due to the widespread usage of concrete, the material accounts for up to 8% of the world's CO_2 emissions, and 95% of the CO_2 emissions associated with concrete result directly from cement production [2]. The majority of greenhouse gas emissions from cement production are from the clinkering process. Ordinary portland cement (OPC) is created by heating limestone, clay, and other raw materials in a kiln, which facilitates the chemical combination of calcium, silicon, aluminum, and iron [1]. During this process, calcium carbonate in the limestone decomposes into calcium oxide and carbon dioxide. Carbon dioxide is also emitted by the burning of fossil fuels required to heat the cement kiln to the extreme temperatures required for the chemical process to take place [3]. Cement is the primary constituent for developing the strength of concrete. There are many different types of cement, all with varying chemical and mechanical properties. Currently, OPC is the most commonly used type of cement. Calcium sulfoaluminate (CSA) cements are promising alternative hydraulic cements with nearly half the CO_2 emissions during production and with high early strength (rapid setting) or controlled expansion (shrinkage compensating). These properties make CSA cement attractive and effective for transportation structure and pavement repair applications by increasing the speed of the repair and/or mitigating shrinkage cracking.

According to the approved consolidated methodology (ACM), there are two methods for reducing greenhouse gas emissions from cement. The first method, ACM0005, is titled "increasing the blend in cement production." This method involves increasing the ratio of other material and decreasing the ratio of clinker in the cement,

which reduces the CO_2 emissions from the combustion of raw materials and emissions from fossil fuels used to heat the cement kiln. The second method, ACM0015, is titled “emission reductions from raw material switch in clinker production.” This method involves replacing limestone with alternative materials not containing carbonates. Replacing limestone eliminates the CO_2 that is released when the material decarbonates. The United Nations Framework Convention on Climate Change (UNFCCC), acting through the Clean Development Mechanism (CDM), approved 17 projects that use these two methods of greenhouse gas reduction. The annual greenhouse gas reduction from these projects was about 2,559,000 tCO_2-eq [4]. CSA cements incorporate both of these greenhouse gas reduction methods by replacing some of the limestone with aluminum oxide and adding mixed material to reduce the amount of clinker in the cement. Furthermore, CSA clinker can be produced at lower kiln temperatures, reducing fuel-related emissions during the production process.

Thus, one potential solution in reducing the carbon emissions associated with concrete production is by using alternative cements, such as CSA cements. These CSA cements can provide additional mechanical benefits, such as high early strength (rapid setting) or controlled expansion (shrinkage compensating), that are especially desirable in bridge and pavement rehabilitation applications. Rapid setting cements can reduce traffic disruptions by decreasing the duration of lane closures. Shrinkage compensating cements can reduce shrinkage cracking and separation of the repair from the base concrete.

There are, however, still some challenges preventing the widespread implementation of CSA cements. First, the mechanical and durability behavior of CSA cement concrete is not as well understood as that of OPC concrete. Additionally, the rapid initial set time of concrete using CSA cement can cause significant barriers during the construction process, including prohibiting the use of ready-mix concrete. Furthermore, as is the case with many developmental materials, the cost of CSA cement is significantly more than that of OPC. In 2017, CSA cement in North America was four times the price of OPC [5]. However, there are many factors to consider relative to material costs, such as service life and environmental impact. Regardless of

long-term cost-benefit analysis, an increased initial cost makes widespread use difficult. There is some cost reduction that would occur if the material was more common, but CSA cement will likely continue to be more costly to produce than OPC because of the requirement for more stringent quality control. There is less margin for variance in the chemical composition of CSA cement, therefore increasing the quality control requirements [5].

1.2. Research Question

CSA cements have proven to be a promising, more environmentally conscious alternative for OPC based on desirable mechanical properties, rapid setting time, and shrinkage compensating behaviors and reduced CO_2 emissions. In addition to mechanical performance, longevity must be considered, as infrastructure is currently aging faster than it can be replaced. Extended serviceability can also be more sustainable than frequent replacement. Thus, there is particular interest in the use of CSA cement as a repair material.

In order to perform as intended, it is vital that concrete repair materials sufficiently bond to the existing concrete. Ideally, both chemical and mechanical bonding occurs. Chemical bonding is affected mostly by the chemical composition of the two concretes. Conversely, physical bonding can be improved by using surface preparation techniques to roughen the surface of the existing concrete.

Vulnerability to freeze-thaw conditions is also an important property to consider when specifying a concrete repair material. During freeze-thaw conditions, water can enter pores in the concrete and freeze, causing it to expand and potentially cause cracking. In repair situations, freeze-thaw resistance of the overlay material and the bond between materials must be considered in areas prone to these conditions. The interface between the existing concrete and the repair material is especially vulnerable because it introduces another zone where water may enter and freeze. It must be ensured that the repair material will not delaminate due to freeze-thaw conditions.

This project investigated the bond strength between superstructure concrete and environmentally friendly, rapid setting, and shrinkage compensating concrete repair materials and freeze-thaw resistance of these interfaces. The mix designs examined in this project use CSA cements and/or supplementary cementitious materials, resulting in decreased greenhouse gas emissions when compared to OPC, along with providing beneficial behaviors.

Chapter 2. Literature Review

2.1. Quantification of CO_2 Emissions from OP, CSA, and HB-CSA Cement

Several researchers have developed methods for quantifying and comparing CO_2 emissions from OPC and CSA cements. Determining how the emissions from CSA cements compare to OPC validates their improved sustainability and provides a basis for estimating the impact of switching to more environmentally friendly repair materials.

Nie et al. [6] developed an analytical approach to quantifying CO_2 emissions from ordinary portland cement (OPC), high-belite cements (HBC), calcium sulfoaluminate (CSA) cements, and high-belite calcium sulfoaluminate (HB-CSA) cements. The methodology of their research was rooted in analyzing chemical processes of cement production and quantifying CO_2 emissions based on these chemical equations. The researchers took a comprehensive approach, accounting for process-related, fuel-related, and electricity-related CO_2 emissions.

Process-related CO_2 emissions were defined as emissions stemming directly from the chemical decomposition of raw materials. The researchers found that this decomposition of raw materials accounted for approximately one-half of the CO_2 emitted in the cement production process. Fuel-related CO_2 emissions accounted for the combustion of fuels required to transform the raw materials. Heat balance equations were used to calculate the theoretical fuel combustion energy, and the fuel-related CO_2 emissions were calculated using the carbon content of the fuel. Lastly, electricity-related CO_2 emissions accounted for the electricity used in plant operations. Emissions from electricity usage were found by multiplying the average electricity consumption by an emission factor. Figure 1 from Nie et al. is a flowchart of the cement production process outlining the steps in which CO_2 emissions occur [6].

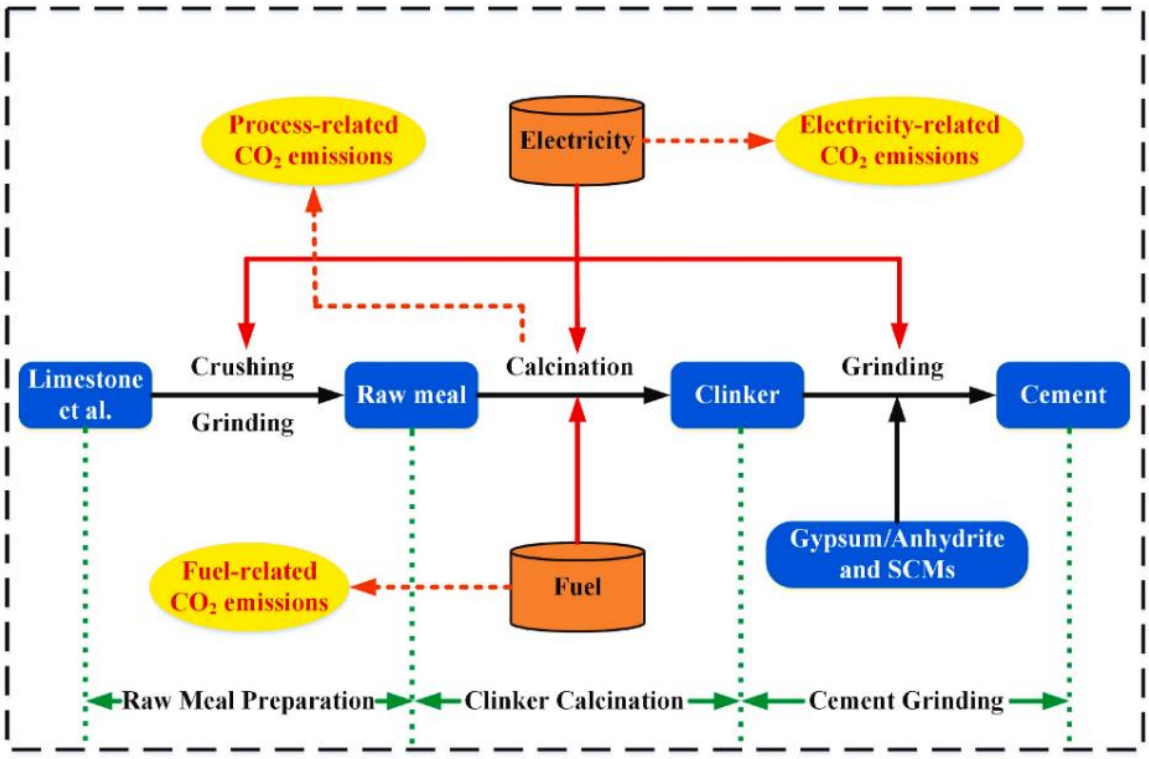


Figure 1: Diagram of Cement Production Process [6]

Jeon et al. [4] developed another, similar method for the quantification of greenhouse gases in CSA cements. The purpose of their research was to effectively account for the simultaneous reduction of greenhouse gas emission that occurs in CSA cements. The theoretical greenhouse gas emissions calculated by Jeon et al. concurred with the values from Nie et al. [6].

Table 1 summarizes the CO_2 emissions of each type of cement analyzed by both groups of researchers. The reduction of CO_2 emissions for CSA cement compared to OPC was 0.252 tCO_2/tCement and 0.281 tCO_2/tCement from Nie et al. [6] and Jeon et al. [4], respectively. The lower overall emissions from the CSA cement production process are a combination of reductions in all three sources of CO_2 (process-related, fuel-related, and electricity-related).

Table 1: Comparison of Theoretical CO_2 Emissions from Cement Production

Cement Type	CO_2 Emissions (tCO_2/tCement) [6]	CO_2 Emissions (tCO_2/tCement) [4]
OPC	0.705	0.810
CSA	0.453	0.529
HB-CSA	0.337	N/A

Nie et al. found that the majority of CO_2 emissions from cement production occur during the process of decomposing raw materials to make clinker. Thus, replacing sources of CaO with alternatives not containing carbonates is an effective way of reducing overall CO_2 emissions. For example, they found that using $Ca(OH)_2$ rather than $CaCO_3$ resulted in a 78% reduction in process and fuel-related CO_2 emissions. The model developed by Nie et al. validated the reduced environmental impact of CSA cements. CSA and HB-CSA cements were found to have 36% and 52% less CO_2 emissions than OPC, respectively.

The reduction in fuel-related CO_2 emissions from CSA cement is mostly attributable to the lower required kiln temperature for CSA clinker production. CSA clinker can be fired at temperatures approximately 150°C lower than OPC clinker, reducing fuel consumption [7]. Electricity-related emissions are also reduced by the increased friability of CSA cement clinker, which refers to the tendency of solid materials to break into smaller pieces under stresses such as abrasion. Because CSA cement clinker is more friable than OPC clinker, less energy is consumed during the grinding process [7].

2.2. Performance of Concrete Using CSA Cements

2.2.1. CSA Cement

The development of calcium sulfoaluminate (CSA) cement dates back to the 1960s, and the material has been used in China for about 50 years. More recently, there has been increasing attention on CSA cement research and implementation in the United States and Europe, with environmental and mechanical benefits being the main motivators [7].

The hydration process of OPC occurs when calcium oxide (CaO), silica (SiO_2), and alumina (Al_2O_3) react with water to form calcium silica hydrate (C-S-H) and calcium hydroxide (CH or portlandite). In OPC, calcium oxide is mainly present in the form of alite (C_3S), belite (C_2S), aluminate (C_3A), and ferrite (C_4AF) [5].

The hydration process of CSA cements differs from that of OPC due to its chemcial composition. CSA cement is contains more alumina (Al_2O_3) and sulfate (SO_3), as well as less calcium oxide (CaO) and silica (SiO_2) than OPC. In CSA cement, calcium oxide is mainly present in the form of Ye'elimite ($C_4A_3\hat{S}$), belite (C_2S), ferrite (C_4AF), and calcium sulfate. The main products of CSA cement hydration are ettringite ($C_6A\hat{S}_3H_{32}$), amorphous aluminite, and monosulfate ($C_4A\hat{S}H_{18}$) [5].

The differing forms of calcium oxide in OPC and CSA cement is one of the reasons for their distinct behaviors. In CSA cements, the presence of ye'elimite facilitates the formation of ettringite. The precipitation of ettringite is the main constituent in the rapidsetting and shrinkage compensating behaviors of CSA cement [5]. The ettringite formation reaction occurs more quickly than the hydration process of OPC, which contributes to the high early strength (or rapid-setting) behavior of CSA cements [8]. In addition to ocurring quickly, the precipitation of ettringite is an expansive process, resulting in volume stability in CSA cements. Relatedly, Type K cements, which are a blend of portland cement, CSA, calcium sulfate, and lime, exhibit shrinkage compensating properties due to this expansive precipitation of ettringite [5]. Rapid setting and shrinkage compentsating CSA cements differ in the timing of ettringite

formation. Rapid setting behavior is promoted by the near immediate onset of ettringite formation. Expansive behavior, on the other hand, occurs when ettringite crystals form after the matrix has started to gain strength [9].

Additionally, the precipitation of needle-like ettringite crystals affects the microstructure of the CSA cement matrix. These ettringite crystals interlock, forming a dense matrix with low porosity and permeability [5], [8]. The matrix structure of CSA cement can further affect concrete properties such as durability.

2.2.2. Challenges of Implementing CSA Cement Concrete

When assessing the viability of a structural material such as CSA cement concrete constructability, mechanical performance, and durability must be considered. Due to the quick precipitation of ettringite crystals, concretes made with CSA cements typically have a quicker initial set time than concretes using OPC. At low water-cemet (*w/c*) ratios and without the use of admixtures, initial setting times of less than 10 minutes can occur. This initial set time can be increased to about an hour through the appropriate proportions of admixtures and water, in addition to reducing the temperature of the concrete. Currently, citric, boric, gluconic, and tartaric acids have proven to be effective retarders of CSA cements, although the availability of a chemical admixture capable of providing an initial set time of more than an hour is limited [5]. The potential for reduced working time is one obstacle preventing the widespread use of CSA cements. Initial set time is an especially pertinent concern for large batches and in higher temperatures, as the concrete sets more quickly when the material is warm.

There are a few reasons why the quick initial set time of CSA cements present significant construction challenges. First, in the current stage of development, rapid setting cements are poorly suited for ready-mix concrete applications. With such rapid setting times, the material can begin to set in the drum of the ready-mix truck before reaching the site. Due to these challenges, rapid setting cements are typically mixed on site for current applications. Additionally, the reduced workability time necessitates

efficient casts for proper placement, consolidation, and avoiding the formation of cold joints. The decreased working time can limit the volume of concrete that can be cast at one time. There may also be a need for additional or more skilled labor to ensure that the material can be placed in a timely manner.

2.2.3. Mechanical Performance of CSA Cement Concrete

Previous research on the mechanical performance of CSA cements shows that some mechanical properties are more favorable than those of OPC, while others are less desirable. The most notable mechanical benefits of using CSA cements are high early compressive strengths and shrinkage compensation. However, CSA cements may also result in strength loss at later ages and carbonation.

2.2.3.1. Mechanical Benefits of CSA Cement

Due to rapid ettringite formation, fifty-percent of the ultimate compressive strength of CSA cement concrete is achieved in the first few hours, and 90% of the ultimate compressive strength is achieved in the first few days [5]. The high early compressive strength of CSA cement concretes make them desireable in infrastructure repair applications due to minimizing disruption/closure times. The rapid strength gain of CSA cements can also be beneficial in precast concrete applications because the members can be demolded quicker and potentially be cured for shorter periods of time, both of which can increase turnover and efficiency [10]. In addition to rapid strength gain, CSA cements can also yield concrete with a relatively high ultimate strength. An ultimate compressive strength of up to 10,000 psi is not uncommon for concrete made with CSA cement, which is more than adequate for most applications [5].

2.2.3.1.1. Time-Dependent Deformation

Roswurm and Starks performed comparable studies of time dependent prestress losses for CSA cement concrete mixes [11], [12]. The research by Roswurm evaluated a rapid-setting, non-expansive BCSA cement self-consolidating concrete. Roswurm found that the shrinkage strain for the non-expansive BCSA concrete was significantly less than for high strength OPC concrete. Starks measured time-dependent strain in a Type K cement concrete and an expansive BCSA cement concrete. In the study, the Type K cement was used as a 25% substitution for OPC, while the expansive BCSA cement concrete mix included no OPC. Both the Type K mix and the expansive BCSA mix exhibited expansive behavior. The Type K mix expanded considerably less, however, and only expanded enough to partially compensate for drying shrinkage. Starks also noted that the expansive behaviors of both types of cement are only observed under wet cure conditions [12].

Furthermore, Roswurm evaluted the impact of BCSA cement concrete age on elastic shortening and creep strain, and found that increased loading age decreased both strain measurements. The ultimate shrinkage values and creep coefficients were significantly lower for the BCSA concrete mix than for high strength OPC concrete. In terms of total time-dependent prestress losses, Roswurm found that the AASHTO LRFD and the American Concrete Institute (ACI) simplified methods both grossly overestimated the long-term losses for prestressed BCSA self-consolidating concrete beams. The predicted losses were 1.86 to 2.75 times higher than the measured values [11].

Similarly, Starks concluded that the addition of Type K cement reduced creep by about half, and the expansive BCSA cement almost completely offset the creep strain. Starks found that the expansion of both the Type K and expansive BCSA cement could offset prestress losses in post-tensioned slabs. Furthermore, the expansive BCSA induced enough chemical prestressing that reduced strand stressing may be possible for prestressed members which use this type of cement, although additional research is needed [12].

2.2.3.1.2. Bond and Development Length of Prestressing Strand

Roswurm further evaluated implications of BCSA cement concrete in prestressing applications by studying strand pullout and embedment lengths. Large block pullout tests completed in the study indicated that bond strength between the concrete and prestressing strand developed quickly. At 3 hours of age, the experimental pullout capacity surpassed the recommended first slip threshold. The peak pullout capacity threshold was met between 1 and 28 days. At one year, the pullout strength was sufficient to achieve the full strength of the prestressing strand, evidenced by 4 out of 6 prestressing strands fracturing during testing. When normalized by compressive strength, the pullout test results suggested that the bond was increased at later ages by the concrete strength gain, rather than by a time-dependent bond mechanism [11].

Furthermore, the development length of the prestressing strands in the study by Roswurm was found to be significantly lower than predicted by the ACI 318 and AASHTO LRFD equations. The experimental development length was found to be 3.5 ft at most, while empirical methods predicted a much higher value of 7.5 ft [11].

2.2.3.1.3. CSA Cement Concrete as a Repair Material

Due to the prevalence of aging concrete infrastructure, concrete repair materials are in increasing demand. The rapid strength gaining and/or shrinkage compensating behavior of CSA cement concrete, combined with the environmental benefits, have led to increased interest in the use of CSA cement concrete as a repair material. The use of rapid-setting CSA cements can reduce the duration of road closures, and shrinkage compensating CSA cements can reduce drying shrinkage, improving dimensional stability and potentially reducing stress at the bond interface [13]. Previous studies by Wirkman and Choate evaluated a fiber reinforced self-consolidating concrete (FR-SCC) repair material containing Type K CSA cement [13], [14].

Wirkman evaluated the performance of FR-SCC as a repair material through bond strength testing and large-scale beam repair specimens. Slant shear testing was done to evaluate the bond strength between conventional concrete and FR-SCC. Two FR-SCC mixes were evaluated, one containing a 10% replacement with Type K cement, and the other containing a 15% replacement. The FR-SCC mix with a 15% CSA cement replacement ratio exhibited a greater average bond strength to the conventional concrete when compared to the 10% replacement mix. Additionally, the flexural strength of large-scale beams repaired with the FR-SCC was “statistically equivalent” to the flexural strength of monolithic conventional concrete beams [13].

Choate expanded on the research done by Wirkman, evaluating the performance of prestressed concrete girders which were shear tested to failure and repaired with FR-SCC. The repaired girders achieved approximately 80% of the original strength and 175% of the required capacity. Furthermore, the girder repaired with FR-SCC experienced a more ductile failure than the original, non-damaged beam, and exhibited no signs of bond failure of the repair concrete [14].

2.2.3.2. Mechanical Challenges of CSA Cement

While many components of CSA cement concrete lead to mechanical benefits, there are also a few challenges that must be considered, namely strength loss at later ages (Section 2.2.3.2.1), modulus of elasticity implications (Section 2.2.3.2.2), and concrete carbonation (Section 2.2.4).

Another challenge regarding CSA cement concrete that cannot be ignored is the less established understanding of mechanical behavior. CSA cement, due to its relatively newer implementation, has not been studied as much as OPC concrete. With less available data on CSA cement concrete performance, there is also a risk associated with applying empirical equations developed for OPC concrete to CSA cement concrete. Research such as the studies completed by Roswurm and Starks indicate that flexural strength, modulus of elasticity, time-dependent losses, and

development length are not accurately predicted by current models [11], [12]. While in some cases, CSA cement concretes may actually perform better than suggested by empirical models, these predictions may not always result in conservative design. For example, an overestimation of prestress losses can result in excess camber. In addition, some designs hinge on a higher concrete stiffness, while others necessitate more flexibility. Therefore, while the modulus of elasticity of CSA cement concrete is not inherently bad, the lack of predictability is an issue in cases where this property is a pertinent factor in design decisions.

2.2.3.2.1. Strength Loss of CSA Cement Concrete

While rapid ettringite formation in CSA cement concrete promotes early strength gain, research suggests that this hydration mechanism can also cause deterioration of the pore structure, which may lead to compressive strength loss at later ages. Previous studies such as by Long et al. suggest that this strength loss behavior can be combatted by using blends of CSA and OPC cements [15].

In addition to the literature showing compressive strength losses of CSA cement concretes at later ages, trends of flexural strength loss over time have been observed as well. A study by Roswurm found that the majority of flexural strength for a rapid setting BCSA cement concrete mix was developed within the first 24 hours. Between the 24 hour and 28 day Modulus of Rupture (MOR) testing, the flexural strength of the material decreased [11]. Similarly, a study by Starks noted flexural strength loss in an expansive Belitic CSA (BCSA) cement at later ages, potentially due to microcracking that occurred after the wet curing period ended [12].

2.2.3.2.2. Modulus of Elasticity of CSA Cement Concrete

The use of CSA cements also may affect the modulus of elasticity (MOE) of concrete compared to OPC. Roswurm discovered a highly linear relationship between

compressive strength and static MOE for a non-expansive BSCA cement concrete. For OPC concrete, MOE is taken as a function of the square root of compressive strength, rather than a linear relationship. This discrepancy suggests that the alternate hydration mechanisms of CSA cements likely impact concrete stiffness differently than the hydration mechanisms of OPC. While Roswurm found that the MOE of the BCSA cement concrete generally increased over time, when normalized by the compressive strength and the square root of the compressive strength, the MOE decreased relative to the compressive strength at later ages [11].

Starks noted a similar linear trend and reduced normalized MOE over time for both expansive BCSA cement and Type K cement concretes. Starks also found that the expansive BCSA cement and the Type K cement concrete both had a lower static MOE compared to the non-expansive BCSA cement concrete in the study by Roswurm and the ACI prediction equations [12], [11]. Starks concluded that the lower MOE of the expansive BCSA and Type K mixes was likely due to the reduced matrix density of expansive concrete mixes [12].

2.2.4. Durability of CSA Cement Concrete

In addition to strength considerations, material durability is of concern for concrete structures, especially when examining environmental and monetary costs. Materials with poor durability potentially require more frequent replacement, which may offset any greenhouse gas emission or monetary savings. Furthermore, according to the Federal Highway Association, repair or replacement is needed in 150,000, or 25%, of the 600,000 bridges in the United States [16]. As deliquent condition is an imminent concern in transportation infrastructure, extending service life of current and future infrastructure is vital in reducing this statistic.

Due to differences in physical and chemical composition, concrete mix designs can vary greatly in durability to various environmental exposure conditions. In general, the literature available on CSA cements suggests adequate durability. The unique

hydration mechanisms of CSA cement yield a matrix with low porosity and permeability, which generally aids in the durability of the material, as the concrete is less penetrable by water and other potentially adverse chemicals [5]. Conclusions by some researchers suggest that this cement matrix structure aids in chloride ion penetration resistance of CSA cements, although a definitive statement cannot be made, as other published literature suggests that CSA cements are more vulnerable to chloride ion penetration [5].

Another concern regarding the durability of CSA cement concrete is that carbonation occurs faster than in OPC concrete due to the absence of portlandite in CSA cement, which serves as a buffer against carbonation in OPC concrete [17]. Carbonation can affect concrete properties such as strength, porosity, pore size distribution, and chemical composition. Additionally, carbonation reduces the pH of concrete, and the pH of CSA cement concrete already tends to be more acidic than OPC concrete. Ordinarily, concrete cover protects steel from oxidation, in part by creating a ferrous oxide film on the surface of the steel. This film forms in highly alkaline conditions (pH > 12) typically present within the concrete matrix, a process known as passivation. However, as carbonation reduces the pH of concrete over time, a more acidic environment can disrupt the protective layer on the steel reinforcenment, making it vulnerable to corrosion. Metals retain a protective barrier against corrosion until the pH is reduced to below the depassivation threshold of the material, which is 9.5 for reinforcing steel. Carbonation can cause the pH of concrete to fall below the depassivation threshold of the reinforcing steel, after which corrosion is a concern if the steel is exposed to water and oxygen [18].

Conversely, CSA cement has proven to be extremely resistant to sulfate attack, showing a promising future in wastewater applications. CSA cement is somewhat unique in its durability against sulfate exposure, compared to other types of cement. CSA cement is already high in sulfate, which limits the number of ions available to react with additional sulfate ions. Additionally, CSA cements do not contain an excess of other constituents that react with sulfate, e.g. lime and aluminates [5].

2.2.4.1. Freeze-Thaw Resistance of CSA Cement Concrete

Freeze-thaw conditions are a common exposure category for concrete structures, as these temperature cycles are naturally-ocurring in many regions. Freeze-thaw damage occurs when moisture penetrates the concrete and freezes. Because water expands when it freezes, internal tensile forces are introduced. Consequently, as concrete is relatively weak in tension, these internal forces can cause significant damage, especially after repeated exposure [19]. Environmental and material properties affect the extent of this damage. For example, moisture, minimum temperature, and rate of temperature change are all environmental factors that impact the harshness of freeze-thaw exposure. Increased moisture, decreased temperature, and a slower rate of freezing are considered to exacerbate concrete freeze-thaw damage [20].

In the laboratory, concrete freeze-thaw conditions are simulated in a chamber which alternates between heating and cooling the specimens. This process in outlined in ASTM C666. To evaluate the effect of the freeze-thaw exposure on the concrete specimens, testing to determing the resonant frequency is performed incrementally following ASTM C215 procedures. Changes to the resonant frequency indicate an alteration in dynamic behavior of the specimen. A reduction in resonant frequency after freeze-thaw exposure can indicate damage to the specimen. For example, microcracking due to freeze-thaw conditions increases damping within the specimen, and conversely the resonant frequency decreases. Similarly, cracking impedes the travel of waves through the specimen, causing them to move more slowly, which also reduces the resonant frequency. Therefore, a reduction in the resonant frequency of a freeze-thaw specimen is indicative of deterioration [21].

Wang et al. also describe concrete properties that can affect freeze-thaw resistance. Water- cement ratio (w/c), aggregate properties, additives, and the air-void system impact durability. These material properties are all heavily related to the concrete pore structure, which most heavily dictates the performance of a concrete exposed to freeze-thaw conditions. More specifically, high w/c ratios decrease density and thus, reduce freeze-thaw durability. Similarly, aggregates with poor gradation

reduce freeze-thaw druability by facilitating larger pore sizes in the concrete. Aggregate moisture content is also relevant to concrete freeze-thaw durability. The inclusion of aggregates with a high moisture content increases the degree of saturation of the concrete, thus increasing vulnerability to freeze-thaw conditions [20].

The most relevant factor of concrete freeze-thaw durability is air content. In order for a concrete material to withstand the expansion of water during freezing and reduce internal tensile forces and correlated cracking, there must be an adequate quanity, size, and distribution of air voids. Previous research suggests that a spacing factor of 0.20 mm (7.87×10^{-3} in.) and air content of 3-6% greatly improve the ability of concrete materials to withstand internal cracking caused by freeze-thaw conditions [20]. Pores in hardened concrete are classified into 3 categories based on diameter: gel pores (1-10 nm), capillary pores (10 nm-500 μm), and air bubbles (> 500 μm). This pore size plays an important role in the interaction between freezing water and the cement matrix. Capillary pores are considered to be the most detrimental to concrete exposed to freeze-thaw conditions. Gel pore water will not freeze, as water molecules attach to the surface of the hydrated cement matrix. Conversely, large air bubble pores, are also not as vulnerable to freeze-thaw damage, as it is difficult for the larger pores to become saturated in standard pressure conditions. Furthermore, these air bubble pores are actually beneficial for freeze-thaw durability, as water begins freezing in the larger pores first, drawing water out of the smaller capillary pores, which are more likely to cause damage to the matrix when frozen [20].

Air entraining admixtures function in accordance with these observed pore size behaviors. These admixtures can be incorperated in order to reduce the internal pressure in the concrete when water freezes. Air entrainment promotes the formation of micropores rather than microcapilaries, which allow more room for expansion [20].

The low porosity and permeability, as well as the high early strength from ettringite formation, are beneficial for freeze-thaw durability of concrete made with CSA cement because water cannot penetrate the material as easily. Lower saturation of the concrete reduces internal tensile forces from the freezing of water. Addditionally higher

strengths may reduce susceptibility to cracking, suggesting that CSA cement concretes could be resistant to freeze-thaw damage at earlier ages [5]. Research by Qin et al. and Li et al. evaluated freeze-thaw durability of OPC-CSA cement blends. Their findings support the early age freeze-thaw resistance of CSA cements, even when used for less than 20% of the overall cementitious materials. The studies showed that the inclusion of CSA cement resulted in improved strength at early ages, and in some concentrations, a more favorable pore structure/microstructure [22], [23]. These studies also discovered that the reduction in compressive strength due to early age frost damage was completely migated by the incorporation of 20% CSA cement at -5°C [22], [23], and was reduced by 80% at exposure temperatures of -15°C [23].

Air entraining admixtures, however, may impact other concrete properties, such as viscosity, which is of notable concern in self-consolidating concrete. Air entraining admixtures can reduce the viscosity of concrete, and self-consolidating concretes are especially sensitive to this viscosity reduction. Adequate viscosity is necessary to prevent segregation of the paste and aggregate. Furthermore, a lack of cohesion can affect the air-void system, reducing frost resistance. Research by Khayat suggests that while these vulnerabilities exist, proper air-entrainment of self-consolidating concrete is possible [24].

In field applications, there are even more factors affecting concrete freeze-thaw performance, including abrasion and exposure to de-icing salts. A study by Su et al. on OPC concrete found that the combination of abrasion and freeze-thaw exposure caused accelerated deterioration in the adhesion of repair specimens. The researchers concluded that as the surface of the concrete was abraded, the pore structure was damaged, and the overlay concrete was more easily penetrable. Consequently, moisture could reach the interface area more easily, where freezing would negatively affect the bond strength between the base and overlay concrete [25]. Their finding is relevant to many concrete applications, including repairs done in the transportation sector.

2.2.4.2. Resistance of CSA Cement Concrete to De-Icing Salts

In conjunction with freeze-thaw durability of concrete in freezing regions, the resistance to de-icing salts must be considered in transportation applications. De-icing salts improve roadway safety, but can also be corrosive to the infrastructure. Chloride ions can cause corrosion of steel reinforcement, which can have adverse effects on structural capacity. There is conflicting research on the performance of CSA cement concrete in chloride-rich environments. Chloride ion penetration through concrete is dependent on both the tortuosity and binding capacity of the material [26].

Tortuosity is dependent on the pore structure of the cement matrix and indicates the complexity of the path of a fluid through the concrete. Higher tortuosity is a likely indicator of better chloride ion resistance, as the fluid containing the chloride ions will take a less direct path when penetrating the concrete. CSA cement matrices tend to have a lower porosity and permeability when compared to OPC matrices [26]. However, a study by Alapati et al. found that the high-belite CSA cement used in their study had a more porous matrix [27]. The pore structure of CSA cement matrices is highly dependent on ettringite formation, which is affected by other factors, namely the sulfate content of the cement [5]. Thus, the pore structure, and consquently, the tortuosity of CSA cement matrices likely varies based on cement composition. Lower porosity and permeability generally lead to higher tortuosity, as the matrix has fewer pores and the pores are less interconnected, increasing the complexity of the path through the material [26].

Binding capacity reduces chloride ion vulnerability of reinforced concrete because ions bound to the cement matrix are prevented from reaching and deteriorating the steel reinforcement. In OPC matrices, binding capacity is dictated by ion exchange with themonosulfate (AFm) and adsorption by the C-S-H gel. AFm dictates the binding capacity of CSA cements as well. However, in CSA cements, the inclusion of gypsum supplies sulfate ions, which inhibits the formation of AFm, as tri-calium aluminate (C_3A) more readily bonds with sulfate ions to form ettringite (AFt) than with chloride ions, which reduces the ability of the cement matrix to bind chloride ions [26], [28].

The reduced presence of themosulfate (AFm) in hydrated CSA cements causes a consquent reduction in binding capacity, and thus a potention vulnerability to chloride ion penetration [26]. The binding capacity of concrete is also impacted by the pH of the material, chloride ion concentration, C_3A concentration, and alkali and sulfate concentration [28]. CSA cement concretes have generally have reduced alkalinity and lower pH, factors which are known to protect steel reinforcement in OPC [17].

It is possible that some of the discrepencies in available research on chloride resistance of CSA cement is due to the interrelated effects of chemical composition of the cement on the tortuosity and binding capacity. For example, some factors such as sulfate ion concentrationn inversely affect tortuosity and binding capacity. The chloride resistance of some CSA cements may be dominated by increased tortuosity due to ettringite formation promoted by the presence of sulfate ions, while the resistance of other CSA cement blends may be dominated by the reduced binding capcity caused by sulfate ion presence.

Ghafoori et al. evaluated the de-icing salt resistance of three high early-strength (HES) concrete mixes, which varied by cement type. The three cement types evaluated in their study were ASTM Type III, ASTM Type V, and CSA. The study indicated that while the mix with CSA cement gained strength the quickest, it had the lowest ultimate strength and was the most vulnerable to deterioration from de-icing salts. For the specimens that were cured for 24 hours before exposure to 25 F-T cycles, the mass of the CSA cement concrete was reduced by 33%, whereas the mass of the Type III and Type IV cement specimens was reduced by only 5% and 3%, respectively. For all three types of cement, the resistance to de-icing salt was higher when the concrete was cured for longer before exposure [29]. This study indicates that CSA cement concretes used for rapid infrastructure repair may be particularly vulnerable to de-icing salt exposure, especially when exposure occurs at an early age.

Shaji et al. researched the resistivity of CSA cement concrete to penetration of chloride ions using other test methods, including surface resistivity measurements, chloride migration, rapid chloride penetration, long-term bulk diffusion, and water

sorptivity. The results of their study indicated that the pore structure of CSA cement matrices can be beneficial against chloride ion penetration while the reduced binding capacity is detrimental. The researchers also cautioned that typical measures of chloride ion penetration must be interpreted with caution for CSA cements. Increased conductivity of the pore solution in CSA cements may falsely inflate the experimental resistivity, and that accelerated research tests may not be the most accurate indicator of CSA cement performance in chloride environments [26].

2.3. Analysis of Supplementary Cementitious Materials

Another method of reducing greenhouse gas emissions in concrete production is by using supplementary cementitious materials (SCMs) to reduce the required quantity of cement. Two such materials are fly ash and ground granulated blast furnace slag (GGBFS).

Fly ash is a fine powder that is a byproduct of coal combustion. It can be used in place of a portion of the portland cement in a concrete mix design. Studies have been conducted on various replacement ratios, but the typical maximum substitution is 15-25%. In addition to reducing concrete CO_2 emissions, fly ash can also provide certain mechanical benefits, including increased workability, reduced suscepability to segregation, and decreased permeability. According to previous studies, fly ash does not significantly affect the freeze-thaw durability of concrete, so long as the strength and air content are kept constant. However, fly ash has been shown to reduce the effectiveness of air-entraining admixtures, which may indirectly introduce challenges with freeze-thaw durability [30].

GGBFS is created from the quenching of molten blast furnace slag. In general, up to 50% of cement can be replaced by GGBFS in applications where there is no exposure to deicing salts, and up to 25% if there will be deicing salt exposure. The benefits of GGBFS as a SCM include increased set time, higher flexural strength, and stronger bonds within the concrete matrix. Due to its fine particle size, GGBFS can also

help to reduce the permeability of concrete. Despite reducing permeability, previous studies suggest that GGBFS does not yield freeze-thaw resistance that is significantly different from that of concrete containing no GGBFS. The freeze-thaw durability of concrete with GGBFS may also be affected by the fineness of the material, which necessitates higher dosages of air-entraining admixture. Additionally, GGBFS does not contain carbon, which can lead to loss of air in concrete [30].

Sakai et al. [31] examined both the environmental and mechanical properties of concrete mix designs using fly ash and GGBFS replacement. Their quantification of unit CO_2 emissions from OPC, fly ash, and ground granulated blast furnace slag are summarized in Table 2. Notably, the CO_2 emissions from fly ash and and GGBFS are only 2.3% and 3.5%, repectively, of the CO_2 emissions from OPC.

Table 2: Quantification of CO_2 Emissions for Supplementary Cementitious Materials [31]

OPC (tCO_2/tCement)	Fly Ash (tCO_2/tCement)	GGBFS (tCO_2/tCement)
0.766	0.018	0.026

However, these supplementary cementitious materials cannot completely replace the OPC in a concrete mix design, so the actual reduction in CO_2 emissions is proportional to the replacement percentage. The reasearch done by Sakai et al. [31] evaluated the mechanical performance and CO_2 emissions for concrete mixtures with 0, 10, and 20% fly ash replacement and 0, 10, 20, 30, and 40% GGBFS replacement. A graph of the CO_2 emissions for each supplementary cementitious material combination can be found in Figure 2.

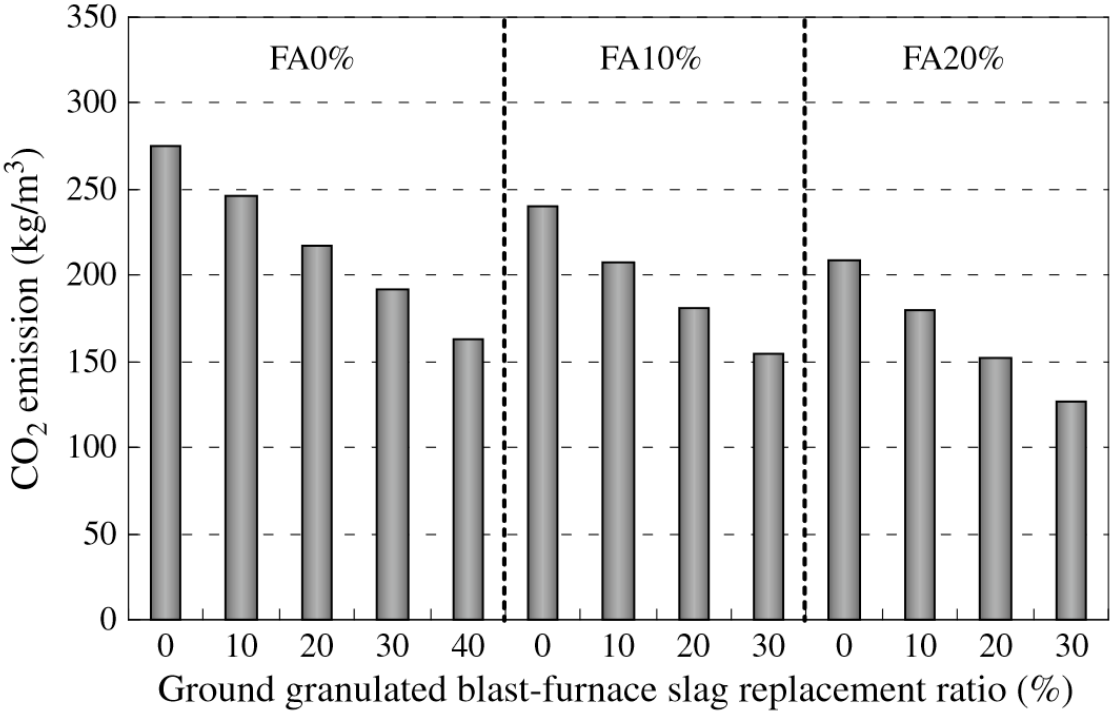


Figure 2: CO_2 Emissions for Concrete with Supplementary Cementitious Materials [31]

In addition to impacting CO_2 emissions, utilizing fly ash and GGBFS as supplementary cementitious materials changed the mechanical properties of the concrete. With higher ratios of fly ash and GGBFS, less water was required due to the spherical shape of the fly ash particles, which increases flowability of the concrete, and the higher specific surface of the fly ash and GGBFS particles. Conversely, increased fly ash replacement necessitated higher quantities of air entraining admixture. In terms of strength, fly ash and GGBFS replacement resulted in a lower compressive strength at early ages, when compared to the mix design that used 100% OPC. The later age compressive strength values differed in whether they were higher or lower than that of the 0% replacement mix. Figure 3 from Sakai et al. [31] compiles the compressive strength data from their study.

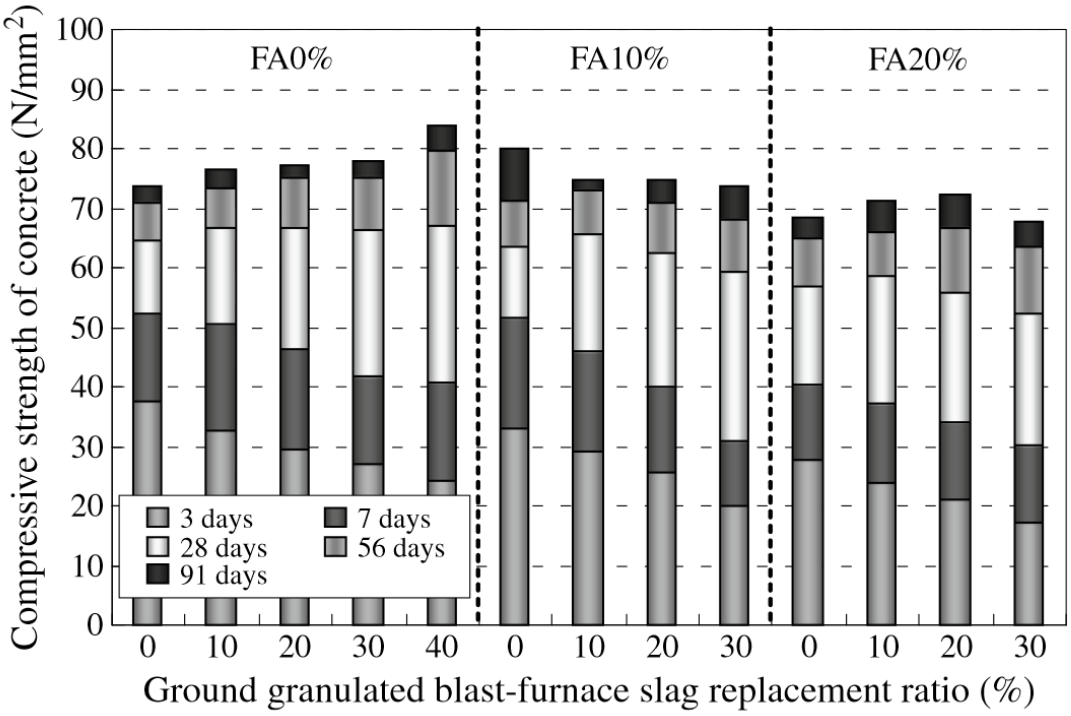


Figure 3: Compressive Strength Data for Fly Ash and GGBFS Replacement Ratios [31]

2.4. Aspects for Future Research

The rapid strength gaining and shrinkage compensating properties, as well as the environmental advantages of calcium sulfoaluminate cement concrete offer promising benefits in infrastructure repair applications. Existing research covers the hydration mechanism, mechanical performance, and durability of CSA cement concrete. However, there is limited literature available on bond behavior between CSA cement concrete and conventional portland cement concrete. As portland cement concrete is widely used, and infrastructure repair is in increasing demand, understanding the bond behavior of CSA cement repair materials is a pertinent topic. Additional research into the bond strength and freeze-thaw resistance of CSA cement concrete as a repair material is needed to evaluate performance and establish best practices.

Chapter 3. Materials and Methodologies

This study consisted of three main components: specimen fabrication, small-scale testing, and large-scale testing. The specimen preparation and small scale testing were completed first in order to evaluate which mix(es) and surface preparation technique(s) demonstrate the most potential to perform well in field applications. All small scale specimens were cast in two layers, consisting of an Oklahoma Department of Transportation (ODOT) Class AA superstructure concrete substrate and a CSA cement based concrete repair material. The surface of each conventional concrete base was prepared with one of four techniques: exposed aggregate, chipping hammer, sandblasted, or sandblasted with surface moistening.

For each repair material/surface preparation combination, one pull-off specimen yielding 5 cores for testing and two freeze-thaw specimens were fabricated. The overall dimensions of the small-scale pull-off test specimens were 14 in. (L) x 14 in. (W) x 3.5 in. (D), with a conventional concrete base thickness of 2 in. and an overlay thickness of 1.5 in. The overall dimensions of the small scale freeze-thaw testing specimens were 15.25 in. (L) x 4 in. (W) x 4 in. (D), with a 2 in. depth of conventional concrete and a 2 in. depth of overlay material. The large-scale repair specimens consisted of chipping hammer and chipping hammer plus sandblasted surface preparations with RS-SCC and FR-SCC repair materials. The repair sections were 46 in. (L) x 6 in. (W) x 4 in. (D).

3.1. Specimen Preparation

3.1.1. Mix Designs

The small scale pull-off and freeze-thaw specimens were cast in two layers. The bottom layer of the specimens was a conventional concrete mix developed at the University of Oklahoma that follows the specifications for ODOT Class AA superstructure concrete [32]. Four different concrete mixes were cast as an overlay to be evaluated for use as a repair material. These mixes were a rapid-setting self-

consolidating concrete (RS-SCC), rapid-setting self-consolidating concrete with a higher coarse aggregate content (RS-SCCHA), fiber-reinforced self-consolidating concrete (FR-SCC), and a rapid-setting self-consolidating concrete mix developed at the University of Arkansas (RS-SCCUA). All rapid setting repair material mixes utilized belitic calcium sulfoaluminate (BCSA) cement, with some also including supplementary cementitious materials. The FR-SCC mix included a combination of OPC and Type K cement, to reduce enviromental impact and provide shrinkage compensating behavior.

References to individual concrete batches will be shortened with a two letter code to indicate the type of concrete and a digit to represent the batch number. Class AA will be represented with “AA”; FR-SCC will be represented with “FR”; RS-SCC will be represented with “RS”; RS-SCCHA will be represented with “HA”; and RS-SCCUA will be represented with “UA”. Some mix names will also include an “X” following the batch number, which indicates that the material was not used to cast specimens. Table 3 below summarizes the completed mixes the corresponding specimens that were cast, if applicable.

Table 3: Summary of Mixes and Corresponding Specimens

Mix Name	Date	Specimens Cast
AA-1	3/29/2024	Monolithic Pull-Off Specimen Bases for RS-SCC Pull-Off Specimens
AA-2X	5/22/2024	Concrete Was Not Used for Testing
AA-3	5/28/2024	Bases for RS-SCCHA Composite Pull-Off Specimens Bases for RS-SCCHA Composite F-T Specimens
AA-4X	6/4/2024	Trial Batch for Exposed Aggregate Technique
AA-5	6/12/2024	Bases for FR-SCC Composite Pull-Off Specimens Bases for FR-SCC Composite F-T Specimens
AA-6X	7/3/2024	Extra Set of Bases for Composite Specimens (Were Not Used for Testing)

Mix Name	Date	Specimens Cast
AA-7	7/23/2024	Bases for RS-SCCUA Composite Pull-Off Specimens
FR-1X	10/23/2024	Trial Batch
FR-2	11/8/2024	Overlays for Composite Pull-Off Specimens Overlays for Composite F-T Specimens
FR-3	4/3/2025	Monolithic Pull-Off Specimen Overlays for Bridge Repair F-T Specimens Large-Scale Repair Slab
RS-1	3/7/2024	Monolithic Pull-Off Specimens (7 and 28 Day)
RS-2	4/26/2024	Overlays for Composite Pull-Off Specimens Monolithic F-T Specimens (7 and 28 Day)
RS-3	2/11/2025	Large Scale Repair Slab
HA-1X	8/27/2024	Trial Batch
HA-2	9/17/2024	Overlays for Composite Pull-Off Specimens Overlays for Composite F-T Specimens
HA-3	3/7/2025	Overlays for Bridge Repair F-T Specimens
HA-4	4/15/2025	Monolithic Pull-Off Specimen Monolithic F-T Specimens
UA-1	1/22/2025	Monolithic Pull-Off Specimen Monolithic F-T Specimens
UA-2	5/13/2025	Overlays for Composite Pull-Off Specimens

The type and nominal maximum size (NMS) of coarse aggregate varied by mix design. The types of coarse aggregates used were ¾ in. NMS limestone (Class AA), ⅝ in. NMS limestone chip (RS-SCC, RS-SCCHA, RS-SCCUA), and ⅜ in. NMS river rock (FR-SCC). The fine aggregate in all mixes was washed river sand. Additional material information is available in Table 4, and mix proportions are presented in Table 5. Note that the dosages of High-Range Water Reducer (HRWR) and Air Entraining Admixture

presented in Table 5 represent the baseline dosage for the mix design. The dosages used in each mix, as well as any adjustments to mixing water proportions, are presented in Table 10 through Table 14, found in Appendix A.

As indicated in the mix designs, the Class AA and FR-SCC mixes are the only to include entrained air. Therefore, freeze-thaw performance of the RS-SCC, RS-SCCHA, and RS-SCCUA (discussed in Sections 3.2.2 and 4.2) represents a worst-case scenario condition.

Table 4: Material Sources

Constituent	Name/Manufacturer
Type IL Portland Limestone Cement	Ash Grove Sourced from Dolese
BCSA Cement	Rapid Set® CTS Cement Manufacturing Corp.
Type K Cement	Komponent® CTS Cement Manufacturing Corp.
Fly Ash	Class C Fly Ash Eco Material Technologies
Polypropylene Fibers	MAC Matrix 2.1 in. Polypropylene Fibers BASF MasterFiber®
High-Range Water Reducer (HRWR)	MasterGlenium 7920 Master Builders
Air Entraining Admixture	AE-90 Master Builders

Table 5: Summary of Mix Designs

Material	Class AA	RS-SCC	RS-SCCHA	FR-SCC	RS-SCCUA
Type I/II Portland Cement (lb/yd^3)	588	0	0	413	0
BCSA Cement (lb/yd^3)	0	752	752	0	792
Type K Cement (lb/yd^3)	0	0	0	113	0
Fly Ash (lb/yd^3)	0	151	151	225	0
Coarse Aggregate (lb/yd^3)	1831	944	1226	1282	1400
Fine Aggregate (lb/yd^3)	1293	1789	1476	1391	1250
Water (lb/yd^3)	211	284	320	196	380
Polypropylene Fibers (lb/yd^3)	0	0	0	7.7	0
HRWR (oz./cwt)	3.5	8	8	8.25	4
Air Entrainer (oz./cwt)	0.7	0	0	1.1	0
Citric Acid (lb./cwt)	0	0.2	0.4	0.05	0.2

3.1.2. Mixing, Casting, and Curing of Class AA Concrete

The Class AA bases for each specimen were cast first. The mix design and procedure for the conventional concrete was from Coleman [33] and was as follows:

1) Add air entraining admixture evenly to the sand;
2) Add coarse aggregate and fine aggregate to the mixer with half of the mixing water and allow to mix for at least two minutes;
3) Mix half of the HRWR with the remaining half of the mixing water;
4) Add the cement to the mixer;
5) Slowly add the remaining mixing water containing half of the HRWR;
6) Slowly add the remaining HRWR;
7) Allow to mix for at least three minutes;
8) Add extra HRWR as necessary to achieve the desired slump, and allow to mix for at least one minute after each addition.

Slump tests were conducted in accordance with ASTM C143 [34] before discharging the material from the mixer. The target slump for the Class AA conventional concrete was 3-6 in. After discharging the material, an air content test was performed in accordance with ASTM C138 [35]. The targeted range for the concrete air content was 4.0-6.0%, however the measured air contents of the batches used to cast specimens ranged from 4.1-7.0%. The fresh properties and compressive strength data of all Class AA concrete mixes are detailed in Table 10 and Table 15, respectively.

Twelve 4 in. x 8 in. compressive strength cylinders were cast for each batch. Casting procedures followed those outlined in ASTM C192 [36]. Four pull-off base specimens with a 2 in. depth and eight freeze-thaw specimens with a 2 in. depth were

cast using each batch of Class AA conventional concrete. For ease of placement and to ensure proper concrete depth within the molds, the inside of the pull-off base specimen forms were marked with a line at the correct level, and a jig was used for measuring depth of the freeze-thaw specimens. All of the conventional concrete specimens were consolidated using a vibratory table. The exposed aggregate surface preparation was performed as described in Section 3.1.3 at the time of casting. After casting, the specimens were placed in a temperature controlled room at 68°F. When the surfaces were firm to the touch, the specimens were covered with wet burlap and plastic. The specimens were then left to cure for 72 hours. Following the initial 72 hour curing period, the specimens were demolded and stored in the same temperature controlled environment.

3.1.3. Surface Preparation

For each of the four repair materials, four surface preparations of the Class AA conventional concrete substrate were evaluated: exposed aggregate (EA), chipping hammer (CH), sand blasted with a dry surface (SB-D), and sand blasted with a moistened surface (SB-MS). The exposed aggregate finish was created at the time of the Class AA concrete casting. The other three surface preparations were performed after the base concrete had cured for at least 28 days. Consistency in execution of the surface preparation techniques was prioritized to allow for relevant comparison between repair specimens. However, the preparation techniques and resulting surfaces were not necessarily done in accordance with the International Concrete Repair Institute (ICRI) guidelines. Future research should expand upon the surface preparation conclusions made in this study with the objective of developing recommendations which meet the ICRI requirements.

Trials were done to evaluate the most effective method for achieving an exposed aggregate finish on the base concrete. In the trial, sugar and Coca-Cola® were tested as surface set retarders and removal of the concrete paste was attempted at both 4-6

hours and 24 hours. The exposed aggregate trial determined that the Coca-Cola® and a 4-6 hour paste removal timeframe was the most effective method. Thus, the exposed aggregate surface was achieved by generously misting the surface of the Class AA concrete with Coca-Cola® while the concrete was still wet. The surface was completely covered with a thin layer of Coca-Cola®. Subsequent mistings were performed as needed to keep the surface moist with Coca-Cola®. After 4-6 hours, when the Class AA concrete was firm enough to remove from the forms without damage, the exposed aggregate base specimens were removed from the forms, and the top layer of paste was removed by gently spraying the specimen with a water hose. Figure 4 (a) shows a defined layer of unset paste from the Coca-Cola® in the exposed aggregate trial. Figure 4 (b) shows a freeze-thaw specimen with the exposed aggregate finish. The exposed aggregate specimens were also lightly sandblasted to remove any remaining concrete that stuck to the aggregate.

3.1.4. Preparation of Small-Scale In-Service Concrete Bases

The specimen bases from in-service concrete were cut from sections taken from the I-35 over Cow Creek bridge deck after approximately 50 years in service using a concrete saw. First, the bridge deck section was cut perpendicular to the top of the deck to create a specimen with a width of 4 in. in order to match the width of the freeze-thaw specimens. Then, the deck section was rotated 90˚ and cut parallel to the deck surface at a depth of approximately 3 in. Next, the pieces were cut to a length of 15 in. Any uneven spots from the initial cuts with the concrete saw were leveled using an angle grinder with a diamond cup wheel. The surface preparation, overlay, and testing for the in-service concrete specimens followed the same procedures as all other freeze-thaw specimens. Four combinations of in-service concrete freeze-thaw specimens were fabricated to test two repair materials (RS-SCCHA and FR-SCC) and two surface preparations (CH and SB-D). Two specimens were tested for each repair material/surface preparation combination, for a total of eight specimens.



Figure 4: Visible Layer of Unset Paste (a) and Exposed Aggregate Finish (b)

The chipping hammer surface preparation was achieved by chiseling the surface of the Class AA concrete with a pneumatic hammer. In order to achieve a more consistent finish amongst specimens, a 1 in. x 1 in. grid was marked on the specimen surface. The chipping hammer was run in one direction, chiseling in between the grid lines. Then, the specimen was rotated 90° and the surface was chiseled between the grid lines in the perpendicular direction. A pull-off specimen with the chipping hammer surface preparation is shown in Figure 5 (a).

The sand blasted surfaces were prepared using the combination of a pressurized canister sandblaster, a handheld sandblasting gun, and a sand blasting cabinet, due to equiptment limitations. The surface of the Class AA concrete bases was sandblasted until the surface appeared evenly rough and the aggregate began to become visible. Figure 5 (b) provides an example of a sandblasted Class AA base for a pull-off specimen. The SB-MS specimens received additional surface preparation at the time of casting the overlay material. The base concrete surface of the SB-MS specimens was misted with water immediately before casting the overlay material. The surface was misted until the entire area was sufficiently wet, but not enough to cause water to pool.

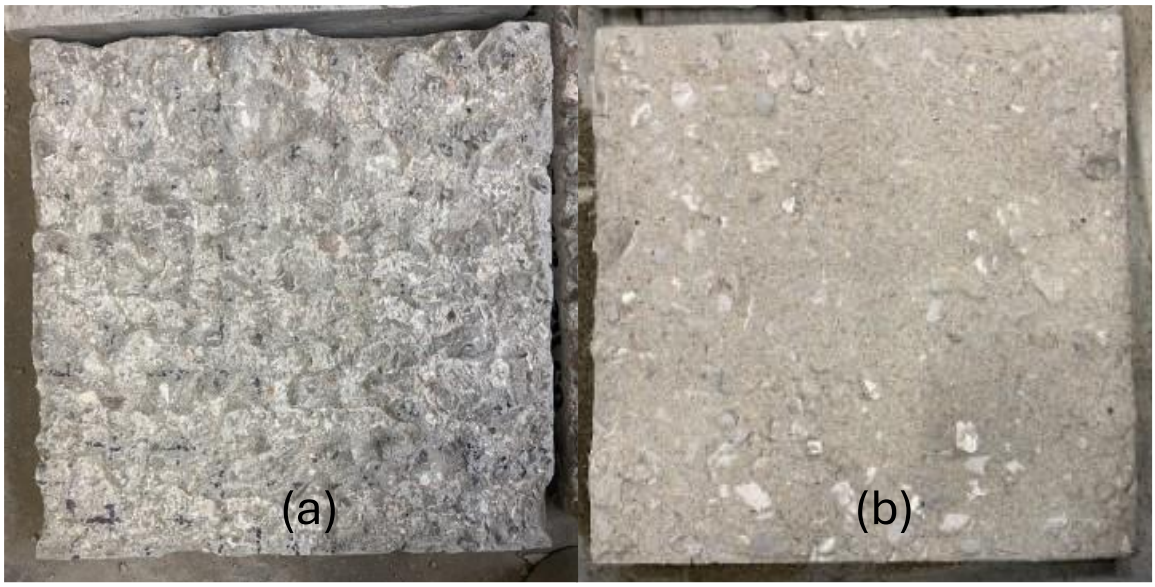


Figure 5: Chipping Hammer (a) and Sandblasted Surface Preparations (b)

3.1.5. Mixing, Casting, and Curing of Overlay Materials

The repair materials were cast onto the Class AA concrete bases after at least 28 days of curing and the completion of surface preparation. The Class AA conventional concrete bases were placed back in the forms before casting the overlays. Special care was taken to avoid contaminating the interface area with form release oil.

The mixing procedure for the repair materials differed slightly, however all of the overlays followed the same casting and curing procedures. In an effort to extend the working time of the rapid-setting materials, the specimens were cast in a 68˚F temperature controlled environment. Fifteen 4 in. x 8 in. compressive strength cylinders were cast in addition to the overlays of the pull-off and freeze-thaw specimens. Alternatively, twelve 6 in. x 12 in. compressive strength cylinders were cast for the FR-SCC mix due to the incorporation of 2.1 in. long fibers. As the repair materials were all self-consolidating, the specimens were cast in one layer. The sides of the cylinders were tapped 9-12 times by hand. The sides of the forms for the pull-off and freeze-thaw specimens were tapped at least 12 times with a rubber mallet. In some cases, as the material stiffened over time, more than 12 taps were required for adequate

consolidation. The pull-off and freeze-thaw forms were filled to the top and the surface smoothed.

The specimens were left to cure in the same temperature controlled environment in which they were cast. Once the surface of the repair material was firm to the touch, wet burlap and plastic were added to cover the surface of the specimens. The covering was removed and the specimens were demolded after 72 hours of curing.

3.1.5.1. RS-SCC and RS-SCCHA Mixing Procedure

The same procedures were followed for mixing the RS-SCC and RS-SCCHA mixes. The RS-SCC and RS-SCCHA mixing procedure was from Roswurm [11] and is as follows:

1) Add coarse aggregate and fine aggregate to the mixer;
2) Thoroughly combine all of the citric acid and half of the HRWR with the mixing water;
3) Add half of the water into the mixer with the coarse and fine aggregate and allow to mix for at least 2 minutes;
4) Add the cement and fly ash to the mixer;
5) Add the remaining water;
6) Add the remaining HRWR;
7) Allow the material to mix for at least 3 minutes from the time of the cement/fly ash addition (more time may be necessary for larger batches);
8) Add extra HRWR as necessary to increase the flow and mix for at least 1 minute following each addition.

Before discharging the material from the mixer, a slump flow test was performed in accordance with ASTM C1611 [37] to ensure adequate workability. The target slump flow for the RS-SCC and RS-SCCHA mixes was 26-30 in. An air content test was not conducted for these materials, as they do not incorporate entrained air. If the slump flow was sufficient, specimens were fabricated with the material. The fresh properties for the RS-SCC and RS-SCCHA are summarized in Table 12 and Table 13, and the compressive strength data is summarized in Table 16 and Table 17 (see Appendix A).

3.1.5.2. FR-SCC Mixing Procedure

The FR-SCC mix design was used previously in research by Wirkman [13], Choate [14], and Ahmadi [38]. The mixing procedure was from Ahmadi [38] and is as follows:

1) Divide the air entrainer evenly amongst the sand;
2) Add the coarse and fine aggregate to the mixer;
3) Add half of the water and allow to mix for at least one minute;
4) Add the ordinary portland and Komponent® cements, as well as the fly ash;
5) Add the HRWR followed by the remaining mixing water;
6) Add additional HRWR as necessary to achieve the desired flow;
7) Add the citric acid and fibers;
8) Allow the mixer to run for 3 minutes, let the concrete rest for 3 minutes, and then mix the material for an additional 2 minutes.

Before discharging the material from the mixer, a slump flow test was performed in accordance with ASTM C1611 [37] to determine workability of the concrete. The target slump flow for the FR-SCC was 26-30 in. However, the slump flow of the mixes used was lower than this range, as there were challenges with the material setting quickly. An air content test was also performed in accordance with ASTM C138 [35]. The target air content was 4-6%, however the measured air content of the FR-SCC-2 mix was 3.1%, as shown in Table 11. For the FR-SCC, larger, 6 in. x 12 in. cylinders were cast for compression testing due to the 2.1 in. long fibers in the mix. The FR-SCC fresh properties and compressive strength data are summarized in Appendix A, Table 11 and Table 19, respectively.

3.1.5.3. RS-SCCUA Mixing Procedure

The mixing procedure for the RS-SCCUA mix was informed by personal communication with Poblete [39] at the University of Arkansas. The material was mixed in accordance with the following steps:

1) Add the coarse and fine aggregate to the mixer;
2) Throughly combine the citric acid with the mixing water;
3) Add half of the water to the mixer and allow the mixer to run for at least 1 minute;
4) Add the cement immediately followed by the other half of the mixing water;
5) Add the HRWR;
6) Mix the material for 2 minutes, allow to rest for 1 minute;
7) Mix for another minute and allow to rest for 1 more minute, during which add any additional HRWR that may be needed to achieve the desired slump;
8) Mix for two additional minutes.

Before discharging the material from the mixer, a slump flow test was performed in accordance with ASTM C1611 to ensure adequate workability. The target slump flow for the RS-SCCUA mix was 23-25 in. An air content test was not conducted for this material, as it did not incorporate entrained air.

3.2. Small-Scale Testing

The small-scale testing consisted of both monolithic and composite specimens. Monolithic pull-off specimens were tested in order to determine a baseline tensile strength of each material. Similarly, monolithic freeze-thaw specimens were tested to evaluate the freeze-thaw durability of each concrete material individually. Composite pull-off and freeze-thaw specimens were used for determination of interfacial bond strength and resistance to freeze-thaw conditions, respectively. The composite specimens were comprised of Class AA concrete bases (as described in Sections 3.1.1 and 3.1.2) and an overlays for each repair material/surface preparation combination.

The pull-off and freeze-thaw testing procedures described in the following sections were followed for each set of pull-off and freeze-thaw specimens.

3.2.1. Pull-Off Testing

Pull-off testing was performed in accordance with ASTM C1583 [40]. The monolithic pull-off specimens were tested at an age of 7-days for the CSA cement repair materials. The monolithic Class AA specimen was tested at 35 days because for the composite specimens, each base was allowed to cure for at least 28 days plus an additional 7 days after the overlay was cast.

The composite pull-off tests were performed at an overlay age of 7 days. Two days before testing, or at an overlay age of 5 days, the specimens were cored in preparation. A drill press with a 2 in. diameter diamond core bit was used for coring.

Water was run during the coring process in order to cool the bit and aid in cutting. The coring depth was 2 in., which was determined based on the 1.5 in. overlay thickness and the ASTM C1583 requirement to extend at least 0.5 in. into the substrate material [40]. One composite specimen for each repair material/surface preparation combination was fabricated, with the exception of a RS-SCC/SB-MS specimen, as the SB-MS surface preparation was added after the RS-SCC pull-off specimens were cast. Thus, a total of 15 composite pull-off specimens were produced. Each specimen yielded 5 cores, 4 located a puck diameter (2 in.) from each corner of the specimen and another in the center. The layout is shown in Figure 6. After coring, the specimens were left to dry for 24 hours.

One day before testing, or at an overlay age of 6 days, the pucks for pull-off testing were affixed to the cores (see Figure 6). The pucks were 2 in. diameter and made out of steel or aluminum. Due to availability, a combination of the steel and aluminum pucks had to be used. The aluminum pucks had a different connection than the testing device and thus required the use of an adapter. In case there was any discrepency in results from the two types of pucks, they were be divided evenly by type amongst the specimens. Although, a statistically significant difference was not observed.

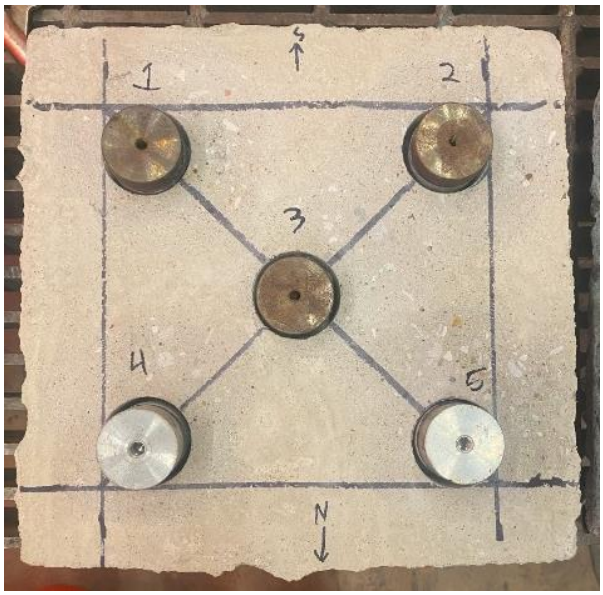


Figure 6: Pull-Off Specimen Before Testing

To help ensure a good bond to the puck, specimens with a particularly rough or uneven surface were first ground until smooth and level with a diamond cup wheel. JB Weld Steel Epoxy was mixed according to manufacturer instructions and used to adhere the pucks onto the cores, as shown in Figure 6. The epoxy was allowed to cure for 24 hours before testing, also following the direction of the manufacturer.

Pull-off testing was conducted in accordance with ATSM C1583. Figure 7 (a) provides a schematic of the testing setup. A Hydrajaws Model 2000 Fixing Tester, pictured in Figure 7 (b), was used. First, the connector that attaches the puck to the testing device was screwed into the puck until hand tight. Then, the reaction frame was placed on top of the specimen so that the hole in the center was over the connector. The three legs of the reaction frame were adjusted until it was level and flush with the connector. For some of the pucks, a thread adapter was required. When the thread adapter was required, steel plates were placed under the legs of the reaction frame so the connector and reaction frame could be level. The steel plates were necessary due to the limited length of the adjustable screws on the reaction frame and the increased height required by the use of the thread adapter.

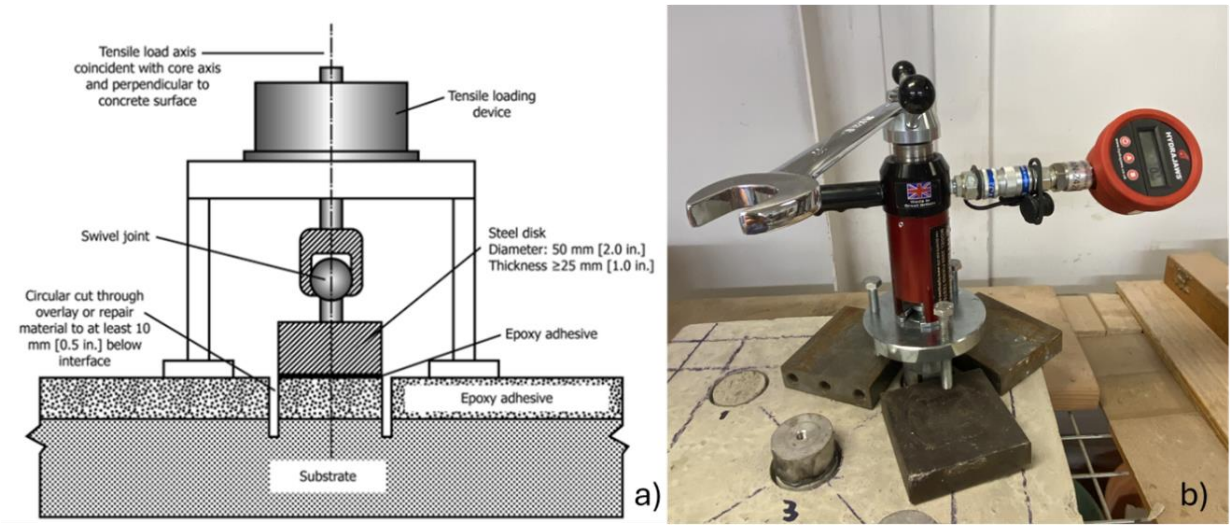


Figure 7: ASTM C1583 [40] Pull-Off Testing Schematic (a) and Testing Device (b)

The testing device was then connected and tensile load manually applied by turning a wrench. While loading, the gauge was monitored in order to apply the load at as consistent of a rate as possible. A digital gauge with a 25 lb sensitivity was used. Both the failure load and the ASTM C1583 [40] failure type were recorded.

There are four failure types included in ASTM C1583: failure in the substrate concrete (a), bond failure at the interface between the substrate and overlay concrete (b), failure in the repair concrete (c), and failure of the adhesive between the steel disk and overlay concrete (d) [40]. Only failure mode b is representative of the bond strength between the base and overlay concrete. The bond strength was calculated using Equation 1.

Failure modes a, c, and d are indicative of the tensile strength of the base concrete, the tensile strength of the repair concrete, and the tensile strength of the adhesive, respectively. The tensile strengths can also be calculated using Equation 1, but cannot be used to directly quantify the bond strength between the Class AA and repair concrete. Strength values calculated from specimens failing in modes a, c, and d can only indicate that the bond strength between the base and overlay concrete is higher than the observed value.

Equation 1: Bond or Tensile Strength of Pull-Off Specimens [40]

$$Bond\ or\ Tensile\ Strength\ [psi] = \frac{Tensile\ Load\ [lbf]}{Area\ of\ Test\ Specimen\ [in^2]}$$

3.2.2. Freeze-Thaw Testing

Freeze-thaw conditions were simulated using the ASTM C666 procedures with some modifications due to equipment limitations [41]. The intention of this study was to test two freeze-thaw specimens for each repair material/surface preparation combination (or a total of 32 specimens). However, due to equiptment limitations, only the RS-SCCHA and FR-SCC composite specimens could be tested (a total of 16 composite specimens). Four combinations of freeze-thaw specimens were fabricated with the in-service bridge deck concrete (RS-SCCHA-CH, RS-SCC-SB-D, FR-SCC-CH, and FR-SCC-SB-D) for eight additional composite specimens. Two monolithic specimens were also tested for the RS-SCC, RS-SCCHA, and RS-SCCUA repair materials (or a total of 6 monolithic specimens). Fundamental resonant frequency testing was used as an indicator of specimen condition over time. The impact resonance method, or method 2 from ASTM C215, was followed for determination of fundamental resonant frequency [42]. Initial resonant frequency readings were taken at an overlay age of 7 days in order to establish a pre-exposure frequency for each specimen.

During resonant frequency testing, the specimens were oriented such that the long sides of the rectangular prism were at the top and bottom of the testing frame, and the side containing the top surface of the overlay was pointed towards the far side of the testing frame (see Figure 8). The monolithic specimens were oriented in the same way, with the rough edge from casting pointing towards the far side of the testing frame. The middle of the specimen was measured lengthwise and marked so that the specimens could be easily aligned when placed in the testing frame. The specimens were also marked so that they would be tested in the same orientation each time. An accelerometer was placed such that it was held lighly in contact with the center of one end of the specimen. This accelerometer was connected to an Emodumeter® frequency analyzer for calculation of the resonant frequency of the specimen. In order to take a reading, the end of the specimen opposite of the accelerometer was tapped with a hardened steel ball, called an impactor. Because the readings can be sensitive to the way in which the specimens are tapped, the freeze-thaw testing was done by a single

researcher and care was taken to provide a consistent tap on each trial. The average of three trials was recorded and taken as the resonant frequency of the specimen at each testing interval.



Figure 8: Specimen Orientation for Resonant Frequency Testing

After taking the initial resonant frequency readings, the specimens were placed in water-filled metal containers in the freeze-thaw chamber. Wires were placed under the specimens to maintain a spacing of 1/8 in. from the bottom of the container. Two different freeze-thaw chambers were used for testing. The temperature of the freeze-thaw chambers cycled from 0°F to 40°F (-18°C to 4°C) and the specimens were left in the chamber for no more than 36 cycles between resonant frequency readings. The water level in the containers was also checked periodically to ensure full submersion of the specimens. Water was added as needed to replace any lost from evaporation or leaking containers.

The targeted temperature fluctuation is illustrated in Figure 9. External conditions, however, likely affected this temperature sequence, although a continuous log of specimen temperature data was not available for confirmation. One of the freeze-thaw chambers required manual operation, so the machine could not realistically be switched between freezing and thawing at exactly 0°F and 40°F. Another factor which likely affected the temperature of the specimens during freeze-thaw testing was the ambient temperature, as the machines were not located in a temperature controlled environment. Fluctuations in ambient temperatures could have affected the cycle duration, which can in turn influence the intensity of freeze-thaw effects.

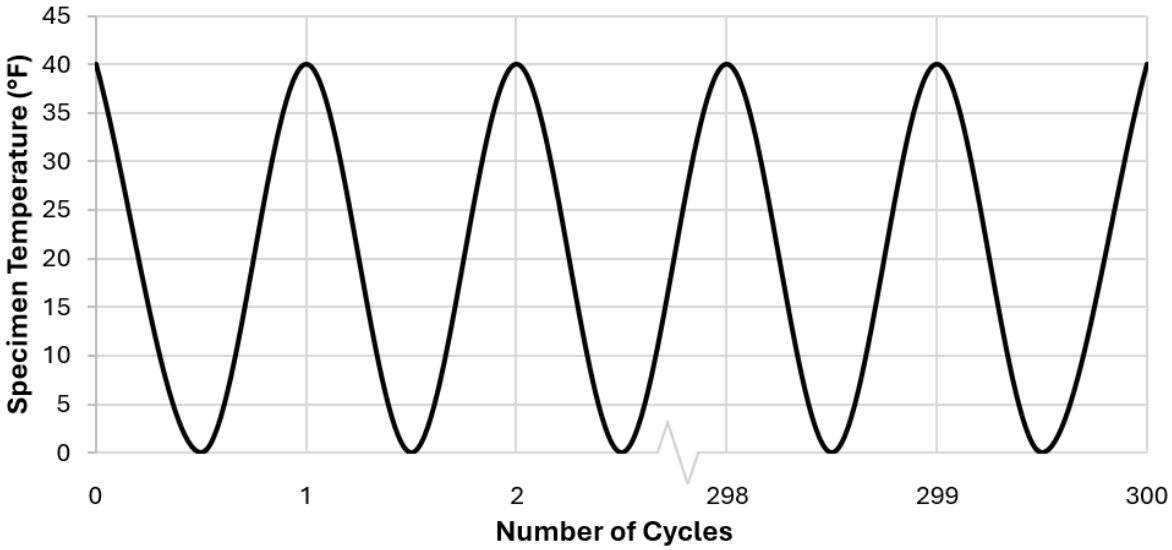


Figure 9: Target Temperature Fluctuation of Freeze-Thaw Specimens

Before resonant frequency readings were taken, the chamber was shut off and the lid left open for 24 hours so that the specimens could be tested at room temperature each time. The specimens were gently towel dried to remove excess water from the surface and were tested using the same procedure described previously. This process was repeated in increments of 36 cycles or less until the specimens had undergone 300 cycles of exposure, the repair material delaminated, or the relative dynamic modulus reached 60% of the initial value, whichever came first.

3.3. Large-Scale Repair Specimens

Once the small-scale testing was complete, the effectiveness of implementation was evaluated with conditions similar to that of a field repair, where sections of Class AA concrete slabs constructed as part of a 2018 research project were intentionally removed and then replaced with CSA cement repair materials. The test slabs were 8 ft long and had a total width of 2 ft, comprised of a 1 ft wide section of conventional concrete and a 1 ft wide section of ultra high-performance concrete (see Figure 10). In order to simulate repair of a conventional concrete bridge deck, the repairs were done on the conventional concrete portion of the slabs.



Figure 10: Large-Scale Slab for Repair

Two slabs were demolished and repaired. One slab was repaired with the RS-SCC material and the other was repaired with the FR-SCC material. Two different surface preparations were performed on each slab: a chipped surface and a chipped plus sandblasted surface. Thus, a total of four repair material/surface preparation combinations were evaluated with the large-scale specimens. In order to remove a section of concrete from the slabs, an angle grinder with a diamond cutting wheel was used to create a grooves to help control the dimensions of the removed section. Two, 8 ft long lines were cut into each slab. The cuts were made perpendicularly at a width of 6 in. and a depth of 4 in, as shown in Figure 11 (a). The depth of the cuts was approximately 1 in., as limited by the 4.5 in. diameter cutting wheel. After the cuts were

made, a pneumatic hammer was used to remove the 6 in. x 4 in. section of concrete. Figure 11 (b) shows the slab during the chipping process. The longitudinal reinforcing bar located in the section of concrete that was removed, was removed during the chipping and sandblasting processes due to the small clearance that may have negatively affected the quality of surface preparation.

Half, or a 4 ft long section of the damaged area was sandblasted. During sandblasting, the rest of the slab was covered with wood and towels to prevent unintentional roughening to any other area of the slabs. Figure 11 (c) shows the slab during sandblasting. Excess sand and dust was removed from the full length of the slab using compressed air. After surface preparation was complete, the longitudinal reinforcement was replaced. In order to ensure that each surface preparation performed independently, a buffer zone was left in the center of the slab between the chipped and sandblasted plus chipped sections. No repair concrete was cast in the center 4 in. of the slab so that the two sides would be separate. The original longitudinal reinforcing bar was also cut into two, 44 in. long, pieces that fit into each half separately.

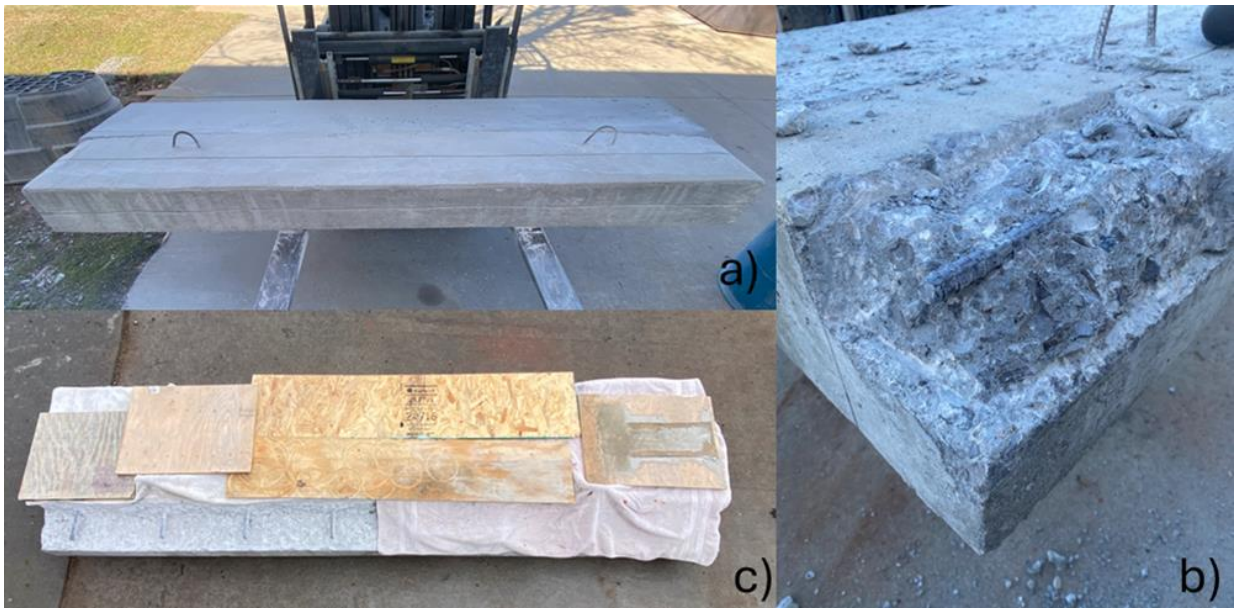


Figure 11: Large Scale Repair Slab During Cutting (a), Chipping (b), and Sandblasting Processes (c)

Forms for the repair section were fabricated using ratchet straps to secure 2x10s along the 3 exposed sides of the removed section. The center divider was made out of scrap lumber and insulation foam, which was cut slightly smaller than the 6 in. x 4 in. repair section. Window seal foam was adhered to the edges of the divider to match the rough contours of the damaged slab and fill the remaining gap. The completed formwork is shown in Figure 12 (a). Silicone caulk was used to fill any remaining gaps in the formwork. The caulk was only applied on the exterior of the formwork to avoid creating any depressions in the repair concrete that may allow water to penetrate the interface more easily. The silicone was allowed to cure fully (at least 24 hours) before casting. The formwork was oiled lightly using a cloth so that the interface area would not be contaminated.

The repairs were cast using the same procedures described in Sections 3.1.5.1 and 3.1.5.2 for the RS-SCC and FR-SCC, respectively. Concrete was added until the repair was flush with the surface of the slab. Due to size limitations, the slabs could not be placed in the same temperature controlled room that the rest of the specimens were cured in. Instead, the slabs were left in a non-temperature controlled room, which had an average temperature of about 68° while the slabs were inside. When the surface of the repair material was firm to the touch, wet burlap and plastic were placed over the concrete. The slabs were cured inside for 2 days before being demolded and placed outside to begin the natural freeze-thaw exposure. A completed slab is shown in Figure 12 (b). One set of 3 compressive strength cylinders was placed outside with the RS-SCC repair slab so that comparisons could be made between the strength of the repair concrete with and without exposure to natural freeze-thaw conditions. Comparisons could not be made for the FR-SCC repair slab due to an insufficient number of compressive strength cylinders.

The repairs were visually inspected over a period of 3-6 months throughout the winter, during which they were left outside and exposed to natural freeze-thaw conditions. The main objective of the large scale testing was to monitor for signs of delamination of the repair material.



Figure 12: Large Scale Repair Slab Formwork (a) and Finished Specimen (b)

Chapter 4. Results and Discussion

4.1. Pull-Off Testing

4.1.1. Monolithic Specimen Pull-Off Testing

For the monolithic specimens, only two failure modes were possible: a bond failure between the puck and concrete core or a tensile failure of the concrete core. A failure of the puck adhesive would indicate that the tensile strength of the concrete specimens was higher than that of the adhesive and corresponding failure stress. None of the specimens exhibited this type of failure. Instead, all the monolithic specimens in this study exhibited a tensile failure of the concrete material. Thus, the recorded stress at failure of all monolithic test cores was indicative of the tensile strength of the concrete. Table 6 summarizes the average failure stress and the standard deviation for each monolithic material.

Table 6: Average Tensile Strength and Standard Deviation for Monolithic Specimens

Concrete Type	Average Stress at Failure (psi)	Standard Deviation of Failure Stress (psi)
Class AA	512	83.2
RS-SCC (7 Days)	624	73.3
RS-SCC (28 Days)	626*	40.8*
RS-SCCHA	618	85.4
RS-SCCUA	427	34.5
FR-SCC	428	31.5

*The average stress and standard deviation values presented in this table for the RS-SCC (28 day) specimens exclude the outlier values discussed in Section 4.1.1.

The tensile strength of the RS-SCC was evaluated at both 7 and 28 days to determine the effect of age on the performance of the material, as well as to dictate the age of subsequent testing. The results of the monolithic RS-SCC pull-off testing indicated that the age of the concrete did not significantly affect the tensile strength of the concrete. While the pull-off tests performed at 28 days resulted in a lower average tensile strength than the tests performed at 7 days, cores 1 and 2 of the 28-day specimen failed at a significantly lower load than the other three cores. The reduced strength of cores 1 and 2 on the 28-day monolithic RS-SCC specimens cannot be explained with certainty, however, there are a couple of possible explanations. Because the specimens were manually cored using a drill press, it is possible that microscopic damage occurred to these two cores, resulting in the observed strength reduction. Another possible explanation for the discrepancy is voids, non-homogeneity, or imperfections in the concrete. The two cores with low strength were adjacent to each other, which could be consistent with either of these explanations.

For the purposes of comparison, the average which excludes the outlier cores (1 and 2) will be used to represent the tensile strength of the 28-day RS-SCC concrete. With the two outlier values removed, the average load at failure and stress at failure of the 28-day specimen cores increase to 1967 lbf and 626 psi, respectively. Excluding the significantly lower tensile strength values associated with cores 1 and 2 resulted in a material tensile strength that was virtually the same at an age of 7 and 28 days. As the material strength was comparable for the two ages, and rapid infrastructure repair is one of the potential implementations of CSA cement concretes, the composite pull-off tests to evaluate bond strength were performed at a repair material age of 7 days. The complete set of pull-off data for the monolithic specimens is available in Appendix B, Table 20 through Table 25.

Two of the repair materials had a tensile strength higher than that of the Class AA concrete (RS-SCCHA and RS-SCC). The other two repair materials (RS-SCCUA and FR-SCC) had a lower tensile strength than the Class AA concrete. The average tensile strength of each repair material compared to the Class AA concrete is illustrated in Figure 13. The monolithic pull-off test data indicates that RS-SCC concrete has an

average tensile strength that is approximately 22% greater than that of the Class AA concrete (624 psi compared to 512 psi). The tensile strength results for the Class AA concrete are summarized in Table 20 (see Appendix B). Similarly, the RS-SCCHA monolithic pull-off specimens had an average tensile strength approximately 21% higher than the Class AA monolithic specimens (618 psi compared to 512 psi). This finding indicates that the RS-SCC and RS-SCCHA materials would not cause a reduction in the overall tensile strength of a structure repaired with the material, provided that an adequate bond is achieved.

Conversely, because the tensile strengths of the RS-SCCUA and FR-SCC were lower than that of the Class AA concrete, using those mixes as a repair material could potentially introduce zones with lower tensile strength, even though the compressive strength of the RS-SCCUA and FR-SCC were higher than that of the Class AA concrete. The lower tensile strength of the RS-SCCUA and FR-SCC could also indicate that the material may crack more easily.

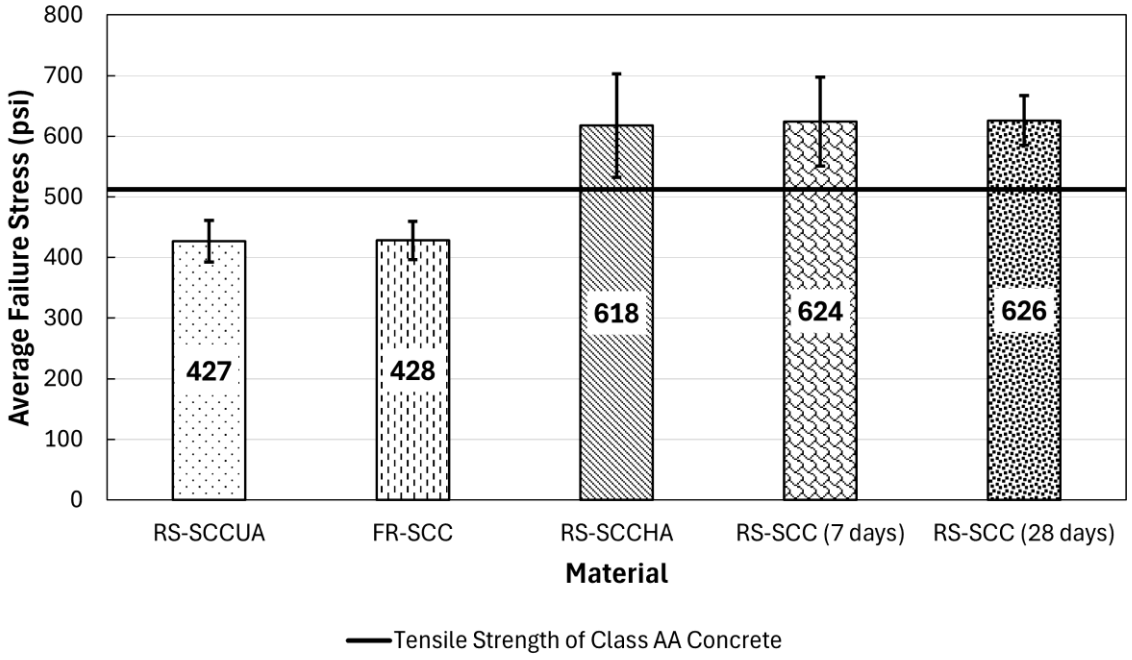


Figure 13: Tensile Strength of Monolithic Materials Measured Using Pull-off Test

The tensile strength results for the monolithic RS-SCCUA specimens are detailed in Table 24 in Appendix B. All failures occurred within the concrete, although cores 1-3 failed closer to the puck and cores 4 and 5 occurred further from the surface. Compared to the other monolithic pull-off specimens, the RS-SCCUA specimens had the second lowest standard deviation of the stress at failure (see Table 6), meaning that the tensile strength of the RS-SCCUA was more consistent than most of the other materials. However, the average tensile strength of the RS-SCCUA was also the lowest at 427 psi.

Although the FR-SCC had a lower tensile strength than the Class AA, RS-SCC, and RS-SCCHA materials, it exhibited some post-cracking tensile strength due to the polypropylene fiber reinforcement. In the monolithic pull-off tests for the FR-SCC, fibers were observed bridging the failure plane on some specimens such as the one shown in Figure 14, which could cause failures in field applications to be less sudden.



Figure 14: Polypropylene Fiber Bridging Failure Plane of Monolithic FR-SCC Pull-Off Specimen

While the RS-SCCUA and FR-SCC mixes exhibited lower tensile strength than the other monolithic materials, they also had the lowest standard deviation, as detailed in Table 6. The lower standard deviation for the RS-SCCUA and FR-SCC pull-off test trials suggests that these concrete mixes may have been more homogenous, leading to more consistent tensile strength. The lower standard deviation of the pull-off test results could also indicate that the specimens were prepared in a more consistent manner, including the surface preparation, coring, and pull-off puck adhering processes. Therefore, although the RS-SCCUA and FR-SCC had a lower tensile strength, it may be possible to predict their tensile strength more accurately.

4.1.2. Composite Specimen Pull-Off Testing

The composite pull-off test results for each repair material/surface preparation combination are shown in Figure 15 through Figure 18. The average values are compiled in Table 7. The results showed that both the repair material and the surface preparation technique affected the bond strength between the base and overlay concrete. For the four repair materials tested, the sandblasted (SB) specimens had higher average pull-off strengths when compared to the exposed aggregate (EA) and chipping hammer (CH) surface preparations. The SB specimens likely performed better in the pull-off test due to the finer, and potentially more distributed, texture of the prepared surface. The CH and EA surface preparation techniques resulted in a much coarser surface texture, and achieving a consistent surface texture across the specimen was more difficult for the CH and EA techniques. The CH preparation technique was also the most aggressive, as it was achieved by repeated impact of the specimen bases with a pneumatic hammer, so the CH specimen bases were particularly vulnerable to damage during the surface preparation process. However, whether the SB-D or SB-MS performed better differed by repair material. Likewise, the comparative performance of the EA and CH specimens also differed by material.

Table 7: Summary of Average Tensile Strength Values (psi)

Surface Preparation	RS-SCC	RS-SCCHA	RS-SCCUA	FR-SCC
EA	261	307	396	360
CH	132	326	146	119
SB-D	466	660	446	453
SB-MS	--	553	465	433

4.1.2.1. Effects of Surface Preparation on Tensile Bond Strength

4.1.2.1.1. Composite Specimens with RS-SCC Overlays

The pull-off test results for the composite RS-SCC specimens are illustrated in Figure 15, where the letters above the bars indicate the ASTM C1583 failure type. All of the exposed aggregate and sandblasted with no surface moistening cores failed in the Class AA concrete (failure mode A), meaning that the bond strength achieved with these surface preparation techniques was higher than the tensile strength of the Class AA concrete. Conversely, all the chipping hammer cores failed at the interface between the Class AA and RS-SCC concrete. Thus, the tensile strength of the bond was less than the tensile strength of each individual material. Due to premature failure at the interface, a significantly lower failure stress was observed for the chipping hammer surface preparation.

Although the EA and SB-D cores all failed in the Class AA concrete, the EA specimens had a much lower average strength (261 psi compared to 466 psi). This strength difference could be due to a number of factors. Some local variation in concrete strength is expected, however, the discrepancies can be exacerbated if the mix is not homogeneous. Additionally, the surface preparation techniques could have impacted the strength of the Class AA bases. For example, using a water hose to remove concrete paste from the surface of the EA specimens at an early age could

have caused damage or further moistened the concrete, potentially affecting cement hydration. Damage during the coring process is also a possible explanation for the strength differences. Lastly, experimental variation such as loading rate and whether the pucks/reaction frame were perfectly level could have impacted the failure loads.

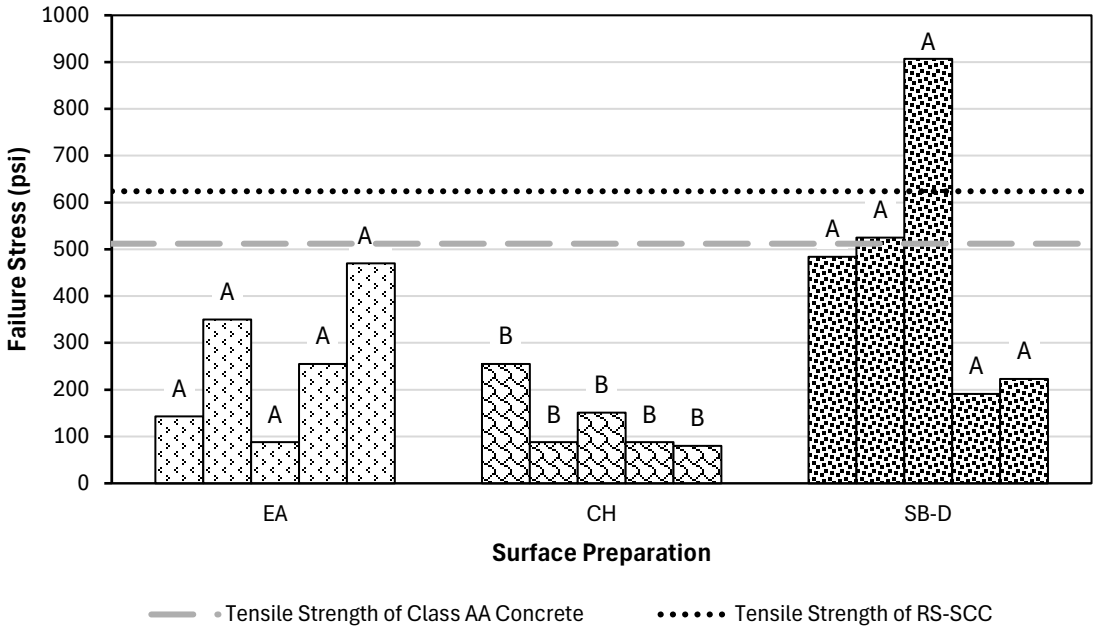


Figure 15: ASTM C1583 Results for Composite Specimens with RS-SCC Overlay

4.1.2.1.2. Composite Specimens with RS-SCCHA Overlays

Similarly, the RS-SCCHA composite pull-off specimens indicated that sandblasting was more effective in facilitating proper bond between the substrate and overlay concrete than an exposed aggregate or chipped surface. The failure stress and failure mode for the RS-SCCHA pull-off specimens are presented in Figure 16. All the test cores for the EA and CH specimens failed at the interface between the Class AA and RS-SCCHA (type B failure). This failure mode indicates that for the EA and CH surface preparations, the bond strength between the two concrete materials was

weaker than the tensile strength of each individual material. For the RS-SCCHA overlay, the specimen with a CH surface exhibited a slightly higher average tensile bond strength than the EA surface (326 psi compared to 307 psi). Between the two sandblasted surfaces, the specimen without surface moistening (SB-D) performed better than the specimen with surface moistening (SB-MS). The average tensile strength of the SB-D specimen was 660 psi, compared to 553 psi for the SB-MS specimen. The bond failures of all test cores for the EA and CH specimens, in conjunction with the lower average failure stresses when compared to the SB-D and SB-MS specimens, suggest that the EA and CH surface preparations resulted in a weaker bond than the sandblasted surfaces.

However, due to the observed failure mechanisms, it is difficult to make a conclusive judgement about the tensile bond strength for the two sandblasted surfaces. All five of the SB-D cores failed in the Class AA concrete, therefore the average recorded tensile strength represents the tensile strength of the Class AA concrete, not the bond strength between the base and overlay concrete. The conclusion that can be drawn based upon the available data is that the tensile bond strength for RS-SCCHA with a SB-D surface preparation is a value greater than the average failure stress of 660 psi. Another notable finding with the SB-D specimen was that although all cores failed in the Class AA concrete, core 3 exhibited a significantly higher tensile strength than the other cores (1249 psi compared to 597 psi for the next highest core). With the removal of this outlier, the average tensile strength for the specimen is reduced to 513 psi, which is consistent with the average tensile strength of 512 psi for the Class AA concrete from the monolithic trial. The abnormally high strength of core 3 may have been impacted by its position within the test slab. Based on the layout of the pull-off cores, as shown in Figure 6, core 3 is directly in the center of the slab, with a greater distance to a free edge than the other four cores. It is possible that the interior most core was the most protected from edge effects and microdamage during surface preparation or that the concrete in the center of the form was consolidated the most effectively, resulting in the higher strength of this core. With such large variability in measurements, it is also possible that there was some measurement error.

Similarly, only one of the SB-MS cores failed at the interface, with the other four failing prematurely in the epoxy or Class AA concrete. The core which failed at the interface between the base and overlay concrete (core 1) is the most indicative of the tensile bond strength for this repair material/surface preparation combination. Core 1 failed at 676 psi, thus based on the available data, the closest estimate for the tensile bond strength of the RS-SCCHA/SB-MS specimen is 676 psi, but this value is drawn from only one trial.

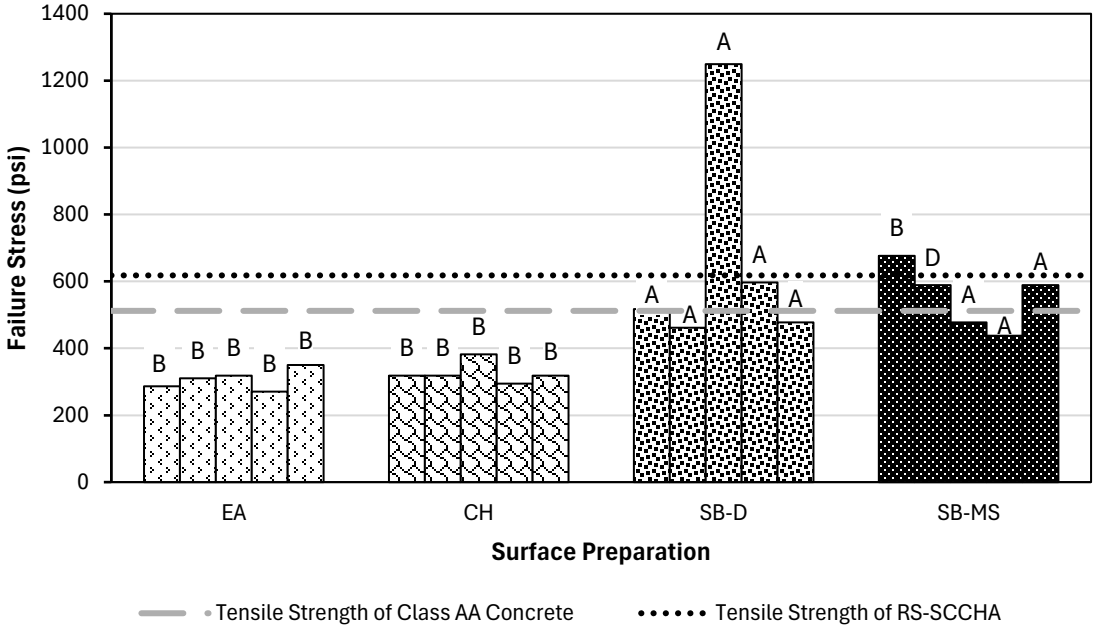


Figure 16: ASTM C1583 Results for Composite Specimens with RS-SCCHA Overlay

4.1.2.1.3. Composite Specimens with RS-SCCUA Overlays

For the RS-SCCUA specimens, the order (lowest to highest) of average pull-off strength for each surface preparation technique was CH (146 psi), EA (396 psi), SB-D (446 psi), and SB-MS (465 psi). Figure 17 shows the stress at failure and failure modes of the RS-SCCUA pull-off specimens. For this repair material, the CH surface preparation resulted in a significantly lower pull-off strength than the EA, SB-D, and SB-

MS. The average failure strength of the CH cores was approximately 1/3 of the strength of the cores for the other three surface preparations. The average pull-off strengths of the EA, SB-D, and SB-MS specimens were 271%, 304%, and 317% of the average pull-off strength of the CH specimen, respectively. In addition to exhibiting the lowest average tensile strength, all five of the RS-SCCUA-CH pull-off cores failed at the interface, meaning that the bond between the base and overlay concrete was the weakest zone on this specimen. The SB surface with and without moistening resulted in similar average pull-off strengths. However, considering both the failure stresses and modes, the SB-MS surface resulted in a better bond than the SB-D surface. Not only was the average pull-off strength greater for the SB-MS surface prep, all five of the SB-MS cores failed in the Class AA concrete, while two of the SB-D cores failed at the interface.

An unexpected finding for the RS-SCCUA overlay was that none of the cores failed in the overlay concrete but several failed in the base concrete, despite the RS-SCCUA concrete having a lower tensile strength than the Class AA concrete in the monolithic pull-off tests. There are a few possible explanations for this discrepancy in composite specimen behavior, the simplest of which being that a different batch of Class AA was used for the monolithic pull-off test and the specimen bases. Another possible reason is that the Class AA monolithic pull-off specimen was tested at 35 days, while the Class AA concrete bases for the RS-SCCHA, RS-SCCUA, and FR-SCC composite specimens were over 100 days old when the composite specimen pull off tests were performed. The compressive strength results for the Class AA concrete (Table 15) suggest some strength loss of the material over time, as the test day strengths are lower than the 28-day strengths for most of the mixes. While tensile strength and compressive strength of concrete are very different, there is often a correlation. At these later ages for the Class AA bases, concrete drying could have also impacted the pull-off test results.

The bases for the RS-SCC composite specimens were cast with the same Class AA concrete batch as the monolithic specimen and were tested at the same age (35 days). However, they still demonstrated the same phenomenon of the Class AA in the

composite specimens failing at a lower tensile strength than indicated by the monolithic trials. Based on these results is presumed that additional factors could be affecting the Class AA concrete rather than or in addition to the natural strength variance by concrete batch or age. One such explanation for the difference in material strength of the composite specimens versus the monolithic specimens is that the deeper coring in the composite specimens may have increased the likelihood of damage during the coring process. As the Class AA concrete was at the base of the cores and the RS-SCCUA was at the surface of the specimens, it is possible that the Class AA concrete sustained more unintentional damage while being cored. This theory is supported by the observation that several cores failed at the bottom of the coring depth. It is also possible that the specimen bases sustained microscopic damage during the various surface preparation processes, causing the Class AA concrete to be weakened compared to the monolithic tests.

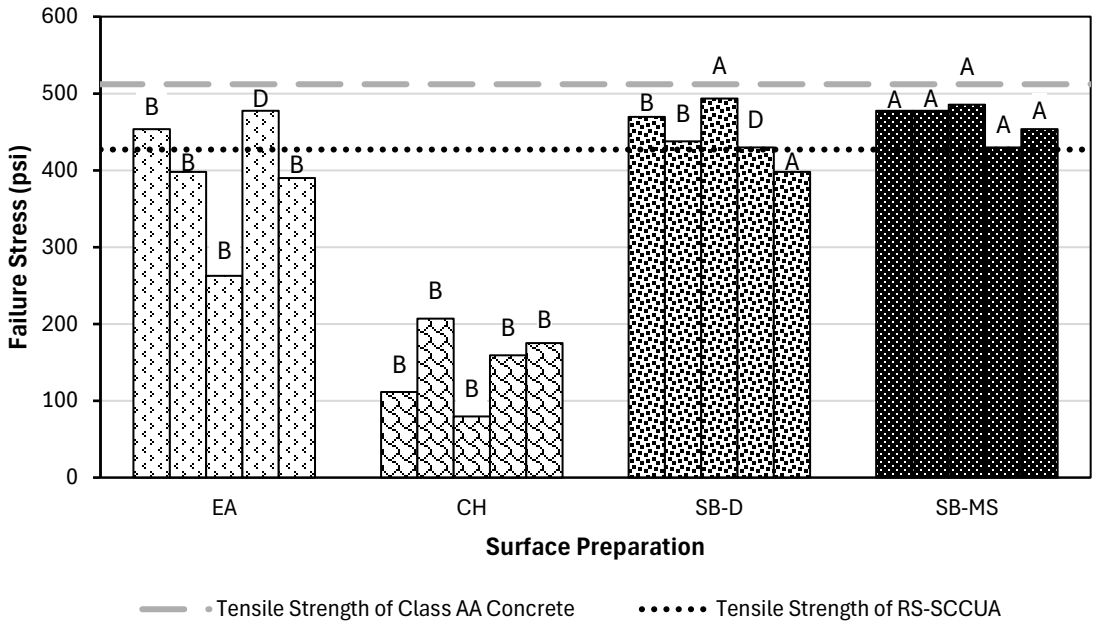


Figure 17: ASTM C1583 Results for Composite Specimens with RS-SCCUA Overlay

4.1.2.1.4. Composite Specimens with FR-SCC Overlays

The composite FR-SCC pull-off specimens behaved similarly to the RS-SCCUA specimens. The pull-off test data for FR-SCC overlays is presented in Figure 18. The CH surface preparation again resulted in the lowest average tensile strength and all five cores failed at the interface, indicating a poor bond with this surface preparation technique. Four out of five of the EA cores also failed at the interface, but at a higher load than each of the chipping hammer cores. The average pull-off strength for the EA specimen was 360 psi, while the average strength for the CH specimen was 119 psi.

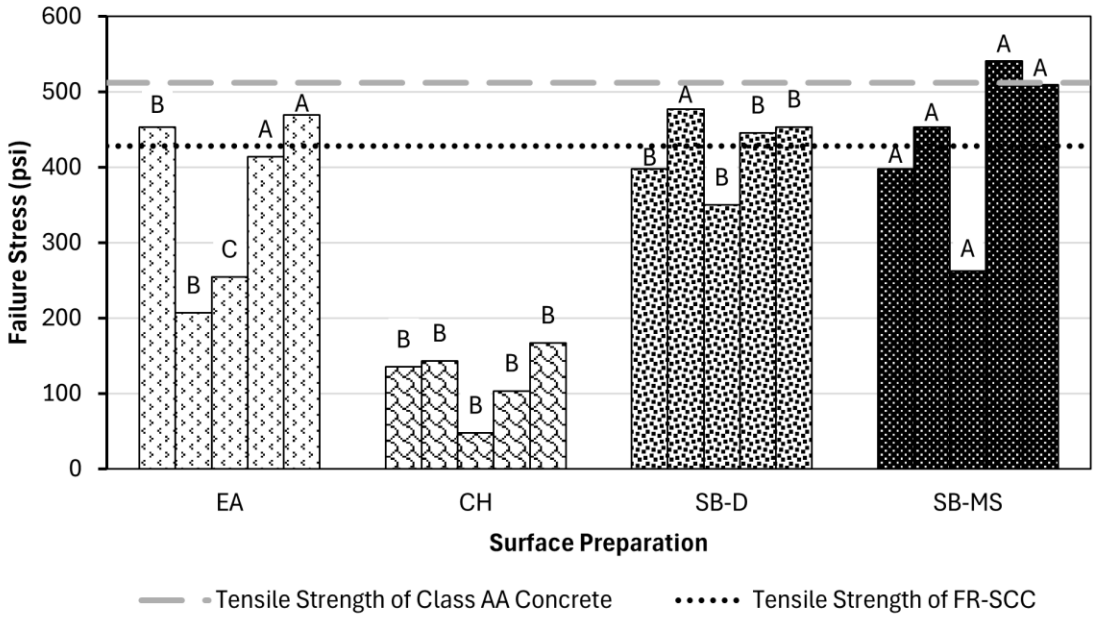


Figure 18: ASTM C1583 Results for Composite Specimens with FR-SCC Overlay

The SB-MS surface preparation performed better than the SB-D surface preparation for the FR-SCC overlay. The average tensile strength for the SB-MS cores was 433 psi, compared to 425 psi for the SB-D cores. Furthermore, all the SB-MS cores failed in the substrate concrete, while four out of five of the SB-D cores failed at the interface.

Like the RS-SCCUA cores, only one of the cores broke in the FR-SCC overlay, while several broke in the Class AA base concrete, despite the higher tensile strength of the Class AA concrete indicated by the monolithic pull-off tests.

4.1.2.2. Effects of Repair Material on Tensile Bond Strength

The composition of the substrate and overlay materials can also influence tensile bond strength, as composition affects adhesion [43]. While the EA and CH surface preparations consistently yielded lower tensile strengths when compared to the sandblasted surfaces, there was no repair material that performed better, regardless of surface preparation technique. Therefore, it seems that regarding tensile strength of composite specimens, surface preparation technique had a more significant impact on bond than the composition of the repair concrete. However, it should be noted that in this study, the mix designs for the RS-SCC, RS-SCCHA, and RS-SCCUA were all very similar. It is possible that the repair material composition would have caused a larger discrepancy in strength, had the mix designs been more varied. For example, different types and quantities of supplementary cementitious materials may have significantly impacted performance.

As shown in Figure 19, the RS-SCCHA yielded the highest average tensile strength for three of the surface preparations: CH, SB-D, and SB-MS. The RS-SCCUA provided the highest average tensile strength out of the composite specimens with an EA surface preparation. As overlay materials, the RS-SCC and FR-SCC did not yield any pull-off specimens with the highest average tensile strength.

Conversely, out of the specimens with an exposed aggregate surface preparation, the RS-SCC overlay had the lowest average pull-off strength. For the SB-D specimens, the RS-SCCUA overlay material had the lowest average pull-off strength. The FR-SCC overlay yielded the lowest average pull-off strength for the composite specimens with the remaining two surface preparation techniques: CH and SB-MS.

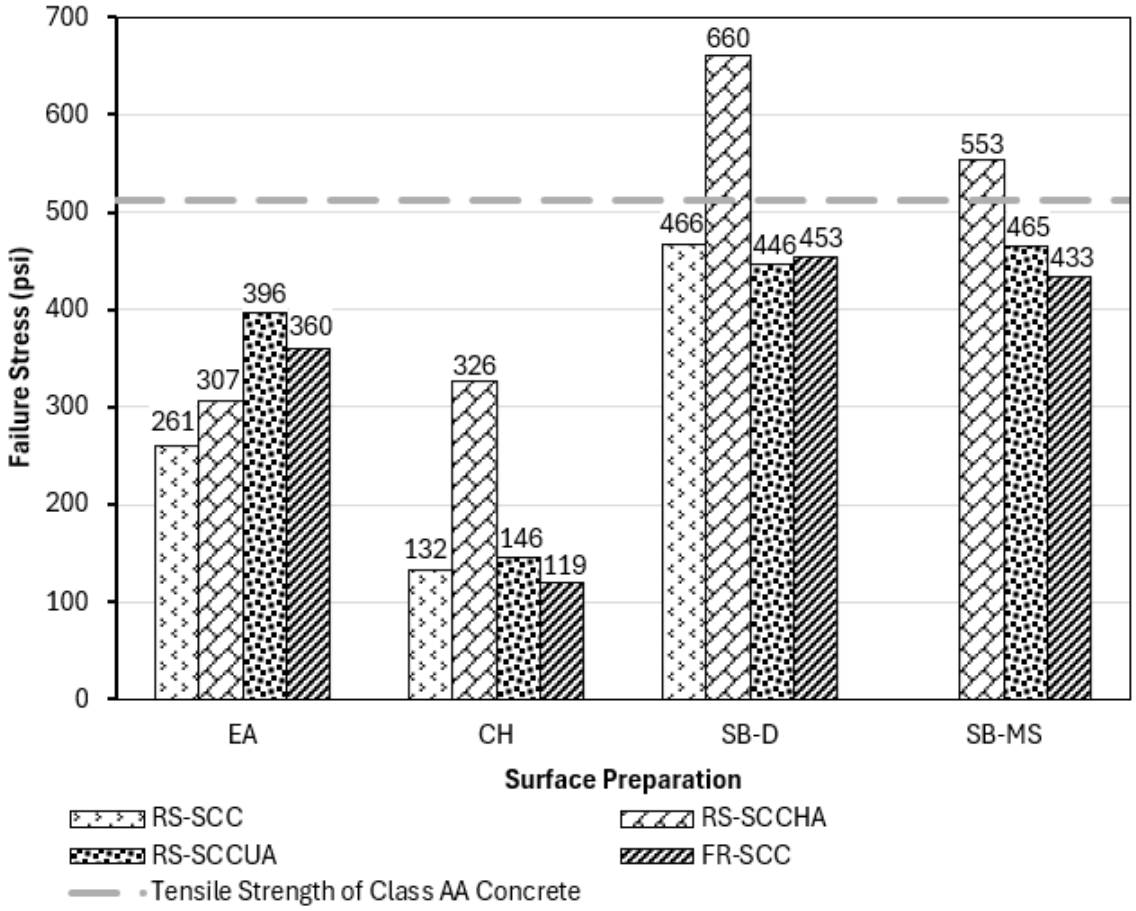


Figure 19: Composite Pull-Off Test Results by Material

4.1.2.3. Summary of Composite Pull-Off Test Results

The pull-off strength values for the composite specimens must be interpreted with caution, as the failure type for each test core is relevant to the meaning of the results. Only a failure at the interface between the two concrete materials is indicative of the tensile bond strength of the overlay. The complete composite pull-off data with failure types can be found in Appendix B, Table 26 through Table 29. All test cores for the RS-SCC-CH, RS-SCCHA-EA, RS-SCCHA-CH, RS-SCCUA-CH, and FR-SCC-CH specimens failed at the interface between the base and overlay concrete, meaning that the bond was the weakest tensile zone for these specimens. All cores for the RS-SCC-EA, RS-SCC-SB-D, RS-SCCHA-SB-D, RS-SCCUA-SB-MS and FR-SCC-SB-MS

specimens failed in the Class AA base concrete, meaning that the tensile strength of the conventional concrete was the weakest zone for these specimens, and the true bond strength between the materials is larger than the recorded values. The percentage of cores that resulted in each failure mode are presented in Table 8. The failure mode data suggests that the CH surface preparation technique was ineffective in facilitating bond between the base and repair concrete, as 100% of the CH cores experienced a type B failure. On the other hand, only 6.67% of the SB-MS test cores failed at the interface between the two types of concrete, suggesting that the SB-MS surface preparation was more effective in promoting tensile bond strength.

Table 8: Percentage of ASTM C1583 Failure Modes by Surface Preparation

ASTM C1583 Failure Mode	EA	CH	SB-D	SB-MS
A	35%	0%	65%	86.7%
B	55%	100%	30%	6.67%
C	5%	0%	0%	0%
D	5%	0%	5%	6.67%

Conversely, only one core out of 75 from all four repair material/surface preparation combination failed in the repair concrete (failure mode C). The core that failed in the repair concrete was from the FR-SCC-EA specimen, and it is shown in Figure 20, where (a) is the failure surface of the concrete adhered to the pull-off puck, and (b) is the failure surface of the concrete remaining attached to the test specimen. The failure surface of this core reveals a weak zone of FR-SCC, which appears to have a pocket of dry material that did not properly hydrate, as indicated by the arrow in Figure 20. The FR-SCC for the composite pull-off specimens was from the FR-2 mix, which began to set and lose workability quickly. Based on the failure surface in Figure 20, there seems to have been some issues with concrete homogeneity as well. The failure

mode data, with only 1 core out of 75 total composite specimen cores failing in the repair material concrete, suggests that the tensile strength of the RS-SCC, RS-SCCHA, and FR-SCC is sufficient for repairs to normal strength concrete, such as ODOT Class AA (provided that the bond strength is adequate).

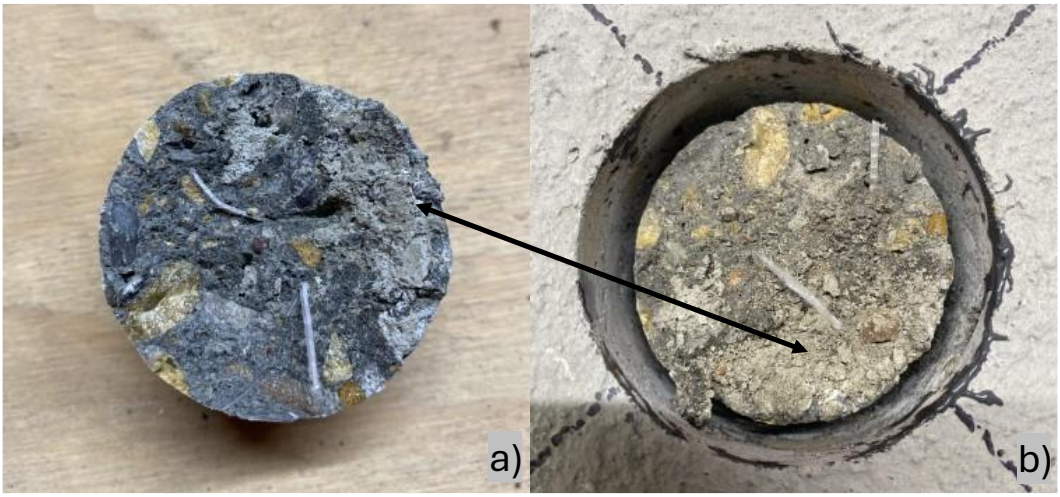


Figure 20: FR-SCC-EA Pull-Off Specimen Failure Surface

For the repair materials in this study, the concrete mix design seemed to have a lesser effect on the pull-off strength than the surface preparation technique. However, it should be noted that the three mix designs with the Rapid Set® BCSA cement were not significantly different from each other in terms of composition. There was no repair mix that consistently achieved higher pull-off strengths than the others, although the RS-SCCHA had the highest average pull-off strength for all surface preparation techniques except EA. The failure modes of the cores must also be considered in this evaluation, as only type B failures can quantify bond strength. Since many of the test cores for each repair material failed in the Class AA concrete, particularly for the SB-D and SB-MS surfaces, the average pull-off strengths are not indicative of bond strength. Furthermore, the strength of cores which exhibit type A failure is dependent on the tensile strength of the Class AA concrete, not factors related to the repair material. Therefore, although the RS-SCCHA failed at higher stresses, it cannot be concluded that the bond strength of this material was higher than that of the other repair materials.

4.2. Freeze-Thaw Testing

The freeze-thaw testing done in this study involved both quantitative and qualitative components. Resonant frequency testing was done at intervals so that the relative dynamic modulus of elasticity could be calculated and interpreted. While the testing intervals were below the 36 cycle maximum defined in ASTM C666, the time elapsed over the exposure period was less consistent [41]. Due to changes in ambient temperatures, the use of two freeze-thaw chambers, and equipment limitations, the time required to freeze and thaw the specimens was variable. Additionally, the available freeze-thaw machines were incapable of reliably fluctuating between freezing and thawing within the durations required by ASTM C666. Variations in cycle duration could cause specimen age to influence durability in a way which is not consistent across all specimens. Furthermore, the rate of temperature change may affect the intensity of freeze-thaw exposure.

Equation 2 is the ASTM C666 equation for the relative dynamic modulus used in this study. The complete data set for relative dynamic modulus of elasticity is presented in Appendix C, Table 30 through Table 41.

Equation 2: Relative Dynamic Modulus of Elasticity [41]

$$P_c = \frac{n_1^2}{n^2} \times 100$$

Where:

P_c = relative dynamic modulus of elasticity, after *c* cycles of freezing and thawing, percent.

n = fundamental transverse frequency at 0 cycles of freezing and thawing

n_1 = fundamental transverse frequency after *c* cycles of freezing and thawing

4.2.1. Monolithic Freeze-Thaw Testing

4.2.1.1. RS-SCC Monolithic Freeze-Thaw Specimen

Freeze-thaw testing was first conducted on monolithic RS-SCC specimens to determine whether pre-exposure curing time would impact the durability of the material. One pair of monolithic specimens was placed in the freeze-thaw chamber at 7 days of age and the other at 28 days. The average relative dynamic modulus of elasticity (MOE) for each age of monolithic RS-SCC specimens are presented in Figure 21. All four specimens experienced an increase in the resonant frequency and relative dynamic modulus during the first round of exposure, which consisted of approximately 30 freeze-thaw cycles. These properties began to decrease again before the specimens underwent approximately 60 cycles of exposure and continuously decreased for the remainder of the exposure period.

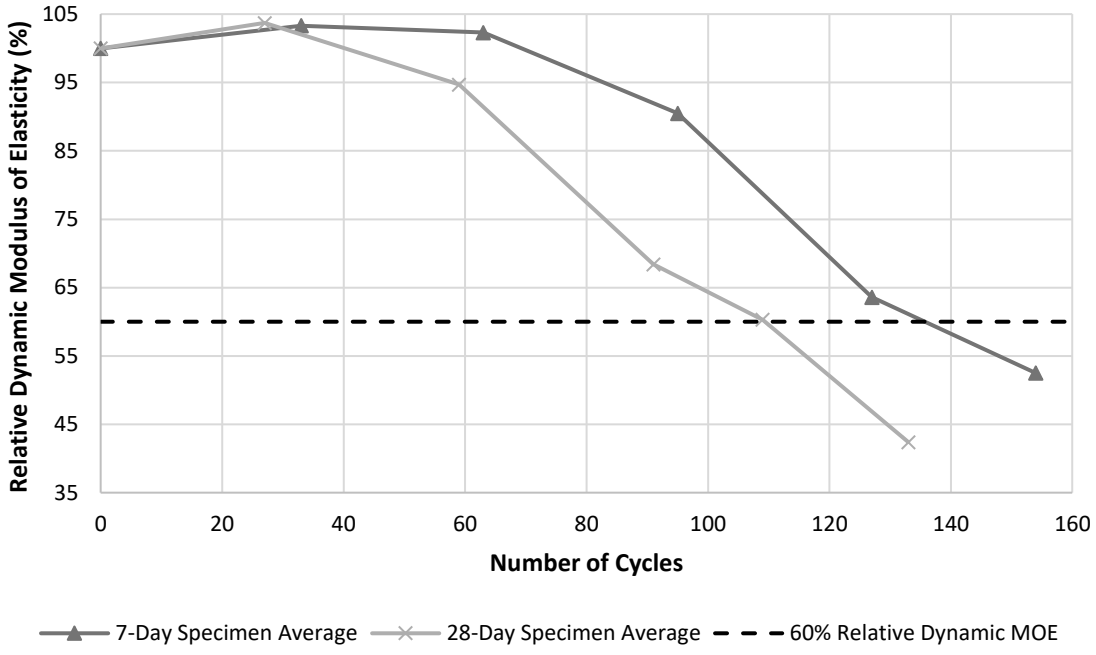


Figure 21: Relative Dynamic Modulus of Elasticity Results for Monolithic RS-SCC

After about 30 cycles of exposure, the 28-day specimens had a slightly higher average relative dynamic MOE. Beyond this first increment of resonant frequency readings, however, the 28-day specimens had a consistently lower average relative dynamic MOE. On average, the relative dynamic MOE of the 7-day RS-SCC specimens reduced to 60% after approximately 130 cycles, compared to about 110 cycles for the 28-day specimens. ASTM C666 permits that freeze-thaw testing be ended when the relative dynamic modulus of elasticity reaches 60%, or after 300 exposure cycles, whichever occurs first [41].

The relative dynamic MOE of the 28-day specimens may have been generally lower than the 7-day specimens due to the relationship between concrete curing and MOE. Because MOE tends to increase over time, the 7-day specimens likely had a lower MOE when the initial resonant frequency readings were taken and experienced some additional curing during freeze-thaw exposure. This additional curing likely increased the MOE and artificially offset some of the effects of freeze-thaw deterioration. Conversely, the 28-day specimens would have already reached a strength plateau before the initial resonant frequency readings were taken, meaning that there was likely not the same level of MOE increase due to additional curing over the testing period. Any potential MOE increases due to curing falsely inflate the relative dynamic MOE used to indicate freeze-thaw durability. Therefore, the 28-day specimens may be a more accurate representation of freeze-thaw deterioration over time.

The pre-exposure resonant frequency readings indicated that the specimens had a higher resonant frequency at 28 days than at 7 days. As both ages of monolithic specimens were cast from the same batch of concrete, this finding suggests that additional curing increases the resonant frequency of the material. However, this increased resonant frequency did not necessarily correlate with better performance. Both the 7-day and 28-day specimens were visually damaged by freeze-thaw exposure, suggesting that the curing age before exposure does not completely dictate freeze-thaw durability. Figure 22 shows a 7-day (a) and 28-day (b) freeze-thaw specimen at the end of freeze-thaw testing. The higher initial resonant frequency of the 28-day specimens supports the notion that the 7-day specimens were still curing when exposure

commenced, which provides a potential explanation for the difference in freeze-thaw performance between the 7-day and 28-day specimens. While the 7-day specimens did not exhibit as fast of a deterioration in relative dynamic MOE, the data was likely skewed. The combination of curing and freeze-thaw deterioration would cause the MOE to simultaneously increase and decrease. Thus, curing which occurred after the initial readings were taken may have disproportionately masked reduction in resonant frequency from freeze-thaw damage. Because concrete gains strength more rapidly at early ages, even if both the 7-day and 28-day specimens experienced additional curing during the exposure period, the data for the 7-day specimens would have been more significantly impacted. Therefore, while the data suggests that the 28-day specimens deteriorated faster than the 7-day specimens, it is likely that this data was at least partially impacted by specimen age in a manner not indicative of actual freeze-thaw performance.



Figure 22: 7-Day (a) and 28-Day (b) Monolithic RS-SCC Specimens After Freeze-Thaw Exposure

4.2.1.2. RS-SCCHA Monolithic Freeze-Thaw Specimens

Testing for the monolithic RS-SCCHA specimens is ongoing due to mechanical challenges with the freeze-thaw chamber. So far, the specimens have been exposed to 93 freeze-thaw cycles. Table 33 in Appendix C includes the resonant frequency and relative dynamic MOE for the two monolithic specimens. Between 0 and 32 exposure cycles, the relative dynamic MOE of specimen 1 decreased to 95.5% and the dynamic MOE of specimen 2 increased to 105.0%, as shown in Figure 23. Between 32 and 93 cycles, the relative dynamic MOE of both specimens increased. After 93 cycles, the relative dynamic MOE of specimens 1 and 2 were 99.6% and 108.3%, respectively. The difference in dynamic MOE behavior between the two specimens is likely due to additional curing of the concrete and/or the position of the specimens within the freeze-thaw chamber. The position in the freeze-thaw chamber may be relevant because proximity to the refrigerant system/circulation fan has had a notable impact on the freezing rate of the specimen containers. Similarly, some of the heating elements worked better than others, so the specimen containers thawed at differing rates. To offset the effects of position in the freeze-thaw chamber as much as possible, specimen position within the chamber was rotated after each incremental round of resonant frequency testing.

Visual inspection of the RS-SCCHA specimens provided additional information about freeze-thaw durability. Figure 24 (a) shows the RS-SCCHA concrete when the initial resonant frequency readings were taken. Figure 24 (b) and (c) show specimens 1 and 2, respectively, after 93 cycles of freeze-thaw exposure. Both specimens had a noticeably rougher surface texture after freeze-thaw exposure, indicating some deterioration. This deterioration seemed to originate around the bubbles on the surface of the specimens, which formed because of the HRWR. Additionally, although the dynamic MOE for specimen 2 increased after 93 cycles, it is clear from Figure 24 (c) that this increase in MOE does not indicate the absence of freeze-thaw damage.

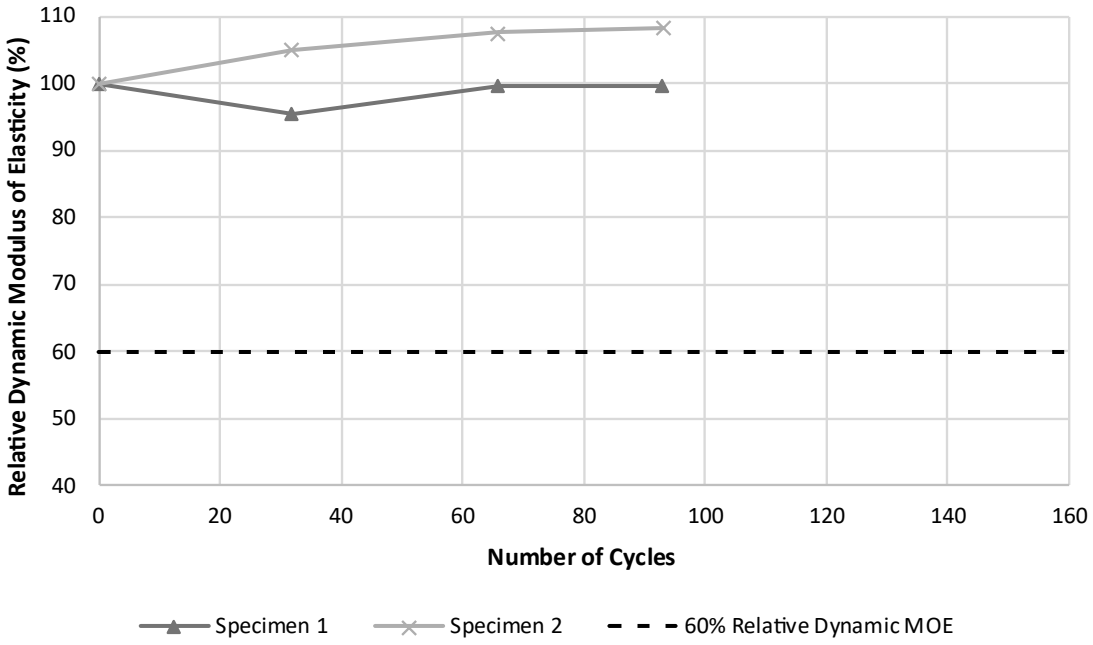


Figure 23: Relative Dynamic Modulus of Elasticity Results for Monolithic RS-SCCHA



Figure 24: RS-SCCHA Monolithic Specimens Before (a) and After (b, c) 93 Freeze-Thaw Cycles

4.2.1.3. RS-SCCUA Monolithic Freeze-Thaw Specimens

Monolithic RS-SCCUA specimen 1 exhibited similar behavior to the monolithic RS-SCC specimens, with an initial increase in relative dynamic modulus of elasticity, followed by an increasingly steep decline. This trend can be observed in Figure 25. Specimen 1 reached 60% of its initial MOE after approximately 150 cycles. This specimen resisted more freeze-thaw cycles than any of the monolithic RS-SCC specimens.

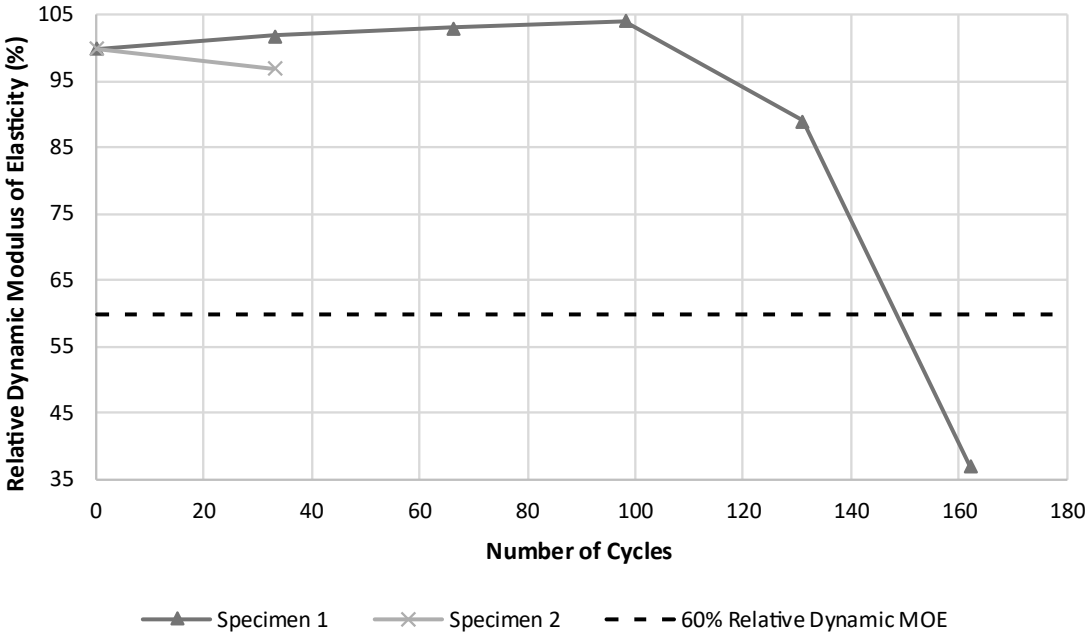


Figure 25: Relative Dynamic Modulus of Elasticity for Monolithic RS-SCCUA Specimens

The second monolithic RS-SCCUA specimen behaved differently, experiencing a much earlier failure and no initial increase in modulus of elasticity. From 0 to 33 cycles of freeze-thaw exposure, the MOE decreased slightly to 97% of the initial value. After an additional 33 cycles of exposure, for a total of 66 cycles, the specimen was too damaged for resonant frequency testing. The deterioration of specimen 2 after 66

exposure cycles is shown in Figure 26. The specimen cracked and broke in half near the center. Pieces of the specimen also broke off surrounding the crack and the bottom of the specimen. This specimen was the only freeze-thaw specimen in the study that cracked into two longitudinal halves.



Figure 26: Deterioration of RS-SCCUA After Freeze-Thaw Exposure

The cause of this large discrepancy in freeze-thaw durability of the RS-SCCUA mix is unknown, and with a sample size of only two specimens, the performance cannot be properly evaluated. It is possible that some of the behavioral differences between the RS-SCC and RS-SCCUA are due to the strength of the concrete. Out of the three mix designs using Rapid Set® cement, the RS-SCCUA concrete took the longest to develop its strength. Because the monolithic RS-SCCUA specimens were exposed to freeze-thaw conditions beginning at 7 days of age, and the compressive strength of this mix did not plateau until closer to 28 days, it is possible that the freeze-thaw durability was impacted. The relative dynamic MOE of specimen 1 increased over a period of more cycles than the RS-SCC specimens, possible due to a longer curing period before the

strength had developed. Additionally, the premature failure of specimen 2 could have been, in part, due to the lower initial strength of the concrete. The discrepancy in behavior between the two RS-SCCUA specimens could have been due to a nonhomogeneous distribution of the citric acid retarder within the concrete, causing the two specimens to develop strength at different rates or a variation in aggregate distribution.

4.2.2. Composite Freeze-Thaw Testing

4.2.2.1. RS-SCCHA Composite Freeze-Thaw Specimens

The relative dynamic MOE for the RS-SCCHA repair specimens are presented in Figure 27. Surface preparation did not have a definable effect on the freeze thaw durability of the composite RS-SCCHA specimens. The dynamic MOE behaved similarly for specimens with each surface preparation technique. Therefore, no surface preparation technique was clearly favorable over the others.

The relative dynamic MOE for all the RS-SCC and RS-SCCHA specimens showed an initial upward trend. This observed trend is likely due to additional curing after the specimens were submerged in water in the freeze-thaw chamber. Further evidence that additional curing occurred upon submersion is that two sets of initial readings were taken due to mechanical issues, which caused a delay between specimens being placed in the freeze-thaw chamber and the commencement of freeze-thaw cycles. When the second initial reading was taken after a delay of eight days, the relative dynamic MOE of all specimens increased, despite no exposure to freeze-thaw conditions during those eight days.

ASTM C666 specifies that concrete specimens should be exposed to freeze-thaw conditions until 300 cycles have passed or the relative dynamic modulus of elasticity has decreased to 60%, whichever comes first [41]. The composite RS-SCCHA specimens were exposed to 300 freeze-thaw cycles, with the lowest relative dynamic

modulus of elasticity for any specimen being 84.0% for the EA-2 specimen. As the specified number of cycles are close to completion, and the relative dynamic modulus of elasticity for all specimens is still within the acceptable range, The RS-SCCHA concrete mix seems to have sufficient freeze-thaw resistance when used as a repair material for air-entrained concrete based on this study.

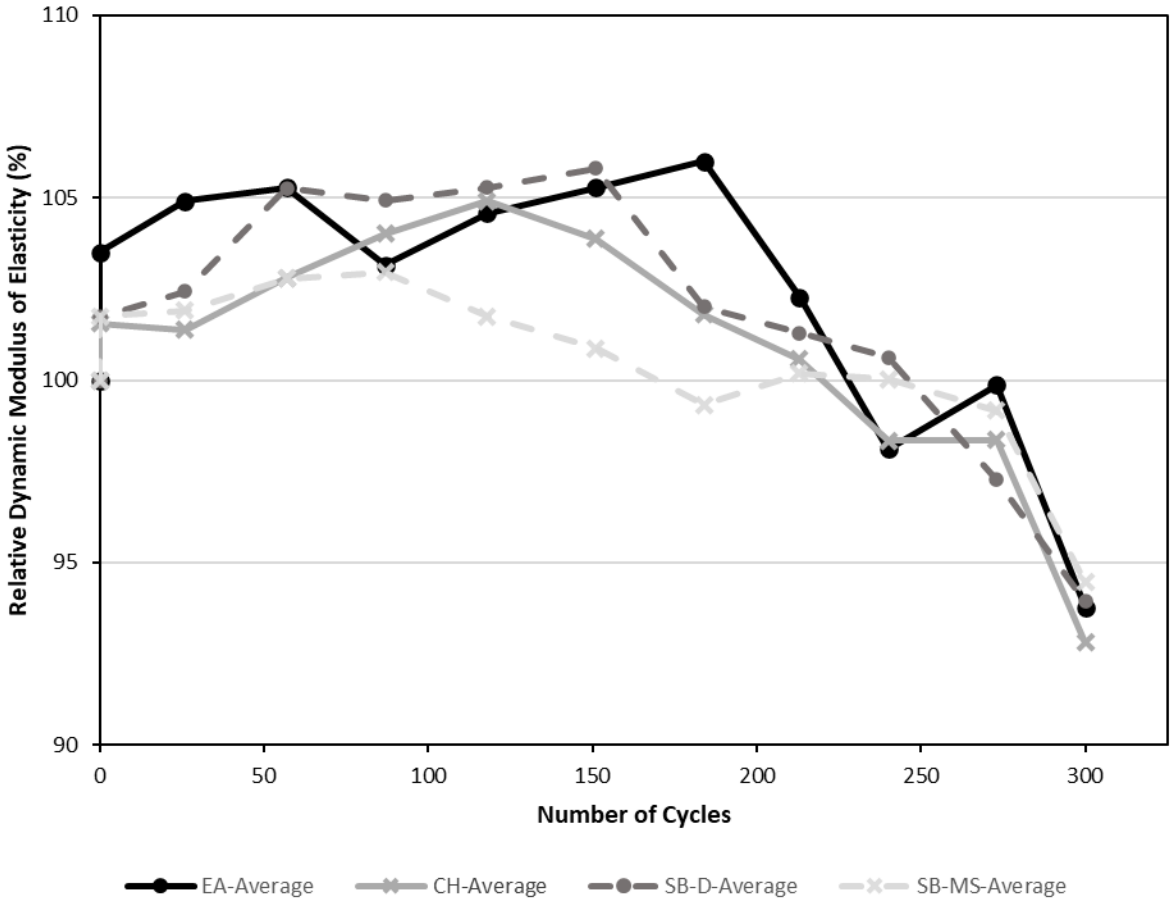


Figure 27: Relative Dynamic Modulus of Elasticity Results for RS-SCCHA Repair

In addition to analysis of the relative dynamic MOE of the specimens, visual degradation of the specimens was monitored and documented. After repeated exposure, the specimens showed increasing signs of deterioration, mainly crumbling of concrete on the edges and scaling of the surfaces of the specimens, such as shown in Figure 28. All of the freeze-thaw specimens appeared visually roughened, and aggregate particles became more visible after freeze-thaw degradation. Figure 29 shows the RS-SCCHA-SB-D1 specimen before (a) and after (b) exposure to 273 freeze-thaw cycles. On the specimen in Figure 29 (b), both the RS-SCCHA and Class AA concrete appear rougher and some of the surface concrete has eroded after exposure. The top of the RS-SCC from the same specimen is magnified in Figure 28, where concrete crumbling and aggregate are visible. These visual markers of deterioration indicate that both the Class AA and RS-SCCHA materials are affected by freeze-thaw exposure. Despite some concrete deterioration, none of the specimens exhibited large cracks or delamination of the repair material.



Figure 28: Crumbling of Edge and Surface of RS-SCCHA Specimen After Freeze-Thaw Exposure

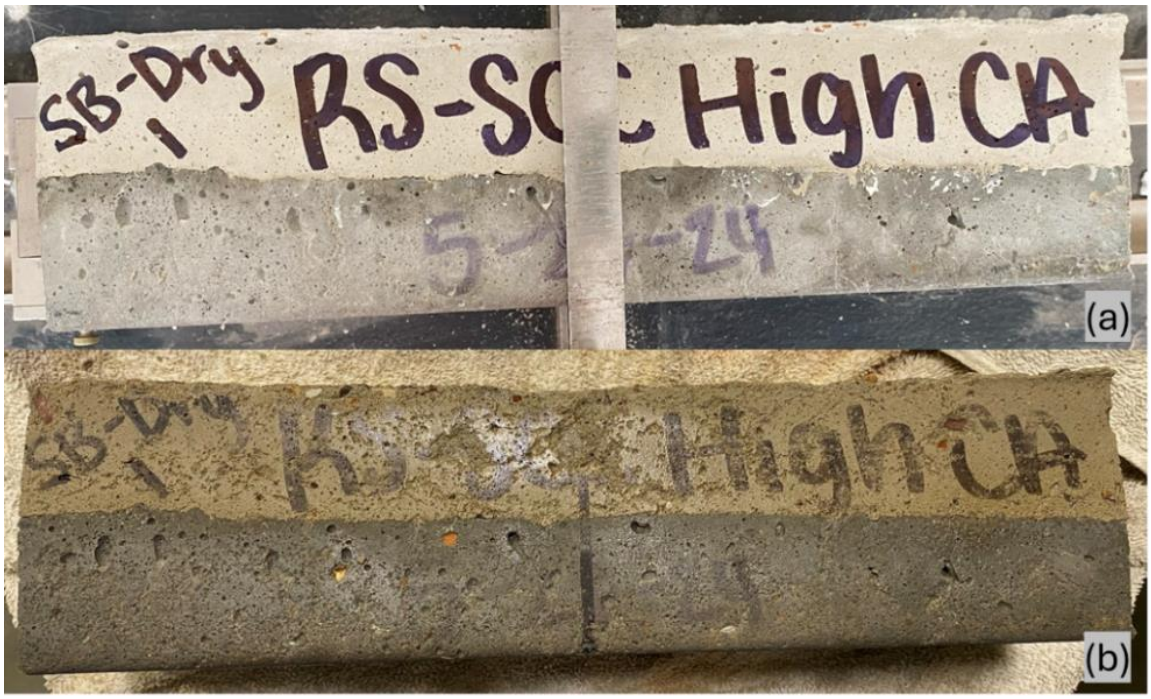


Figure 29: RS-SCCHA-SB-D1 Specimen Before (a) and After (b) Freeze-Thaw Exposure

The freeze-thaw durability results varied considerably between the monolithic RS-SCC and the composite RS-SCCHA specimens. The composite specimens had a much smaller reduction in the relative dynamic MOE, quantitatively indicating that the composite specimens performed better under freezing-thaw conditions. However, the results for the composite RS-SCCHA specimens were also less consistent than for the monolithic RS-SCC specimens. In Figure 21, the relative dynamic MOE for all monolithic specimens constantly decreased after the first round of approximately 30 cycles. However, results for the composite specimens illustrated in Figure 27, showed considerably more variation in specimen behavior. Most notably, several of the composite specimens exhibited a less defined downward trend of the relative dynamic modulus of elasticity, varying considerably between measurements throughout the exposure period.

4.2.2.2. FR-SCC Composite Freeze-Thaw Specimens

Delamination is a pertinent concern regarding composite concrete sections that are exposed to freeze-thaw conditions. Water that freezes and expands in the interface can cause the two layers of concrete to separate, i.e. delaminate. Specimens with a poor bond between concrete layers are particularly vulnerable to delamination from freeze-thaw conditions for two reasons: water penetrates the interface more easily and less force is required to separate the two layers of concrete.

Delamination was observed in the FR-SCC-SB-D1 specimen after 32 cycles of freeze-thaw exposure and in the FR-SCC-SB-D2 specimen after 227 cycles. Some of the FR-SCC composite specimens were particularly vulnerable to delamination because the material lost workability quickly during casting. The abrupt lack of workability of the FR-SCC was due to high ambient temperature during casting, the rapid-setting nature of the Komponent® cement, and the incorporation of polypropylene fibers.

As a result, the repair material did not consolidate very well for some of the specimens, leaving voids that water could easily enter. Figure 30 documents the delamination of the FR-SCC-SB-D1 repair specimen that was not well consolidated. Figure 30 (a) was taken before exposure to freeze-thaw cycles, in which honeycombing was prominent at the interface between the Class AA concrete and the FR-SCC. The overlay delaminated cleanly at the interface for both sandblasted specimens, suggesting that water readily penetrated the interface (likely aided by the poor consolidation of the FR-SCC) and that the bond between the two concrete materials was susceptible to freeze-thaw damage, as shown in Figure 30 (b).



Figure 30: Poorly Consolidated FR-SCC Specimen Before (a) and After (b) Freeze-Thaw Exposure

The failure surfaces of the FR-SCC and Class AA concrete are aligned in Figure 31. In the figure, the FR-SCC interface is on top and the Class AA interface is on the bottom. As illustrated in Figure 31, some aggregate was fractured along the failure plane, with part of the rock bonded to the Class AA concrete and the corresponding part bonded to the FR-SCC overlay. Conversely, little to no transfer of one type of concrete paste onto the other was observed at the interface of this specimen, indicating that the failure of this specimen was caused by inadequate bond between the substrate and overlay concrete. The presence of fractured aggregate combined with the absence of paste transfer suggests that the FR-SCC bonded to the Class AA aggregate, which was slightly exposed from sandblasting, more effectively than the FR-SCC bonded to the paste of the Class AA concrete.

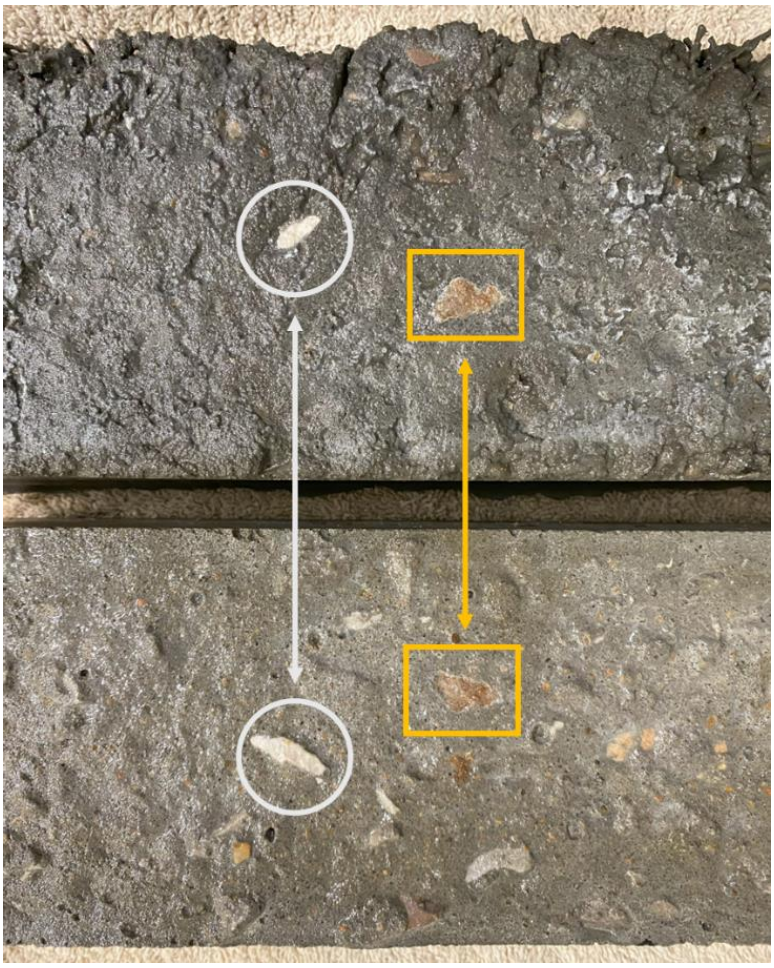


Figure 31: Failure Surface of FR-SCC-SB-1 Specimen Showing Fractured Aggregate Particles at the Interface

The relative dynamic modulus of elasticity data from the composite FR-SCC freeze-thaw testing is shown in Figure 32. The average modulus was plotted for each surface preparation, except for the SB-D technique, as specimen 1 only yielded the initial resonant frequency reading before the repair delaminated. The complete resonant frequency and relative dynamic MOE data is provided in Appendix C, Table 36 and Table 37, respectively.

The CH and EA surface preparation techniques generally had a higher average relative dynamic MOE than the SB-D and SB-MS specimens, suggesting that sandblasting may not be the best surface preparation technique for freeze-thaw

considerations. However, the degree of consolidation likely had a greater impact on specimen performance. Regardless, all specimens except the SB-D specimens had a relative dynamic MOE greater than 100% after 307 cycles of exposure.

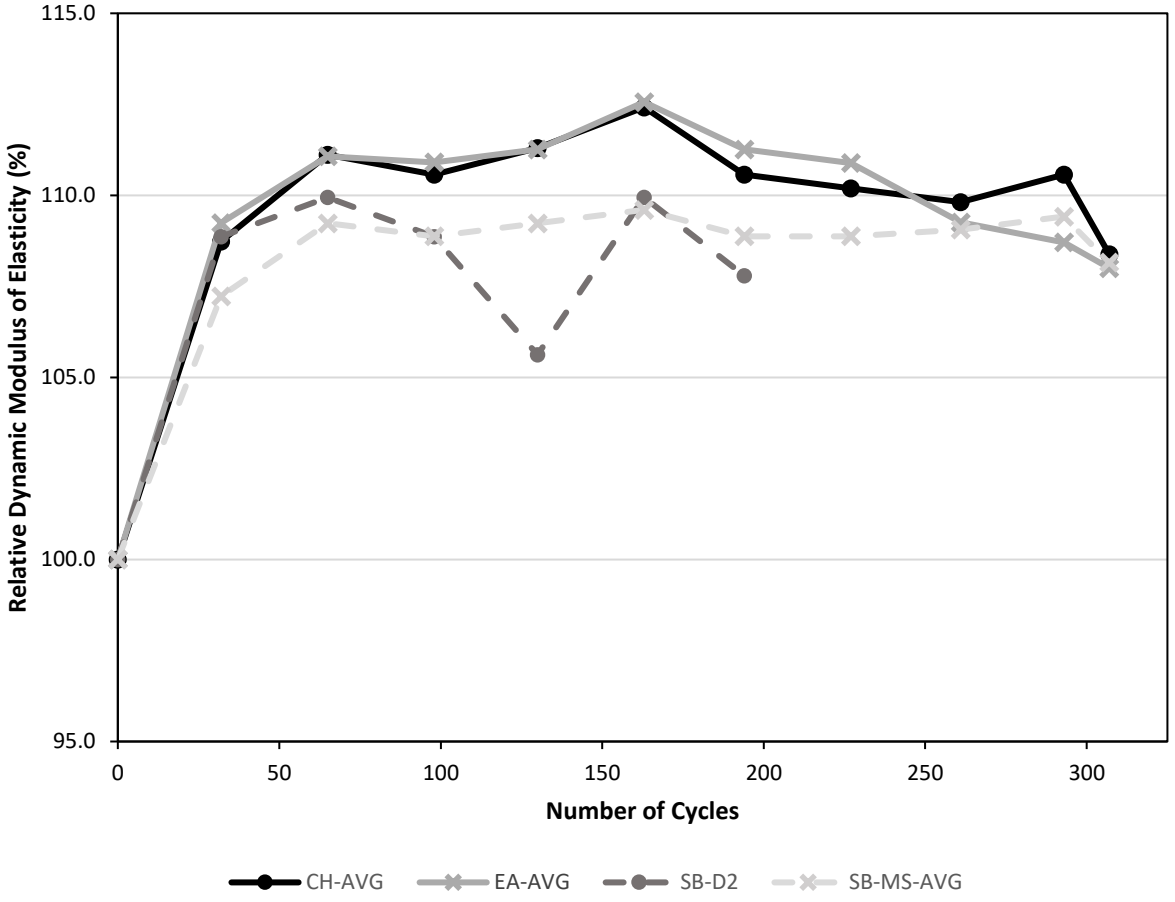


Figure 32: Relative Dynamic Modulus of Elasticity Results for FR-SCC Repair

Additional curing throughout the exposure period may have been the cause of the increased MOE values. The FR-SCC overlays were cast with concrete from the FR-2 mix and were placed in the freeze-thaw chamber at an overlay age of 7 days. The average compressive strength for this mix, presented in Appendix A (Table 19), was 6709 psi at 7 days and 9199 psi at 28 days. The increase in strength between 7 and 28 days indicates that the concrete had not reached ultimate strength at 7 days when the

initial resonant frequency readings were taken. The increase in compressive strength indicates additional curing beyond the beginning freeze-thaw exposure, which may explain the increase in relative dynamic modulus of elasticity.

Another likely reason that the freeze-thaw data for the FR-SCC specimens did not indicate deterioration (aside from the delaminated repairs) is that both the Class AA concrete and the FR-SCC were air entrained. Air entrainment has proven to be beneficial in concrete durability against freeze-thaw conditions. Figure 33 shows one of the specimens after 307 cycles of freeze-thaw exposure. The concrete is noticeably less damaged than for some of the other repair materials. Even the specimens which delaminated (see Figure 30) did not experience significant visual damage to the Class AA concrete or the FR-SCC.



Figure 33: FR-SCC Composite Specimen after 307 Exposure Cycles

4.2.2.3. Composite Freeze-Thaw Specimens with In-Service Class AA Concrete

The data for the repair specimens with Class AA concrete from a former bridge deck is summarized in Appendix C, Table 38 through Table 41. Due to equipment limitations with the freeze-thaw chamber, most of the composite freeze-thaw specimens with in-service Class AA concrete have not reached the end of the required exposure period. Testing for the RS-SCCHA-CH repair specimens finished when the repairs for each of the specimens delaminated. RS-SCCHA-CH specimen 2, shown in Figure 34 (a) delaminated first after 132 cycles. RS-SCCHA-CH specimen 1, shown in Figure 34 (b) delaminated after 164 cycles.

The Class AA bases that were cut from the bridge deck slab had an existing overlay, which can also be seen in Figure 34, where the top layer is the RS-SCCHA, the middle layer is the overlay on the bridge deck, and the bottom layer is the base Class AA concrete from the bridge deck. The existing overlay from the bridge deck is worth considering, as the RS-SCCHA overlay delaminated before the overlay that was on the bridge deck while it was in service. The bond behavior may be influenced by the maturity of each layer of concrete.

However, more research with in-service concrete should be done. If the bond between CSA cement concrete and conventional concrete is less resistant to freeze-thaw conditions than the bond between conventional concrete and conventional concrete, CSA cement concrete could be a less desirable repair material in regions where freeze-thaw conditions are of concern.

The relative dynamic MOE trend of the RS-SCCHA-CH bridge deck repair specimens was also different than for the composite specimens with Class AA concrete cast more recently. As shown in Figure 35, the RS-SCCHA-CH specimens did not have an initial increase in the MOE. The RS-SCCHA-SB relative dynamic modulus data is also presented in Figure 35, although testing is ongoing. Unlike the CH specimens, the SB specimens did show an initial increase in MOE.



Figure 34: Delamination of RS-SCCHA-CH Repairs on Bridge Deck Specimens, (a) RS-SCCHA-CH Specimen 2 and (b) RS-SCCHA-CH Specimen 1

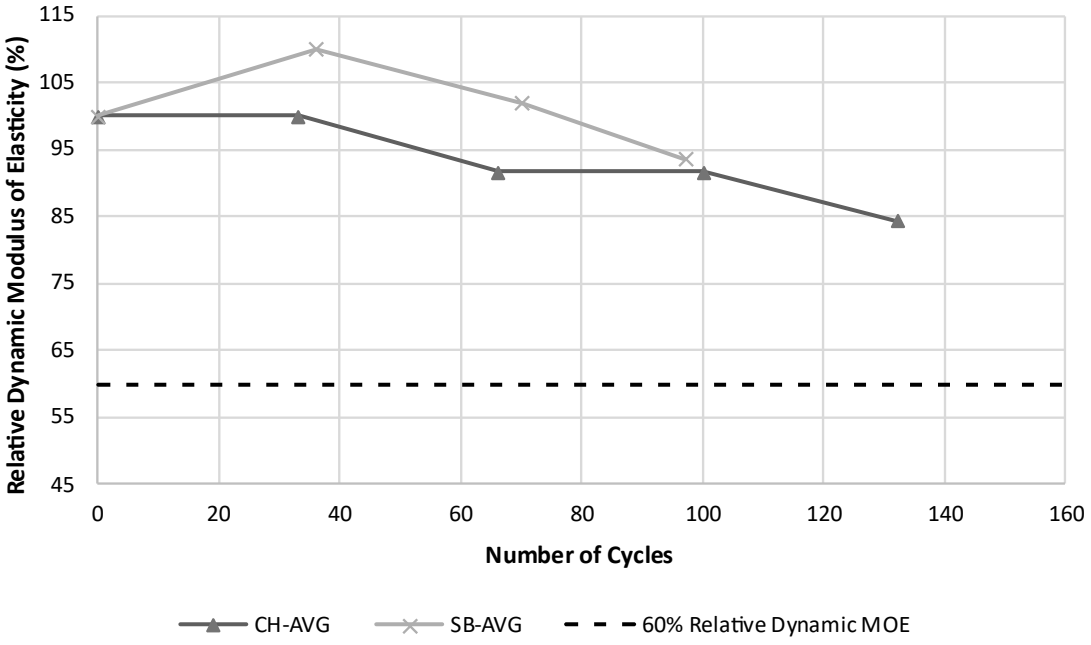


Figure 35: Relative Dynamic MOE Data for RS-SCCHA Bridge Deck Repair Specimens

Bridge deck repair specimens were also cast with FR-SCC as a repair material. Testing for the FR-SCC-CH and FR-SCC-SB specimens is ongoing. The FR-SCC repair specimen have been exposed to 95 freeze-thaw cycles so far. The initial relative dynamic MOE trend for the FR-SCC repair specimens is shown in Figure 36.

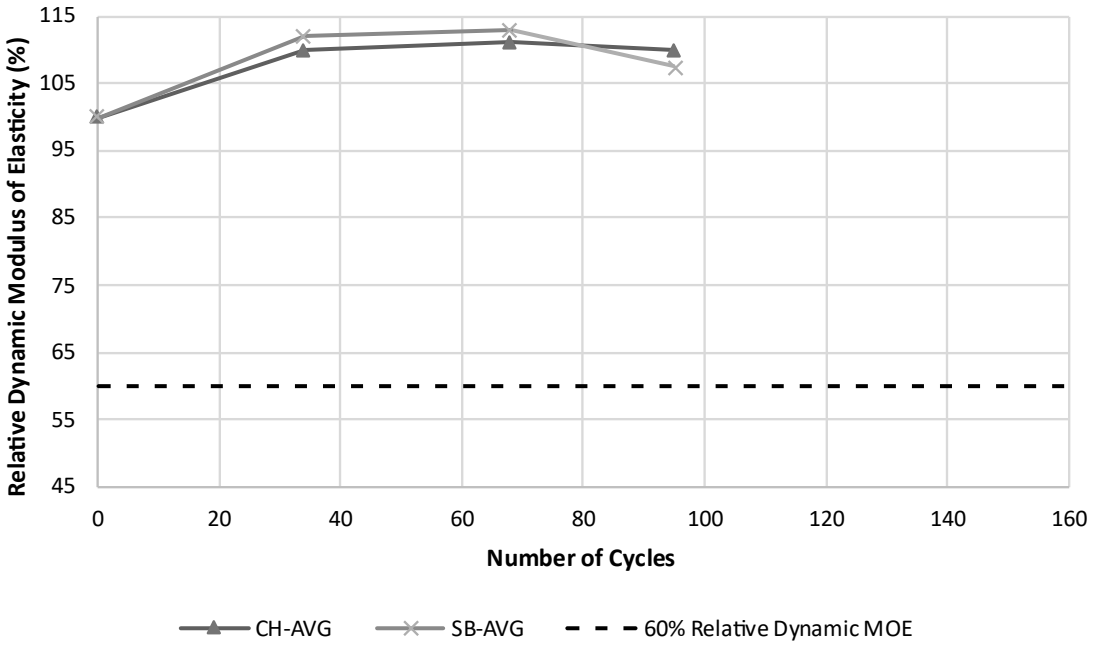


Figure 36: Relative Dynamic MOE Data for FR-SCC Bridge Deck Repair Specimens

The overlays on the FR-SCC-CH and FR-SCC-SB bridge deck repair specimens did not sustain significant visual damage during the first 95 exposure cycles, although the Class AA concrete on the FR-SCC-SB specimen appears to be slightly more textured. The repair concrete on the RS-SCCHA-SB specimen was visibly roughened after 97 cycles. Figure 37 shows a RS-SCCHA-SB specimen after 97 cycles (a), a FR-SCC-CH specimen after 95 cycles (b), and a FR-SCC-SB specimen after 95 cycles (c). After exposure to approximately the same number of cycles, visual observation and resonant frequency data indicate that the RS-SCCHA repair concrete was more damaged than the FR-SCC repair concrete. The RS-SCCHA appears more textured

than the FR-SCC, with small pieces of the repair concrete beginning to flake away from the surface. The average dynamic MOE of the RS-SCCHA-SB specimens was 93.7% after 97 cycles, compared to 109.9% and 107.6% after 95 cycles for the FR-SCC-CH and FR-SCC-SB specimens, respectively. Although the RS-SCCHA-SB specimens were exposed to two more freeze-thaw cycles than the FR-SCC specimens at the time of evaluation, the differences in condition are more significant than would be expected from two additional cycles. Instead, the differences in condition are more likely to be indicative of the freeze-thaw durability of the repair materials. The lack of entrained air in the RS-SCCHA is likely the reason that the material deteriorated faster than the FR-SCC, which is air entrained.



Figure 37: Bridge Deck Repair Specimens After Initial Exposure Period: RS-SCCHA-SB Specimen After 97 Cycles (a), FR-SCC-CH Specimen After 95 Cycles (b), and FR-SCC-SB Specimen after 95 Cycles (c)

4.2.3. Durability of Monolithic Versus Composite Freeze-Thaw Specimens

An additional finding was that the monolithic CSA cement concrete freeze-thaw specimens generally deteriorated after fewer exposure cycles than the composite specimens. This observed behavior may be explained by the air void system of the CSA cement repair materials. The RS-SCC, RS-SCCHA, and RS-SCCUA mixes were not air entrained, while the FR-SCC and Class AA concrete were. Without entrained air, the dense matrix of the CSA cement repair materials may have been more vulnerable to cracking and deterioration from freeze-thaw exposure.

The monolithic specimens had a larger volume and surface area of the CSA cement concrete than the composite specimens, which may have caused the monolithic specimens to deteriorate more rapidly than the composite specimens if the CSA cement concrete materials were more vulnerable to freeze-thaw exposure than the Class AA concrete. It is also possible that the interface region provided room for expansion, relieving some of the internal pressure from freezing. The difference in performance between monolithic and composite specimens may have additionally been caused in part by the Class AA concrete, which was air entrained, providing some restraint for the repair materials. The monolithic specimens did not have this restraint.

4.2.4. Large-Scale Repair Specimens

Long-term observation of the repair slabs was not possible within the timeframe of this project, however, they will continue to be observed for resistance to extended exposure. Thus, the results for the large-scale repair slabs are centered on feasibility of casting (consolidation, set time, and repair material strength), as well as initial behavior (early cracking or signs of separation at the interfaces).

So far, the RS-SCC repair slab has been outdoors for over 4 months, and the FR-SCC slab has been outdoors for over 2 months. Although due to the timing of

casting and the local climate, there was minimal natural freezing during this initial exposure period. The RS-SCC specimen was exposed to freezing temperatures for a short period of time. The FR-SCC repair was not cast until after freezing conditions had subsided for the year. The casting dates of the corresponding mixes (RS-3 and FR-3) are presented in Table 3. Neither repair slab has shown signs of repair material delamination or degradation at this time.

4.2.4.1. RS-SCC Repair Specimen

The RS-SCC repair material consolidated well, as evidenced by Figure 38. Figure 38 (a) shows the outer edge of the chipping hammer section, and Figure 38 (b) is the interior edge of the sandblasted section. On both ends, the RS-SCC filled the contours of the conventional concrete without leaving voids. An initial slump flow of 25 in. and proper dose of citric acid (0.2 wt.%) ensured that the material had sufficient workability and remained workable for long enough to conform to the varying surface of the conventional concrete. The satisfactory consolidation of the RS-SCC should help ensure the strength of the repair, as well as preventing excess water from entering the interface, although the observation period of the study was not long enough to confirm this conjecture.



Figure 38: RS-SCC Interfaces on Large-Scale Repair Slab

As the RS-SCC repair concrete cured, some shrinkage cracking was observed. These shrinkage cracks mainly occurred near the interface between the RS-SCC and conventional concrete in regions where the RS-SCC was filled flush with the conventional concrete during casting. Figure 39 shows a shrinkage crack on the CH surface preparation side of the RS-SCC repair slab. The pictured shrinkage crack is representative of other shrinkage cracks that occurred throughout the length of the slab. There was no noticeable difference in shrinkage cracking behavior between the CH and CH plus SB surface preparations.

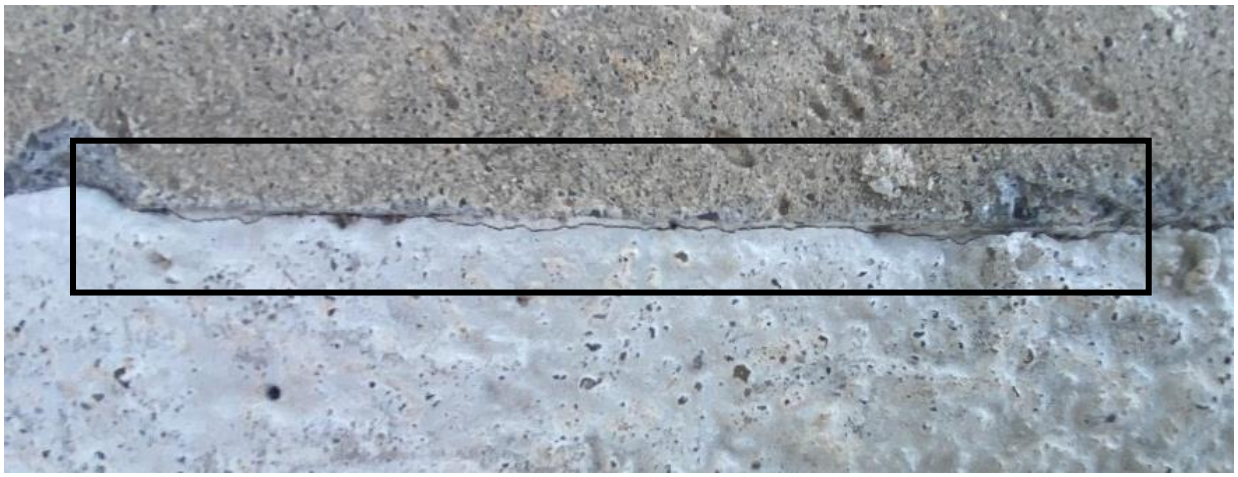


Figure 39: Shrinkage Crack on Large-Scale RS-SCC Repair Slab

During the limited exposure period, the RS-SCC repair slab was exposed to a short duration of ambient freezing temperatures, as well as ice accumulation. Figure 40 shows the slab (a) and compressive strength cylinders (b) with ice accumulation due to freezing rain. The RS-SCC repair concrete was 7-days old during the exposure event pictured in Figure 40.



Figure 40: RS-SCC Large-Scale Repair Slab (a) and Compressive Strength Cylinders (b) with Ice Accumulation

The specimen has not noticeably deteriorated with environmental exposure during the initial observation period. Figure 41 (a) and (b) shows the current condition of the slab, after approximately 4 months of environmental exposure. The side of the slab with the CH plus SB surface is shown in Figure 41 (a). The repair section looks visually similar to the pre-exposure condition and the repair has not exhibited signs of delamination. The same is true of the CH side of the repair slab. Figure 41 (b) shows the condition of the RS-SCC material after exposure. There was no observable cracking or deterioration of the repair concrete to indicate damage from exposure.

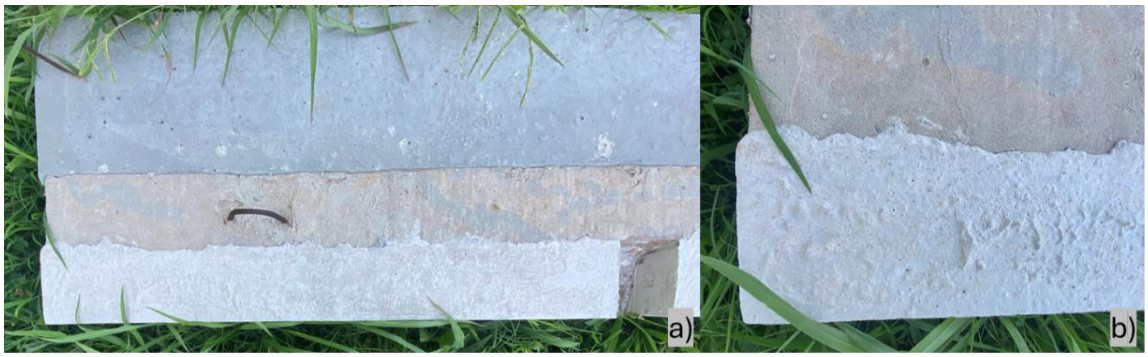


Figure 41: RS-SCC Large-Scale Repair Slab with the CH plus SB Surface Condition (a) and Close-up of the RS-SCC Material (b) After Environmental Exposure

Another consideration for the repair material was whether the compressive strength would be affected by freeze-thaw exposure and/or curing temperature. The 28-day compressive strength was compared for cylinders that were placed outside with the slab and cylinders that were placed in a 68°F temperature-controlled environment. There was not a significant difference between the average compressive strength of the outdoor versus temperature-controlled specimens. The specimens that were cured outdoors were subjected to temperature variation (including freezing temperatures) and precipitation, as evidenced in Figure 40 (b). The specimens cured in a regulated environment were maintained at a constant temperature and were not exposed to moisture beyond ambient conditions. The specimens that were exposed to environmental conditions exhibited slightly higher average compressive strength (10,710 psi compared to 10,290 psi), although the strength difference was minute and likely due to natural variation of concrete specimens, rather than the exposure conditions. Table 9 details the compressive strength data for the specimens cured outdoors and in a controlled environment.

Table 9: 28-Day Compressive Strength of RS-SCC Specimens for Environmental and Controlled Curing Conditions

Cylinder Number	**Compressive Strength Under Environmental Curing Conditions (psi)**	**Compressive Strength Under Controlled Curing Conditions (psi)**
1	10,400	10,063
2	10,811	10,544
3	10,909	10,250
Average	**10,710**	**10,290**

4.2.4.2. FR-SCC Repair Specimen

The large-scale FR-SCC repair specimen casting went as intended and the repair consolidated well. The material used for the repair was from mix FR-3. The workability of the repair slab material was a significant improvement from the FR-2 mix, which was used to cast overlays for the composite pull-off and freeze-thaw specimens. The slump flow of the FR-3 mix was 25 in., compared to 17.5 in. for the FR-2 mix. The difference in workability between the two mixes cannot be properly explained, as the FR-2 mix included a higher dosage of HRWR (10.11 oz/cwt compared to 9.25 oz/cwt) and was cast at a lower ambient temperature. Differences in behavior between the FR-2 and FR-3 mixes were therefore most likely due to the cementitious materials used. Several months elapsed between the casting of mixes FR-2 and FR-3, and as a result, separate shipments of OPC and different bags of Type K cement from the same pallet were used in the two mixes. The age and storage conditions of the Type K cement may have had an especially significant impact on the behavior of the concrete. The Type K cement used in this study came in 50 lb bags, and when a new bag was opened, the leftover cement was stored in a closed 5-gallon bucket for use in future batches. With several months in between the FR-2 and FR-3 mixes, separate bags of the Type K cement would have been used. It is possible that if the buckets were not completely air tight, one bag of cement may have been exposed to more moisture than the other. Additionally, the Type K cement used in the second batch was several months older than in the first batch. It is possible that Type K cement used in the two batches had differing levels of reactivity due to moisture exposure and/or age.

The large-scale FR-SCC repair specimen after demolding is shown in Figure 42. It was clear that the FR-SCC consolidated well, as there were no visible voids or honeycombing at the interface or in the FR-SCC. The repair cast on this slab suggests that a similar size and complexity of repair would be possible in the field, provided that ambient temperatures are low enough to prevent rapid workability loss of the material.

The FR-SCC repair slab, like the RS-SCC slab, did not exhibit visual signs of deterioration after the approximately 2-month exposure period completed during this

study. However, sub-freezing temperatures did not occur during the FR-SCC repair slab exposure period, so freeze-thaw damage would not have occurred. Figure 43 shows the end of the FR-SCC repair before (a) and after (b) exposure. The images are from the end of the slab with the CH plus SB surface preparation, but the same behavior was observed for the other end with only the CH surface preparation. This figure further proves the adequate consolidation of the FR-SCC, as it conforms to the shape of the existing slab and no gaps are visible. Good consolidation is important for the durability of concrete repairs subject to freeze-thaw conditions, as water can readily penetrate voids and increase the risk of delamination. As evidenced by Figure 43, there was no visual difference between the condition of the FR-SCC before and after being placed outside.



Figure 42: Large-Scale FR-SCC Repair Slab Before Exposure

The RS-SCC and FR-SCC repair slabs differed in shrinkage behavior of the repair concrete. Unlike for the RS-SCC, shrinkage cracking was not observed in the FR-SCC repair concrete. Figure 44 shows a zone at the interface between the FR-SCC and existing slab, which is comparable to the RS-SCC repair interface shown in Figure 39. Despite similar interface conditions, shrinkage cracking is not seen on the FR-SCC repair slab. There is a difference in age between the RS-SCC and FR-SCC, with the materials being approximately 4 months and 2 months old, respectively. However,

shrinkage occurs most rapidly at the beginning of the curing period, so the age difference is likely not the reason for the difference in shrinkage cracking behavior. Instead, the lack of shrinkage cracking is an indication that the shrinkage compensating property of the Type K cement used in the FR-SCC mix design helped to offset shrinkage, thereby reducing shrinkage cracking.



Figure 43: Comparison of FR-SCC Repair Material Before (a) and After (b) Exposure



Figure 44: Interface Zone of FR-SCC Repair Slab

Chapter 5. Conclusions and Recommendations

Based on the data collected, CSA cements are a promising material for rapid infrastructure repair based on their reduced environmental impact, rapid strength gaining behavior, adequate bond to conventional concrete, and sufficient freeze-thaw durability. A few conclusions and recommendations can be made regarding CSA cement concrete repair materials and surface preparations. However, these interpretations should be refined/expanded through future research, and the conditions under which the data in this study was collected should be considered when interpreting the results. A few such limitations include failure mode of composite pull-off specimens, maturity of the base and repair concrete, uncertainty in freeze-thaw exposure temperatures, and development of concrete strength during the freeze-thaw exposure period.

5.1. Conclusions on General Material Performance

- All four CSA cement repair materials (RS-SCC, RS-SCCHA, RS-SCCUA, and FR-SCC) exhibited adequate compressive strength to be considered for use as repair materials.
- Sensitivity of CSA cement concrete to high temperatures and challenges with workability must be considered when determining feasibility of use.
- The workability of the FR-SCC was particularly challenging, partially due to the inclusion of fibers.
- Refinement of air-entraining admixture dosage or procedure should be pursued in order to provide an air content that is consistently within the acceptable range.
- It is possible to cast and consolidate moderately sized repairs with CSA cement concrete.

5.2. Conclusions on Bond Strength

- The tensile strength of the concrete mixes in this study (based on ASTM C1583 Direct Tension) from strongest to weakest was RS-SCC, RS-SCCHA, Class AA, FR-SCC, and RS-SCCUA.
- The FR-SCC had a comparatively low tensile strength, but the inclusion of polypropylene fibers gave the material post-cracking tensile strength.
- The pull-off strength of the overlay specimens was heavily impacted by surface preparation method and execution, but was not significantly impacted by concrete type.
- The SB-D and SB-MS surfaces generally performed better in pull-off testing than the CH and EA surfaces.
- Coring and/or surface preparation may damage the underlying concrete.

5.3. Conclusions on Freeze-Thaw Durability

- The lack of entrained air may have negatively affected the freeze-thaw durability of the RS-SCC CSA cement concrete repair materials in this study.
- Monolithic freeze-thaw specimens tended to deteriorate after fewer cycles than composite freeze-thaw specimens.
- The freeze-thaw resistance of concrete repairs can be highly affected by improper consolidation.
- Surface preparation technique did not seem to have as large of an impact on freeze-thaw resistance as it did for pull-off strength.
- Many freeze-thaw specimens showed increases in dynamic MOE over the course of freeze-thaw testing, which was likely related to curing of the concrete,

rather than an indicator of freeze-thaw resistance.

- Only a few composite freeze-thaw specimens had delamination of the repair material, and most of the specimens reached 300 cycles of exposure before reaching the 60% threshold for relative dynamic MOE, suggesting that the freeze-thaw resistance of the bond between Class AA and CSA cement concretes may be adequate.

5.4. Recommendations for Future Research

Additional research in the following areas would further the understanding of CSA cement concrete behavior and help facilitate implementation efforts:

- Bond strength of CSA cement concrete repairs using surface preparation techniques approved by the International Concrete Repair Institute (ICRI).
- Effects of air-entrainment on CSA cement concrete behavior and freeze-thaw resistance.
- The effects of supplementary cementitious materials on mechanical performance and bond strength/durability.
- Bond behavior between CSA cement concrete and in-service conventional concrete.
- Bond performance of CSA cement concrete repairs after service level wear.
- Optimal air content of CSA cement concrete subject to freeze-thaw conditions.
- Adjusted practices for mixing rapid-setting CSA cement materials in extreme temperatures.
- Corrosion resistance of reinforced CSA cement concrete, especially when exposed to deicing salts.

References

[1] R. Meininger, “Alternative Cementitious Materials in Transportation - Sustainable, Durable Substitutes for Portland Cement | FHWA,” Federal Highway Administration. Accessed: Nov. 15, 2024. [Online]. Available: https://highways.dot.gov/research/publications/ear/FHWA-HRT-18-031

[2] Y. Cancio Díaz *et al.*, “Limestone calcined clay cement as a low-carbon solution to meet expanding cement demand in emerging economies,” *Dev. Eng.*, vol. 2, pp. 82–91, Jan. 2017, doi: 10.1016/j.deveng.2017.06.001.

[3] R. M. Andrew, “Global CO_2 emissions from cement production, 1928–2018,” *Earth Syst. Sci. Data*, vol. 11, no. 4, pp. 1675–1710, Nov. 2019, doi: 10.5194/essd-11-1675-2019.

[4] E. Jeon, K. Lee, and C. Lee, “Development of a New Clean Development Mechanism Methodology for the Quantification of Greenhouse Gas in Calcium Sulfoaluminate Cement,” *Sustainability*, vol. 11, no. 5, Art. no. 5, Jan. 2019, doi: 10.3390/su11051482.

[5] R. J. Thomas, M. Maguire, A. D. Sorensen, and I. Quezada, “Calcium Sulfoaluminate Cement,” 2018, Accessed: Nov. 27, 2024. [Online]. Available: https://www.concrete.org/publications/internationalconcreteabstractsportal.aspx?m=details&ID=51702289

[6] S. Nie *et al.*, “Analysis of theoretical carbon dioxide emissions from cement production: Methodology and application,” *J. Clean. Prod.*, vol. 334, p. 130270, Feb. 2022, doi: 10.1016/j.jclepro.2021.130270.

[7] C. W. Hargis, A. Telesca, and P. J. M. Monteiro, “Calcium sulfoaluminate (Ye’elimite) hydration in the presence of gypsum, calcite, and vaterite,” *Cem. Concr. Res.*, vol. 65, pp. 15–20, Nov. 2014, doi: 10.1016/j.cemconres.2014.07.004.

[8] S. Park, Y. Jeong, J. Moon, and N. Lee, “Hydration characteristics of calcium

sulfoaluminate (CSA) cement/portland cement blended pastes," *J. Build. Eng.*, vol. 34, p. 101880, Feb. 2021, doi: 10.1016/j.jobe.2020.101880.

[9] G. Le Saoût, B. Lothenbach, A. Hori, T. Higuchi, and F. Winnefeld, "Hydration of Portland cement with additions of calcium sulfoaluminates," *Cem. Concr. Res.*, vol. 43, pp. 81–94, Jan. 2013, doi: 10.1016/j.cemconres.2012.10.011.

[10] C. D. Murray, R. W. Floyd, and C. C. E. Ramseyer, "Using Belitic Calcium Sulfoaluminate Cement For Precast, Prestressed Concrete Beams," Precast/Prestressed Concrete Institute. Accessed: Dec. 06, 2024. [Online]. Available: https://www.pci.org/PCI/PCI/Publications/PCI_Journal/Issues/2019/March-April/Using_belitic_calcium_sulfoaluminate_cement_for_precast_prestressed_concrete_beams.aspx

[11] S. Roswurm, "Application of Rapid-Setting Belitic Calcium Sulfoaluminate Cements in Pretensioned, Prestressed Concrete," May 2023, Accessed: Dec. 06, 2024. [Online]. Available: https://shareok.org/handle/11244/337148

[12] J. Starks, "Mechanical Performance of Post-Tensioned Residential Foundation Slabs Using Expansive BCSA Cements." 2023.

[13] C. Wirkman, "Performance of Fiber-Reinforced Self-Consolidating Concrete for Repair of Bridge Sub-Structures," May 2016, Accessed: Jul. 21, 2025. [Online]. Available: http://hdl.handle.net/11244/34596

[14] J. Choate, "Implementing Fiber-Reinforced, Self-Consolidating Concrete as a Repair Material for AASHTO Prestressed Concrete Girders," Aug. 2018, Accessed: Jul. 21, 2025. [Online]. Available: https://hdl.handle.net/11244/301337

[15] Z. Long *et al.*, "Hydration, strength, and microstructure evolution of Portland cement-calcium sulphoaluminate cement-CSH seeds ultra-early strength cementitious system," *Constr. Build. Mater.*, vol. 430, p. 136492, Jun. 2024, doi: 10.1016/j.conbuildmat.2024.136492.

[16] Federal Highway Administration, “ABC - Accelerated - Technologies and Innovations - Construction - Federal Highway Administration.” Accessed: Mar. 02, 2025. [Online]. Available: https://www.fhwa.dot.gov/bridge/abc/

[17] M. Shakouri, A. A. Ahmed, M. Teymouri, and D. Trejo, “Corrosion Resistance of Calcium Sulfoaluminate Cementitious Systems,” *J. Mater. Civ. Eng.*, vol. 35, no. 8, p. 04023238, Aug. 2023, doi: 10.1061/JMCEE7.MTENG-15178.

[18] B. Šavija and M. Luković, “Carbonation of cement paste: Understanding, challenges, and opportunities,” *Constr. Build. Mater.*, vol. 117, pp. 285–301, Aug. 2016, doi: 10.1016/j.conbuildmat.2016.04.138.

[19] D. Lv *et al.*, “Freeze–Thaw Damage Characteristics of Concrete Based on Compressive Mechanical Properties and Acoustic Parameters,” *Materials*, vol. 17, no. 5, p. 1010, Feb. 2024, doi: 10.3390/ma17051010.

[20] R. Wang, Z. Hu, Y. Li, K. Wang, and H. Zhang, “Review on the deterioration and approaches to enhance the durability of concrete in the freeze–thaw environment,” *Constr. Build. Mater.*, vol. 321, p. 126371, Feb. 2022, doi: 10.1016/j.conbuildmat.2022.126371.

[21] J. Tanesi and R. Meininger, “Freeze-Thaw Resistance of Concrete With Marginal Air Content, December 2006 - FHWA-HRT-06-117.” Accessed: May 30, 2025. [Online]. Available: https://www.fhwa.dot.gov/publications/research/infrastructure/pavements/pccp/06117/

[22] L. Qin, X. Gao, and A. Zhang, “Potential application of Portland cement-calcium sulfoaluminate cement blends to avoid early age frost damage,” *Constr. Build. Mater.*, vol. 190, pp. 363–372, Nov. 2018, doi: 10.1016/j.conbuildmat.2018.09.136.

[23] P. Li, X. Gao, K. Wang, V. W. Y. Tam, and W. Li, “Hydration mechanism and early frost resistance of calcium sulfoaluminate cement concrete,” *Constr. Build. Mater.*, vol. 239, p. 117862, Apr. 2020, doi: 10.1016/j.conbuildmat.2019.117862.

[24] K. H. Khayat, “Optimization and performance of air-entrained, self-consolidating concrete,” *ResearchGate*, Sep. 2000, Accessed: Mar. 23, 2025. [Online]. Available: https://www.researchgate.net/publication/279894168_Optimization_and_performance_of_air-entrained_self-consolidating_concrete

[25] F. Su, T. He, Q. Yu, X. Ma, Y. Ke, and G. Chen, “The adhesion performance of concrete repair interface under the coupling abrasion and freeze-thaw,” *Constr. Build. Mater.*, vol. 487, p. 142146, Aug. 2025, doi: 10.1016/j.conbuildmat.2025.142146.

[26] P. Shaji and P. Chaunsali, “Durability Assessment of Expansive and Nonexpansive Calcium Sulfoaluminate Belite Cement Concrete in Chloride-Rich Environments,” *J. Mater. Civ. Eng.*, vol. 36, no. 7, p. 04024195, Jul. 2024, doi: 10.1061/JMCEE7.MTENG-17544.

[27] P. Alapati, M. K. Moradllo, N. Berke, M. T. Ley, and K. E. Kurtis, “Designing corrosion resistant systems with alternative cementitious materials,” *Cement*, vol. 8, p. 100029, Jun. 2022, doi: 10.1016/j.cement.2022.100029.

[28] A. M. Abd El Fattah and I. N. A. Al-Duais, “Modeling of Chloride Binding Capacity in Cementitious Matrices Including Supplementary Cementitious Materials,” *Crystals*, vol. 12, no. 2, Art. no. 2, Feb. 2022, doi: 10.3390/cryst12020153.

[29] N. Ghafoori, M. O. Maler, M. Najimi, and A. Hasnat, “De-icing salt resistance of high early-strength concrete for rapid repairs,” *MATEC Web Conf.*, vol. 361, p. 03001, 2022, doi: 10.1051/matecconf/202236103001.

[30] S. M. Levy, “Section 5 - Calculations Relating to Concrete and Masonry,” in *Construction Calculations Manual*, S. M. Levy, Ed., Boston: Butterworth-Heinemann, 2012, pp. 211–264. doi: 10.1016/B978-0-12-382243-7.00005-X.

[31] K. Sakai, T. Matsuka, and Y. Suzuki, “Low-Carbon Concrete Using Ground Granulated Blast-Furnace Slag and Fly Ash,” in *Innovative Materials and Techniques in Concrete Construction*, M. N. Fardis, Ed., Dordrecht: Springer

Netherlands, 2012, pp. 101–114. doi: 10.1007/978-94-007-1997-2_6.

[32] Oklahoma Department of Transportation Transportation Commission, “Oklahoma Department of Transportation 2019 Standard Specifications for Highway Construction.” Oklahoma Department of Transportation. [Online]. Available: https://www.odot.org/c_manuals/specbook/2019%20-FULL-SPEC-Web-Version.pdf

[33] R. Coleman, “Comparative Study of Surface Preparation And Bond Angle Combinations For Bridge Repair Using Ultra-High Performance Concrete Alternative,” Dec. 2018, Accessed: Dec. 06, 2024. [Online]. Available: https://hdl.handle.net/11244/316286

[34] *ASTM C143/C143M-20 Standard Test Method for Slump of Hydraulic-Cement Concrete*, 2020. Accessed: Dec. 06, 2024. [Online]. Available: https://compass.astm.org/content-search/?content=c143&stype=A&page=0

[35] *ASTM C138/C138M-24a Standard Test Method for Density (Unit Weight), Yield, and Air Content (Gravimetric) of Concrete*, 2024. Accessed: Dec. 06, 2024. [Online]. Available: https://compass.astm.org/document/?contentCode=ASTM%7CC0138_C0138M-24A%7Cen-US

[36] *ASTM C192/C192M-24 Standard Practice for Making and Curing Concrete Test Specimens in the Laboratory*, 2024. Accessed: Dec. 06, 2024. [Online]. Available: https://compass.astm.org/document/?contentCode=ASTM%7CC0192_C0192M-24%7Cen-US

[37] *ASTM C1611/C1611M-21 Standard Test Method for Slump Flow of Self-Consolidating Concrete*, 2021. Accessed: Dec. 06, 2024. [Online]. Available: https://compass.astm.org/document/?contentCode=ASTM%7CC1611_C1611M-21%7Cen-US

[38] M. Ahmadi, “End Regions Repair of Prestressed Girders for Restoring the Shear

Capacity Using UHPC, FR-SCC, and MALP," Jan. 2021, Accessed: Dec. 06, 2024. [Online]. Available: https://www.academia.edu/83433309/End_Regions_Repair_of_Prestressed_Girders_for_Restoring_the_Shear_Capacity_Using_UHPC_FR_SCC_and_MALP

[39] B. Poblete, "CSA Cement Mix Design," Jul. 15, 2024.

[40] *ASTM C1583/C1583M-20 Standard Test Method for Tensile Strength of Concrete Surfaces and the Bond Strength or Tensile Strength of Concrete Repair and Overlay Materials by Direct Tension (Pull-off Method)*, 2020. Accessed: Dec. 06, 2024. [Online]. Available: https://compass.astm.org/document/?contentCode=ASTM%7CC1583_C1583M-20%7Cen-US

[41] *ASTM C666/C666M-15 Standard Test Method for Resistance of Concrete to Rapid Freezing and Thawing (Withdrawn 2024)*, 2015. Accessed: Dec. 06, 2024. [Online]. Available: https://compass.astm.org/document/?contentCode=ASTM%7CC0666_C0666M-15%7Cen-US

[42] "ASTM C215-19 Standard Test Method for Fundamental Transverse, Longitudinal, and Torsional Resonant Frequencies of Concrete Specimens," ASTM Compass. Accessed: May 30, 2025. [Online]. Available: https://compass.astm.org/document/?contentCode=ASTM%7CC0215-19%7Cen-US

[43] A. A. Semendary and D. Svecova, "Bond Characterization and Interfacial Coefficients at Precast UHPC and Cast-in-Place UHPC Interface," *J. Mater. Civ. Eng.*, vol. 33, no. 7, p. 04021143, Jul. 2021, doi: 10.1061/(ASCE)MT.1943-5533.0003755.

Appendix A: Fresh Properties and Compressive Strength Data

Table 10: Admixture Dosages, Slump, and Air Content of Class AA Concrete

Property	AA-1	AA-2X	AA-3	AA-4X	AA-5	AA-6X	AA-7
HRWR Dosage (oz./cwt)	**3.50**	**4.79†**	**4.79‡**	**9.92**	**5.58**	**4.58**	**5.57**
Air Entrainer Dosage (oz./cwt)	**0.70**	**0.70**	**0.35**	**0.35**	**0.35**	**0.41**	**0.60**
Slump (in.)	3.0	5.5	5.5	--	4.25	6.0	7.0
Air Content (%)	5.10	7.00	4.60	--	4.10	3.90	7.00

†Included additional mixing water proportional to 22.2 lb/yd^3
‡Included additional mixing water proportional to 6.3 lb/yd^3

Table 11: Admixture Dosages, Slump Flow, and Air Content of FR-SCC

Property	FR-1X	FR-2	FR-3
HRWR Dosage (oz./cwt)	10.08	10.11	9.25
Air Entrainer Dosage (oz./cwt)	1.1	1.1	1.1
Slump Flow (in.)	24	17.5	25
Air Content (%)	3.6	3.1	4.0

Table 12: Admixture Dosage and Slump Flow of RS-SCC

Property	RS-1	RS-2	RS-3
HRWR Dosage (oz./cwt)	8.19	11.72‡	9.00
Slump Flow (in.)	24.75	21	25

‡Used Advacast 575 HRWR and additional mixing water proportional to 57.9 lb/yd^3

Table 13: Admixture Dosage and Slump Flow of RS-SCCHA

Property	RSHA-1X	RSHA-2	RSHA-3	RSHA-4
HRWR Dosage (oz./cwt)	10.56	8.64	11.00	9.50
Slump Flow (in.)	27	23.5	29	24.5

Table 14: Admixture Dosage and Slump Flow of RS-SCCUA

Property	UA-1	UA-2
HRWR Dosage (oz./cwt)	4.00	2.00
Slump Flow (in.)	24	21

Table 15: Compressive Strength Data for Class AA Concrete

Test Result	AA-1	AA-3	AA-5	AA-6X	AA-7
3-Day Average	**4650**	**5180**	**4940**	**4860**	**4860**
Cylinder 1	5122	5182	4601	4728	4718
Cylinder 2	3872	5173	5191	4938	5001
Cylinder 3	4966	5173	5033	4920	4859
7-Day Average	**--**	**6170**	**5870**	**5990**	**5930**
Cylinder 1	--	6080	5782	5872	5932
Cylinder 2	--	6119	6184	5976	6196
Cylinder 3	--	6325	5647	6112	5659
28-Day Average	**--**	**6610**	**6130**	**6530**	**6210**
Cylinder 1	--	6819	6127	6370	6353
Cylinder 2	--	6458	6356	6706	6107
Cylinder 3	--	6542	5892	6498	6168
Test-Day Average	**6910**	**6510**	**5780**	**--**	**6080**
Cylinder 1	7107	6513	5726	--	6206
Cylinder 2	6941	6530	5873	--	6069
Cylinder 3	6680	6479	5732	--	5960

Table 16: Compressive Strength Data for RS-SCC

Test Result	RS-1	RS-2	RS-3
6-Hr Average	**--**	**5030**	**6280**
Cylinder 1	--	5106	6127
Cylinder 2	--	4971	6244
Cylinder 3	--	5012	6372
1-Day Average	**8080**	**6420**	**8290**
Cylinder 1	8305	6669	8384
Cylinder 2	7829	6097	8807
Cylinder 3	8118	6499	7668
3-Day Average	**--**	**7610**	**--**
Cylinder 1	--	7580	--
Cylinder 2	--	7408	--
Cylinder 3	--	7842	--
7-Day Average	**9070**	**8220**	**10250**
Cylinder 1	9270	8175	10556
Cylinder 2	8876	8245	10422
Cylinder 3	9473	8226	9767
28-Day Average	**9370**	**8870**	**10290**
Cylinder 1	9390	8875	10063
Cylinder 2	9816	8888	10544
Cylinder 3	8893	8851	10250

Table 17: Compressive Strength Data for RS-SCCHA

Test Result	HA-2	HA-3	HA-4
6-Hr Average	**6400**	**5810**	**5060**
Cylinder 1	6394	5910	5065
Cylinder 2	6535	5689	4914
Cylinder 3	6255	5816	5192
1-Day Average	**7530**	**8320**	**7620**
Cylinder 1	7783	8659	7517
Cylinder 2	7240	7820	7781
Cylinder 3	7560	8471	7565
3-Day Average	**9080**	**9700**	**8670**
Cylinder 1	9108	9710	8645
Cylinder 2	9200	9203	9026
Cylinder 3	8940	10187	8336
7-Day Average	**9640**	**10540**	**8990**
Cylinder 1	9914	10280	8996
Cylinder 2	9538	10300	9195
Cylinder 3	9452	11047	8772
28-Day Average	**9420**	**10670**	**8740**
Cylinder 1	9781	11238	9226
Cylinder 2	9152	10125	8381
Cylinder 3	9329	10637	8606

Table 18: Compressive Strength Data for RS-SCCUA

Test Result	UA-1	UA-2
6-Hr Average	**4700**	**4190**
Cylinder 1	4614	4224
Cylinder 2	4840	4195
Cylinder 3	4658	4149
1-Day Average	**5600**	**5330**
Cylinder 1	5584	5330
Cylinder 2	5310	--
Cylinder 3	5919	--
3-Day Average	**6190**	**--**
Cylinder 1	6379	--
Cylinder 2	6024	--
Cylinder 3	6153	--
7-Day Average	**6930**	**5750**
Cylinder 1	7041	6051
Cylinder 2	6578	5606
Cylinder 3	7171	5598
28-Day Average	**7080**	**5710**
Cylinder 1	7144	5997
Cylinder 2	7412	4954
Cylinder 3	6676	6185

Table 19: Compressive Strength Data for FR-SCC

Test Result	FR-2	FR-3
3-Day Average	**6160**	**--**
Cylinder 1	6234	--
Cylinder 2	5969	--
Cylinder 3	6268	--
7-Day Average	**6710**	**6910**
Cylinder 1	6850	7022
Cylinder 2	5550	6774
Cylinder 3	7728	6920
28-Day Average	**9200**	**8400**
Cylinder 1	8741	8392
Cylinder 2	9102	8453
Cylinder 3	9753	8357

Appendix B: Pull-Off Test Data

Table 20: Pull-Off Results for Class AA Monolithic Specimen

Core Number	Failure Load (lbf)	Failure Stress (psi)	Failure Type
1	1200	382	Monolithic†
2	1850	589	Monolithic†
3	1575	501	Monolithic†
4	1825	581	Monolithic†
5	1600	509	Monolithic†
Average	**1610**	**512**	**N/A**

†Specimen failed in the monolithic concrete layer

Table 21: Pull-Off Test Results for 7-Day RS-SCC Monolithic Specimen

Core Number	Failure Load (lbf)	Failure Stress (psi)	Failure Type
1	1700	541	Monolithic†
2	2000	637	Monolithic†
3	1800	573	Monolithic†
4	2300	732	Monolithic†
5	2000	637	Monolithic†
Average	**1960**	**624**	**N/A**

†Specimen failed in the monolithic concrete layer

Table 22: Pull-Off Test Results for 28-Day RS-SCC Monolithic Specimen

Core Number	Failure Load (lbf)	Failure Stress (psi)	Failure Type
1	775	247	Monolithic†
2	750	239	Monolithic†
3	2075	660	Monolithic†
4	1825	581	Monolithic†
5	2000	637	Monolithic†
Average	**1485**	**473**	**N/A**

†Specimen failed in the monolithic concrete layer

Table 23: Pull-Off Test Results for RS-SCCHA Monolithic Specimen

Core Number	Failure Load (lbf)	Failure Stress (psi)	Failure Type
1	2100	668	Monolithic†
2	1600	509	Monolithic†
3	2300	732	Monolithic†
4	1825	581	Monolithic†
5	1875	597	Monolithic†
Average	**1940**	**618**	**N/A**

†Specimen failed in the monolithic concrete layer

Table 24: Pull-Off Test Results for RS-SCCUA Monolithic Specimen

Core Number	Failure Load (lbf)	Failure Stress (psi)	Failure Type
1	1300	414	Monolithic†
2	1500	477	Monolithic†
3	1350	430	Monolithic†
4	1350	430	Monolithic†
5	1200	382	Monolithic†
Average	**1340**	**427**	**N/A**

†Specimen failed in the monolithic concrete layer

Table 25: Pull-Off Test Results for FR-SCC Monolithic Specimen

Core Number	Failure Load (lbf)	Failure Stress (psi)	Failure Type
1	1450	462	Monolithic†
2	1325	422	Monolithic†
3	1325	422	Monolithic†
4	1200	382	Monolithic†
5	1425	454	Monolithic†
Average	**1345**	**428**	**N/A**

†Specimen failed in the monolithic concrete layer

Table 26: Pull-Off Results for RS-SCC Composite Specimens

Core	Failure Load (lbf)	Failure Stress (psi)	Failure Type
EA 1	450	143	A
EA 2	1100	350	A
EA 3	275	88	A
EA 4	800	255	A
EA 5	1475	470	A
EA Average	**820**	**261**	**N/A**
CH 1	800	255	B
CH 2	275	88	B
CH 3	475	151	B
CH 4	275	88	B
CH 5	250	80	B
CH Average	**415**	**132**	**N/A**
SB-D 1	1520	484	A
SB-D 2	1650	525	A
SB-D 3	2850	907	A
SB-D 4	600	191	A
SB-D 5	700	223	A
SB-D Average	**1464**	**466**	**N/A**

Table 27: Pull-Off Results for RS-SCCHA Composite Specimens

Core	Failure Load (lbf)	Failure Stress (psi)	Failure Type
EA 1	900	286	B
EA 2	975	310	B
EA 3	1000	318	B
EA 4	850	271	B
EA 5	1100	350	B
EA Average	**965**	**307**	**N/A**
CH 1	1000	318	B
CH 2	1000	318	B
CH 3	1200	382	B
CH 4	925	294	B
CH 5	1000	318	B
CH Average	**1025**	**326**	**N/A**
SB-D 1	1625	517	A
SB-D 2	1450	462	A
SB-D 3	3925	1249	A
SB-D 4	1875	597	A
SB-D 5	1500	477	A
SB-D Average	**2075**	**660**	**N/A**
SB-MS 1	2125	676	B
SB-MS 2	1850	589	D
SB-MS 3	1500	477	A
SB-MS 4	1375	438	A
SB-MS 5	1850	589	A
SB-MS Average	**1740**	**554**	**N/A**

Table 28: Pull-Off Results for RS-SCCUA Composite Specimens

Core	Failure Load (lbf)	Failure Stress (psi)	Failure Type
EA 1	1425	454	B
EA 2	1250	398	B
EA 3	825	263	B
EA 4	1500	477	D
EA 5	1225	390	B
EA Average	**1245**	**396**	**N/A**
CH 1	350	111	B
CH 2	650	207	B
CH 3	250	80	B
CH 4	500	159	B
CH 5	550	175	B
CH Average	**460**	**146**	**N/A**
SB-D 1	1475	470	B
SB-D 2	1375	438	B
SB-D 3	1550	493	A
SB-D 4	1350	430	D

Core	Failure Load (lbf)	Failure Stress (psi)	Failure Type
SB-D 5	1250	398	A
SB-D Average	**1400**	**446**	**N/A**
SB-MS 1	1500	477	A
SB-MS 2	1500	477	A
SB-MS 3	1525	485	A
SB-MS 4	1350	430	A
SB-MS 5	1425	454	A
SB-MS Average	**1460**	**465**	**N/A**

Table 29: Pull-Off Results for FR-SCC Composite Specimens

Core	Failure Load (lbf)	Failure Stress (psi)	Failure Type
EA 1	1425	454	B
EA 2	650	207	B
EA 3	800	255	C
EA 4	1300	414	A
EA 5	1475	470	A
EA Average	**1130**	**360**	**N/A**
CH 1	425	135	B
CH 2	450	143	B
CH 3	150	48	B
CH 4	325	103	B
CH 5	525	167	B
CH Average	**375**	**119**	**N/A**
SB-D 1	1250	398	B
SB-D 2	1500	477	A
SB-D 3	1100	350	B
SB-D 4	1400	446	B
SB-D 5	1425	454	B
SB-D Average	**1335**	**425**	**N/A**
SB-MS 1	1250	398	A
SB-MS 2	1425	454	A
SB-MS 3	825	263	A
SB-MS 4	1700	541	A
SB-MS 5	1600	509	A
SB-MS Average	**1360**	**433**	**N/A**

Appendix C: Freeze-Thaw Test Data

Table 30: Monolithic RS-SCC (7-Day) Freeze-Thaw Data

Test Result	0 Cycles	33 Cycles	63 Cycles	95 Cycles	127 Cycles	154 Cycles
Resonant Frequency (Hz) Specimen 1	7227	7324	7285	6650	5397	5156
Relative Dynamic Modulus of Elasticity (%) Specimen 1	100.0	102.7	101.6	84.7	55.8	50.9
Resonant Frequency (Hz) Specimen 2	7217	7354	7324	7080	6100	5312
Relative Dynamic Modulus of Elasticity (%) Specimen 2	100.0	103.8	103.0	96.2	71.4	54.2

Table 31: Monolithic RS-SCC (28-Day) Freeze-Thaw Data

Test Result	0 Cycles	27 Cycles	59 Cycles	91 Cycles	109 Cycles	133 Cycles
Resonant Frequency (Hz) Specimen 1	7266	7363	7207	5605	5537	4466
Relative Dynamic Modulus of Elasticity (%) Specimen 1	100.0	102.7	98.4	59.5	58.1	37.8
Resonant Frequency (Hz) Specimen 2	7275	7441	6937	6393	5755	4987
Relative Dynamic Modulus of Elasticity (%) Specimen 2	100.0	104.6	90.9	77.2	62.6	47.0

Table 32: Monolithic RS-SCCUA Freeze-Thaw Data

Test Result	0 Cycles	33 Cycles	66 Cycles	98 Cycles	131 Cycles	162 Cycles
Resonant Frequency (Hz) Specimen 1	5127	5176	5205	5234	4837	3125
Relative Dynamic Modulus of Elasticity (%) Specimen 1	100.0	101.9	103.1	104.2	89.0	37.2
Resonant Frequency (Hz) Specimen 2	5117	5039	N/A*	N/A*	N/A*	N/A*
Relative Dynamic Modulus of Elasticity (%) Specimen 2	100.0	97.0	N/A*	N/A*	N/A*	N/A*

*Data not available due to specimen failure

Table 33: Monolithic RS-SCCHA Freeze-Thaw Data

Test Result	0 Cycles	32 Cycles	66 Cycles	93 Cycles
Resonant Frequency (Hz) Specimen 1	5547	5420	5537	5537
Relative Dynamic Modulus of Elasticity (%) Specimen 1	100.0	95.5	99.6	99.6
Resonant Frequency (Hz) Specimen 2	5518	5654	5723	5742
Relative Dynamic Modulus of Elasticity (%) Specimen 2	100.0	105.0	107.6	108.3

Table 34: Composite RS-SCCHA Resonant Frequency Data (Hz)

Specimen	0 Cyc.	0 Cyc.	26 Cyc.	57 Cyc.	87 Cyc.	118 Cyc.	151 Cyc.	184 Cyc.	213 Cyc.	240 Cyc.	273 Cyc.	301 Cyc.
EA 1	5615	5703	5742	5781	5713	5762	5713	5781	5693	5625	5732	5713
EA 2	5625	5732	5771	5752	5703	5732	5820	5791	5674	5508	5498	5156
CH 1	5703	5742	5732	5752	5820	5811	5752	5684	5654	5566	5557	5361
CH 2	5605	5654	5654	5713	5713	5771	5771	5723	5684	5645	5654	5527
SB-D 1	5703	5752	5752	5820	5791	5791	5811	5605	5605	5566	5420	5459
SB-D 2	5615	5664	5703	5791	5801	5820	5830	5820	5781	5781	5732	5508
SB-MS 1	5654	5703	5703	5732	5732	5742	5713	5703	5664	5645	5742	5664
SB-MS 2	5635	5684	5693	5713	5723	5645	5625	5547	5635	5645	5498	5303

Table 35: Composite RS-SCCHA Relative Dynamic Modulus of Elasticity Data (%)

Specimen	0 Cyc.	0 Cyc.	26 Cyc.	57 Cyc.	87 Cyc.	118 Cyc.	151 Cyc.	184 Cyc.	213 Cyc.	240 Cyc.	273 Cyc.	301 Cyc.
EA 1	100.0	103.2	104.6	106.0	103.5	105.3	103.5	106.0	102.8	100.4	104.2	103.5
EA 2	100.0	103.8	105.3	104.6	102.8	103.8	107.1	106.0	101.7	95.9	95.5	84.0
CH 1	100.0	101.4	101.0	101.7	104.1	103.8	101.7	99.3	98.3	95.3	94.9	88.4
CH 2	100.0	101.8	101.8	103.9	103.9	106.0	106.0	104.3	102.8	101.4	101.8	97.2
SB-D 1	100.0	101.7	101.7	104.1	103.1	103.1	103.8	96.6	96.6	95.3	90.3	91.6
SB-D 2	100.0	101.8	103.2	106.4	106.7	107.4	107.8	107.4	106.0	106.0	104.2	96.2
SB-MS 1	100.0	101.7	101.7	102.8	102.8	103.1	102.1	101.7	100.4	99.7	103.1	100.4
SB-MS 2	100.0	101.7	102.1	102.8	103.1	100.4	99.6	96.9	100.0	100.4	95.2	88.6

Table 36: Composite FR-SCC Resonant Frequency Data (Hz)

Specimen	0 Cyc.	32 Cyc.	65 Cyc.	98 Cyc.	130 Cyc.	163 Cyc.	194 Cyc.	227 Cyc.	261 Cyc.	293 Cyc.	307 Cyc.
EA 1	5625	5869	5918	5938	5947	5977	5928	5918	5820	5830	5811
EA 2	5596	5859	5908	5879	5889	5928	5908	5898	5908	5869	5850
CH 1	5625	5859	5918	5908	5938	5967	5918	5908	5898	5918	5850
CH 2	5557	5801	5869	5850	5859	5889	5840	5830	5820	5840	5791
SB-D 1	5566	N/A*	N/A*	N/A*	N/A*	N/A*	N/A*	N/A*	N/A*	N/A*	N/A*
SB-D 2	5625	5869	5898	5869	5781	5898	5840	N/A*	N/A*	N/A*	N/A*
SB-MS 1	5586	5771	5820	5791	5791	5801	5781	5781	5791	5801	5762
SB-MS 2	5645	5859	5918	5928	5947	5957	5938	5938	5938	5947	5918

*Data not available due to specimen failure

Table 37: Composite FR-SCC Relative Dynamic Modulus of Elasticity Data (%)

Specimen	0 Cyc.	32 Cyc.	65 Cyc.	98 Cyc.	130 Cyc.	163 Cyc.	194 Cyc.	227 Cyc.	261 Cyc.	293 Cyc.	307 Cyc.
EA 1	100.0	108.9	110.7	111.4	111.8	112.9	111.1	110.7	107.1	107.4	106.7
EA 2	100.0	109.6	111.5	110.4	110.7	112.2	111.5	111.1	111.5	110.0	109.3
CH 1	100.0	108.5	110.7	110.3	111.4	112.5	110.7	110.3	109.9	110.7	108.2
CH 2	100.0	109.0	111.5	110.8	111.2	112.3	110.4	110.1	109.7	110.4	108.6
SB-D 1	100.0	N/A*	N/A*	N/A*	N/A*	N/A*	N/A*	N/A*	N/A*	N/A*	N/A*
SB-D 2	100.0	108.9	109.9	108.9	105.6	109.9	107.8	N/A*	N/A*	N/A*	N/A*
SB-MS 1	100.0	106.7	108.6	107.5	107.5	107.8	107.1	107.1	107.5	107.8	106.4
SB-MS 2	100.0	107.7	109.9	110.3	111.0	111.4	110.7	110.7	110.7	111.0	109.9

*Data not available due to specimen failure

Table 38: RS-SCCHA/CH Bridge Repair Freeze-Thaw Data

Specimen	0 Cyc.	33 Cyc.	66 Cyc.	100 Cyc.	132 Cyc.	164 Cyc.
CH 1 Resonant Frequency (Hz)	4951	4961	4814	4873	4549	N/A*
CH 1 Relative Dynamic Modulus of Elasticity (%)	100.0	100.4	94.5	96.9	84.4	N/A*
CH 2 Resonant Frequency (Hz)	5127	5117	4834	4766	N/A*	N/A*
CH 2 Relative Dynamic Modulus of Elasticity (%)	100.0	99.6	88.9	86.4	N/A*	N/A*

*Data not available due to specimen failure

Table 39: RS-SCCHA/SB-D Bridge Repair Freeze-Thaw Data

Specimen	0 Cyc.	36 Cyc.	70 Cyc.	97 Cyc.
SB-D 1 Resonant Frequency (Hz)	5205	5439	5400	5059
SB-D 1 Relative Dynamic Modulus of Elasticity (%)	100.0	109.2	107.6	94.5
SB-D 2 Resonant Frequency (Hz)	5166	5439	5068	4980
SB-D 2 Relative Dynamic Modulus of Elasticity (%)	100.0	110.8	96.2	92.9

Table 40: FR-SCC/CH Bridge Repair Freeze-Thaw Data

Specimen	0 Cyc.	34 Cyc.	68 Cyc.	95 Cyc.
CH 1 Resonant Frequency (Hz)	5029	5332	5342	5332
CH 1 Relative Dynamic Modulus of Elasticity (%)	100.0	116.0	116.4	116.0
CH 2 Resonant Frequency (Hz)	4951	5225	5273	5225
CH 2 Relative Dynamic Modulus of Elasticity (%)	100.0	103.9	105.8	103.9

Table 41: FR-SCC/SB-D Bridge Repair Freeze-Thaw Data

	0 Cyc.	34 Cyc.	68 Cyc.	95 Cyc.
SB-D 1 Resonant Frequency (Hz)	5176	5469	5488	5400
SB-D 1 Relative Dynamic Modulus of Elasticity (%)	100.0	110.4	111.2	107.6
SB-D 2 Resonant Frequency (Hz)	5205	5508	5537	N/A*
SB-D 2 Relative Dynamic Modulus of Elasticity (%)	100.0	113.7	114.9	N/A*

*Data not available